Universidade do Estado do Rio de Janeiro
Centro Biomédico
Instituto de Biologia Roberto Alcântara Gomes

Rickson Souza Ribeiro

Efeitos de LED azul e *laser* vermelho de baixa potência na sobrevivência celular e expressão gênica de fotoliases em culturas de *Escherichia coli* e na viabilidade celular e expressão de genes circadianos em células de câncer de mama

Rio de Janeiro
2023

Rickson Souza Ribeiro

Efeitos de LED azul e *laser* vermelho de baixa potência na sobrevivência celular e expressão gênica de fotoliases em culturas de *Escherichia coli* e da viabilidade celular e expressão de genes circadianos em células de câncer de mama

Dissertação apresentada como requisito parcial para obtenção do Título de Mestre em Biociências ao Programa de Pós-Graduação em Biociências da Universidade do Estado do Rio de Janeiro.

Orientador: Prof. Dr. Adenilson de Souza da Fonseca

Coorientador: Prof. Dr. Andre Luiz Mencalha

Rio de Janeiro

2023

CATALOGAÇÃO NA FONTE
UERJ/REDE SIRIUS/BIBLIOTECA CB-A

R484 Ribeiro, Rickson Souza.
Efeitos de LED azul e laser vermelho de baixa potência na sobrevivência celular e expressão gênica de fotoliases em culturas de Escherichia coli e da viabilidade celular e expressão de genes circadianos em células de câncer de mama / Rickson Souza Ribeiro. - 2023.
114 f.

Orientador: Prof. Dr. Prof. Dr. Adenilson de Souza da Fonseca
Coorientador: Prof. Dr. Andre Luiz Mencalha

Dissertação (Mestrado) - Universidade do Estado do Rio de Janeiro, Instituto de Biologia Roberto Alcântara Gomes. Pós-graduação em Biociências.

1. Terapia a Laser – Instrumentação – Teses. 2. Neoplasias da mama – Radioterapia – Teses. 3. Terapia com luz de baixa intensidade – Instrumentação – Teses. I. Fonseca, Adenilson de Souza da. II. Mencalha, Andre Luiz. III. Universidade do Estado do Rio de Janeiro. Instituto de Biologia Roberto Alcântara Gomes. IV. Título.

CDU 618.19-006:535.21

Bibliotecário: Felipe Caldonazzo CRB7/7341

Rickson Souza Ribeiro — Assinatura

24/08/2023 — Data

Rickson Souza Ribeiro

Efeitos de LED azul e *laser* vermelho de baixa potência na sobrevivência celular e expressão gênica de fotoliases em culturas de *Escherichia coli* e da viabilidade celular e expressão de genes circadianos em células de câncer de mama

Dissertação apresentada como requisito parcial para obtenção do Título de Mestre em Biociências ao Programa de Pós-Graduação em Biociências da Universidade do Estado do Rio de Janeiro.

Aprovado em 24 de agosto de 2023

Coorientador: Prof. Dr. Andre Luiz Mencalha

Instituto de Biologia Roberto Alcântara Gomes - UERJ

Banca Examinadora:

Prof. Dr. Adenilson, de Souza da Fonseca (Orientador)

Instituto de Biologia Roberto Alcântara Gomes - UERJ

Prof.ª Dra. Flávia de Paoli

Universidade Federal de Juiz de Fora

Prof.ª Dra. Tatiana de Almeida Simão

Instituto de Biologia Roberto Alcântara Gomes – UERJ

Rio de Janeiro

2023

DEDICATÓRIA

Dedico este trabalho ao meu querido pai que me incentivou a chegar até aqui, à minha querida mãe e irmão por sempre ter me apoiado, à minha namorada por ter enfrentado os desafios comigo e aos meus queridos amigos que me acompanham desde a infância.

AGRADECIMENTOS

Agradeço primeiramente à Deus, pela vida, oportunidade e aprendizados para que conseguisse chegar até onde cheguei e por tudo mais que virá.

Agradecer também à minha mãe Maria das Graças de Souza Ribeiro, meu falecido pai Jayme Moreira Ribeiro Junior, meu irmão Acácio Luiz de Souza Rezende e minha namorada Eshilley de Souza Alves por toda dedicação, amor, carinho e incentivos que me tornaram o homem que sou e me fizeram chegar até aqui.

Aos meus colegas de laboratório, Ana Carolina Ferreira, Thayssa Gomes, Juliana Alves, Pryscianne Siqueira, Mariana Moreno e Márcia Soares um muito obrigado pelas ajudas e contribuições para que esse trabalho fosse concluído com êxito.

Ao meu querido orientador, companheiro e amigo, professor Dr. Adenilson de Souza da Fonseca, muito obrigado, por ter aceitado me orientar durante esta etapa e também pelas maravilhosas conversas que tivemos ao longo dessa jornada e também por me incentivar a seguir na carreira cientifica e acadêmica. Agradeço também ao professor Dr. Andre Luiz Mencalha por ter aceitado ser meu coorientador e me dar *insghts* sobre os experimentos desenvolvidos durante a minha jornada acadêmica.

Por fim, agradeço o suporte da Fundação de Amparo à Pesquisa do Estado do Rio de Janeiro (FAPERJ) e à Universidade do Estado do Rio de Janeiro (UERJ).

RESUMO

RIBEIRO, Rickson Souza. **Efeitos de LED azul e *laser* vermelho de baixa potência na sobrevivência celular e expressão gênica de fotoliases em culturas de *Escherichia coli* e da viabilidade celular e expressão de genes circadianos em células de câncer de mama**. 2023. 114 f. Dissertação (Mestrado em Biociências) – Instituto de Biologia Roberto Alcântara Gomes, Universidade do Estado do Rio de Janeiro, Rio de Janeiro, 2023.

Lasers e LEDs terapêuticos de baixa potência são usados com base na fotobiomodulação, mas os efeitos da fotobiomodulação nos mecanismos de reparo do DNA em células bacterianas e na expressão dos genes envolvidos no ciclo circadiano de células tumorais de mamíferos ainda não foram avaliados. Assim, o objetivo desse trabalho foi avaliar os efeitos do *laser* vermelho (658 nm) e LED azul (470 nm) terapêuticos de baixa potência nos genes da família das flavoproteínas utilizando modelos procarióticos e eucarióticos. Alíquotas do plasmídeo pUC19 e culturas de *E. coli* C600, MCF-7 e MDA-MB-231 foram expostos ao LED azul (470 nm) e ao *laser* vermelho (658 nm) em diferentes fluências. Outras culturas de *E. coli* C600 foram expostas a radiação UVC e em seguida ao LED azul e ao *laser* vermelho de baixa potência. Após irradiação, os plasmídeos foram submetidos a eletroforese em gel de agarose para avaliar as formas plasmidiais, culturas bacterianas foram semeadas em placas de *Petri* contendo meio nutritivo para avaliar a sobrevivência e proliferação bacteriana, e os níveis de mRNA da fotoliase em células bacterianas foram avaliados por reação em cadeia da polimerase quantitativa em tempo real. Culturas de MCF-7 e MDA-MB-231, após irradiação, também foram cultivadas em meio DMEM e RPMI, respectivamente, suplementado com soro fetal bovino. Os níveis de mRNA dos genes circadianos também foram avaliados por reação em cadeia da polimerase quantitativa em tempo real. O ensaio de viabilidade celular por WST-1 foi realizado após 24, 48 e 72 horas após irradiação. Os resultados sugeriram que a exposição ao LED azul e ao *laser* vermelho de baixa potência não causam quebra na fita de DNA em plasmídeos bacterianos e não altera a sobrevivência e os níveis de mRNA do gene da fotoliase em células de *E. coli*, mas aumenta a sobrevivência e proliferação em culturas de *E. coli* expostas a radiação ultravioleta C dependendo da fluência do *laser*. A viabilidade celular, e os níveis de mRNA dos genes circadianos em células MCF-7 e MDA-MB231 após exposição ao LED azul e ao *laser* vermelho de baixa potência não foram alterados nas fluências avaliadas.

Palavras-Chaves: Câncer de mama; *Escherichia coli*; Fotobiomodulação; Genes circadianos; *Laser*.

ABSTRACT

RIBEIRO, Rickson Souza. *Effects of low-power blue LED and red laser on cell survival and gene expression of photolyases in Escherichia coli cultures and cell viability and circadian genes expression on breast cancer cells*. 2023. 114 f. Dissertação (Mestrado em Biociências) – Instituto de Biologia Roberto Alcântara Gomes, Universidade do Estado do Rio de Janeiro, Rio de Janeiro 2023.

Therapeutic low-power LEDs and *lasers* are used based on photobiomodulation, but the photobiomodulation effects on DNA repair mechanisms in bacterial cells and the expression of circadian genes in mammalian tumor cells have not yet been explored. Thus, the objective of this work was to evaluate the effects of low-power therapeutic blue LED and red *laser* on the genes of the flavoprotein family by prokaryotic and eukaryotic models. Aliquots of plasmid pUC19 and cultures of *E. coli* C600, MCF-7 and MDA-MB-231 were exposed to blue LED (470 nm) and red *laser* (658 nm) at different fluences. Other cultures of *E. coli* C600 were exposed to UVC radiation, followed by low-power blue LEDs and red *laser*. After irradiation, plasmids were subjected to agarose gel electrophoresis to evaluate the plasmidial forms, bacterial cultures were spread on *petri* dishes containing nutritive medium to evaluate the bacterial survival and proliferation, and photolyase mRNA levels of bacterial cells were assessed by real-time quantitative polymerase chain reaction. Cultures of MCF-7 and MDA-MB-231, after irradiation, were also cultivated in DMEM and RPMI medium, respectively, supplemented with fetal bovine serum. The mRNA levels of circadian genes were also assessed by real-time quantitative polymerase chain reaction. The cell viability assay by WST-1 was performed at 24, 48 and 72 hours after irradiation. The results suggest that exposure to low-power blue LED and red *laser* do not cause DNA strand breaks in bacterial plasmids and do not alter survival and the mRNA levels of the photolyase gene in *E. coli* cells, but increase survival and proliferation in *E. coli* cultures exposed to ultraviolet C radiation depending on the *laser* fluence. The cell viability and the mRNA levels of the circadian genes in MCF-7 and MDA-MB-231 cells after exposure to low-power blue LED and red *laser* did not change in evaluated fluences.

Keywords: Breast cancer; *Escherichia coli*; Photobiomodulation; Circadian genes; *laser*.

LISTA DE FIGURAS

LISTA DE TABELAS

LISTA DE ABREVIATURAS E SIGLAS

ACTB	Beta actina
AlGaInP	Gálio-Alumínio-Indio-fósforo
araC	proteína reguladora responsiva a arabinose
ATP	Adenosina trifosfato
BMAL1	Basic helix-loop-helix ARNT like 1
cDNA	DNA complementar
CLOCK	Regulador do relógio circadiano
CO_2	Dióxido de carbono
CPD	Ciclobutanos de pirimidina
CRY-DASH	Criptocromo-DASH
CRY1	Criptocromo 1
CRY2	Criptocromo 2
DMEM	Meio Eagle modificado
DMRL	6, 7-dimetil-8- ribityl lumazine
dNTP	Trifosfatos de desoxinucleotídeos
DNA	Ácido desoxirribonucleico
ERO	Espécies reativas de oxigênio
FAD	flavina-adenina dinucleotídeo
FA	Fração de área
FS	Fração de sobrevivência
gyrA	Subunidades da DNA girase
HER2	Receptor tipo 2 do fator de crescimento epidérmico humano
JR	Junior
Lasers	Amplificação da luz por emissão estimulada de radiação
LEDs	Diodos emissores de luz
$MgCl_2$	Cloreto de magnésio
mRNA	Ácido ribonucleico mensageiro
MTHF	Metil-tetra-hidro-folato
PBS	Tampão fosfato-salino
PER1	Período 1

PER2	Período 2
PER3	Período 3
Phr	Fotoliase
RNA	Ácido ribonucleico
RPMI	Meio de Roswell park memorial institute
rpoA	Subunidade da enzima central da RNA polimerase
RT-qPCR	Reação em cadeia da polimerase quantitativa em tempo real
TNFα	Fatores de necrose tumoral alfa
UFC	Unidades formadoras de colônias
UV	Ultravioleta
UVA	Ultravioleta A
UVC	Ultravioleta C
XPA	Xeroderma pigmentosum A
6-4 PP	Fotoprodutos 6-4 pirimidina pirimidona
8-HDF	8-hidroxi-7, 8 dimetil-5 deazariboflavina

LISTA DE SÍMBOLOS

cm	centímetro
cm²	centímetro quadrado
µl	microlitro
h	hora
J/cm²	Joules por centímetro quadrado
kJ/cm²	kilojoules por metro quadrado
mA	miliampére
min	minutos
mJ/cm²	milijoules por centímetro quadrado
ml	mililitros
mm²	milímetros quadrados
mW	miliwatts
ng	nanogramas
nm	nanômetros
RPM	rotações por minuto
s	segundos
V	volts
W	watts
W/cm²	watts por centímetro quadrado
%	por cento
±	mais ou menos
=	igual
°C	graus Celsius
+	mais
<	menor que
>	maior que

SUMÁRIO

INTRODUÇÃO

Equipamentos *Lasers* são dispositivos que utilizam o fenômeno físico de emissão estimulada para emitir um feixe de luz monocromática e coerente com pouca divergência. A palavra *laser* é um acrônimo para "*light amplification by stimulated emission of radiation*" (amplificação da luz por emissão estimulada de radiação). (HEISKANEN, HAMBLIN, 2018). O primeiro *laser* funcional foi desenvolvido por Theodore Maiman, nos anos de 1960, ao incidir luz sobre um cristal sintético de rubi, obtendo um feixe com comprimento de onda de 694 nm (MAIMAN, 1960). Mas o dispositivo já havia sido hipotetizado por Albert Einstein em 1917 através de seu trabalho "*Zur quantum Theories der Strahlung*" (Teoria quântica da radiação) (Einstein, 1917).

O equipamento *laser* é um dispositivo que emite feixes de radiações com características bem definidas quando comparadas com fontes ordinárias. Dentre essas características está a monocromaticidade, onde a radiação emitida apresenta um comprimento de onda dentro de uma faixa bem definida do espectro eletromagnético, outra característica é a sua coerência temporal e espacial, que pode ser entendida radiações com mesma frequência e direção que mantém uma relação de fase constante entre si, a colimação é outra característica a se destacar na qual os feixes de radiação se tornam paralelos, atingindo um ponto bem definido e a por fim, sua alta densidade de energia, que consiste na energia total transmitida pelo laser por unidade de área (BIRNGRUBER, 1989).

Os *lasers* também variam de acordo com sua potência. Os *lasers* de alta potência apresentam geram efeitos térmicos, ablação, sendo comumente utilizado na medicina em procedimentos cirúrgicos (DANTAS *et al*, 2021). Os *lasers* de média potência também geram efeitos térmicos, mas não abrasivos, sendo utilizados em procedimentos estéticos como fotodepilação (MARTINS, PAULA, SIMÕES, 2017). Os *lasers* de baixa potência não geram efeitos térmicos e são utilizados para terapias de fotobiomodulação, que se baseia na interação dos fótons com as células desencadeando eventos celulares, moleculares e sistêmicos (SILVA *et al*, 2023).

Para avaliar os efeitos dos *lasers* de baixa potência, são analisados alguns parâmetros como a fluência, medida em J/cm², que é a grandeza física que avalia a possibilidade de estimulação, inibição ou não manifestação dos efeitos terapêuticos; são avaliadas também a irradiância, medida em W/cm², que é o cálculo da potência de saída de luz por unidade de área e avalia a possibilidade de danos térmicos (RIBEIRO *et al*, 2011).

Outro fator relevante nos tratamentos com *lasers* de baixa potência é a escolha do dispositivo. Existem diferentes meios emissores capazes de emitir radiações pelo processo *laser* com diferentes comprimentos de onda, como o He-Ne (632,8 nm), rubi (694 nm) e Nd-YAg (1064 nm) (OLIVEIRA *et al*, 2013; YU, LAN, YU, 2019; YANG, *et al*, 2022). A escolha do dispositivo e comprimento de onda é de grande importância para estudar os fenômenos celulares, visto que as células apresentam cromóforos que absorvem radiação de comprimentos de onda em faixas específicas, desencadeando assim os efeitos envolvidos na fotobiomodulação (KARU, PYATIBRAT, KALENDO, 2003).

Os equipamentos LEDs são dispositivos baseados em materiais semicondutores que realizam um fenômeno denominado de eletroluminescência. Esse fenômeno ocorre quando uma corrente elétrica passa por materiais semicondutores, liberando energia luminosa (RENK, 2012). Diferente dos *lasers*, as radiações emitidas por esses equipamentos não são coerentes, são quase monocromáticas e os feixes da radiação emitida apresenta divergência (Figura 1) (HEISKANEN, HAMBLIN, 2018). O primeiro LED de luz visível foi desenvolvido por Nick Holonyak Jr. Em 1962. Estudos posteriores foram feitos e novos LEDs foram criados, dentre esses, LEDs emissores de luz no espectro da luz laranja, amarela e verde entre os anos de 1962 e 1970 (COURTLAND, 2014).

Os LEDs apresentam vantagens em relação aos *lasers*, devido ao seu custo mais reduzido, vida útil maior, emissão em diversas faixas de comprimento de onda (380 – 1200 nm) e tamanho pequeno. Entretanto, na prática experimental e clínica ainda há estudos comparativos sendo realizados para demonstrar a eficácia desses dispositivos em terapias baseadas na fotobiomodulação, visto que as características de coerência e colimação são levadas em consideração durante a irradiação do tecido para atingir um resultado esperado (ENWEMEKA, 2006; ANTIPA *et al*., 1996).

Figura 1 - Esquema representativo da radiação emitida por *laser* e LEDs.

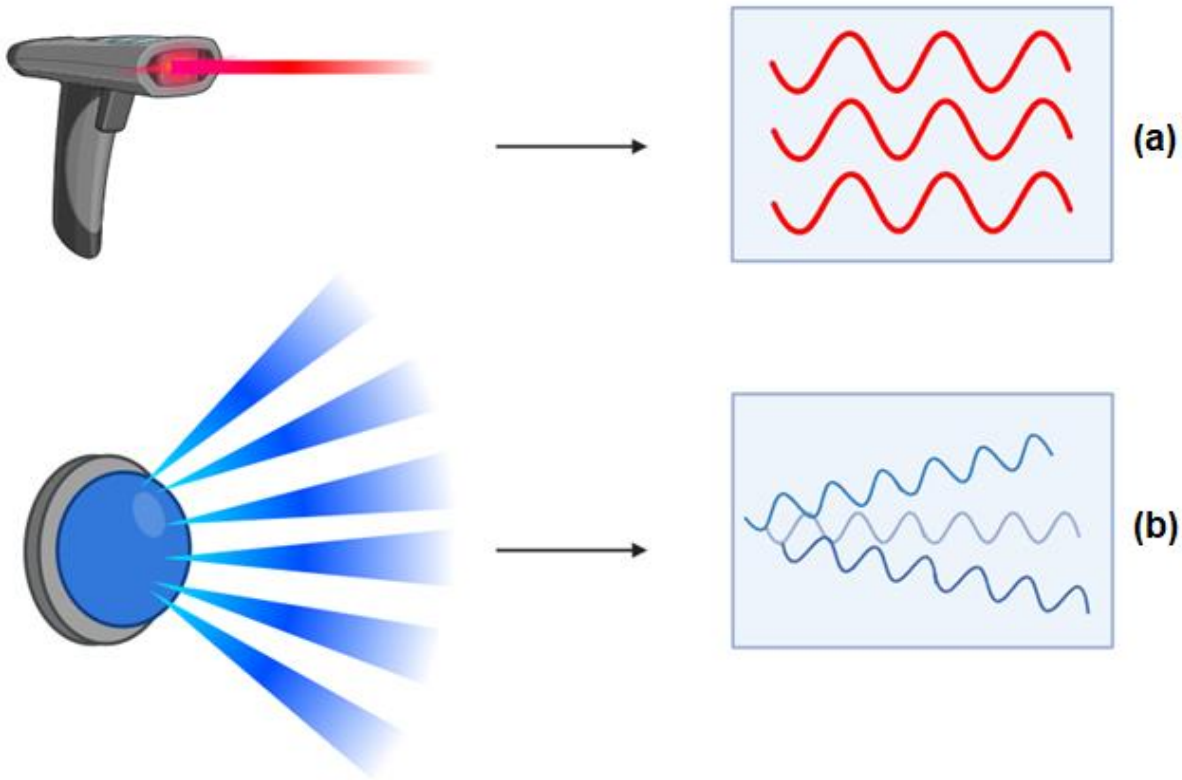

Legenda: (a) radiação emitida por *laser* com características de monocromaticidade, coerência e colimação. (b) radiação emitida por LEDs com radiação quase monocromática, sem colimação e se coerência.

Fonte: O autor, 2023.

1. **REVISÃO DA LITERATURA**

1.1 **Efeitos fotobiomoduladores**

Alguns anos após o desenvolvimento do dispositivo *laser*, foram realizados os primeiros estudos sobre os efeitos biológicos das radiações emitidas por esses dispositivos. O físico Leon Goldman foi o primeiro a estudar os efeitos do laser sobre lesões na pele, que publicou os resultados da sua pesquisa avaliando os efeitos do *laser* rubi na destruição de melanomas malignos em 1964. No mesmo ano, Endre Master se interessou pelas aplicações clínicas no tratamento de melanomas (STRAIGHT, 2016; MCGUFF *et al*., 1964; MESTER, MESTER, 2017).

Endre Master iniciou seus estudos sobre os efeitos da radiação emitida pelo *laser* rubi de baixa potência na pele de camundongos e demonstrou que os pelos da pele dos camundongos irradiadas com o *laser* cresce de forma mais acelerada quando comparada com os pelos da pele do grupo não irradiado. Entretanto, quando a dose aplicada era aumentada, os pelos não cresciam mais, o oposto do que acontecia com o grupo não irradiado onde os pelos cresciam normalmente (MESTER, MESTER, 2017). Este foi o primeiro experimento documentando a aplicação da lei biofísica de Arndt-Schulz para *lasers*, onde o *laser* pode apresentar efeitos estimulatórios ou inibitórios dependendo da dose aplicada (MESTER *et al*, 1969).

As contribuições de Tiina Karu também tiveram grande impacto na compreensão dos efeitos da fotobiomodulação. Seus estudos explorando os efeitos de *lasers* em células HeLa auxiliou na elucidação da interação da radiação vermelha e infravermelha no aumento da atividade mitocondrial e síntese de ATP, DNA e proteínas (KARU, PYATIBRAT, KALENDO, 2003). Assim como seus estudos sobre os efeitos dessas radiações em procariotos, elucidando suas interações e consequências nesses organismos (KARU *et al*, 1994).

Embora terapias baseadas na fotobiomodulação sejam utilizadas para diversos propósitos terapêuticos, como a cicatrização de feridas, alívio da dor, tratamentos odontológicos e de acne, ainda há controvérsias sobre o uso dessa terapia em pacientes oncológicos (HAMBLIN, NELSON, STRAHAN, 2018). Essas controvérsias se devem as propriedades proliferativas encontradas nas terapias de fotobiomodulação, que poderiam resultar em uma piora do quadro clínico de um paciente com o aumento da atividade proliferativa das células tumorais (HAMBLIN, NELSON, STRAHAN, 2018). Entretanto, há

estudos demonstrando terapias baseadas em fotobiomodulação no tratamento de mucosite oral em pacientes submetidos a quimioterapia e radioterapia (CRONSHAW *et al*, 2020).

1.2 **Família das flavoproteínas**

1.2.1 Fotoliases

As fotoliases são enzimas pertencentes a família das flavoproteínas. Essas enzimas apresentam um cofator enzimático derivado da riboflavina, o dinucleotídeo de flavina e adenina (FAD). As flavinas foram descobertas e caracterizadas em 1930, sendo reconhecidas por processos biológicos de transferência de um ou dois elétrons para oxidação de substratos orgânicos e transferência de elétrons na cadeia respiratória (MASSEY, 2000).

As enzimas fotoliases estão presentes em quase todos os grupos de seres vivos, com algumas exceções como os mamíferos placentários (SANCAR, 2004). Em bactérias, o gene responsável por codificar a fotoliase é o gene *phr*. Essas enzimas desempenham função vital no processo de reparo de lesões no DNA induzido por radiação ultravioleta (LIU, WANG, ZHONG, 2015).

As lesões provocadas pela radiação ultravioleta (UV), em especial a radiação ultravioleta C (UVC), podem ser causadas por duas vias, direta e indireta. Na via direta, a molécula de DNA absorve a energia do fóton de radiação UV nas regiões com bases pirimidínicas adjacentes (SINHA, HÄDER, 2002, JIANG *et al*., 2009). Após a absorção da energia, essas bases formam ligações covalentes, gerando uma deformação na fita de DNA que impedem a transcrição e replicação (ZHANG, WANG, ZHONG, 2017). Essas lesões são chamadas de dímeros de pirimidina e podem ser de dois tipos, os ciclobutanos de pirimidina (CPD) e os fotoprodutos 6-4 pirimidina-pirimidona (6-4 PP), cuja diferença está nas ligações covalentes formadas entre os carbonos nas bases pirimidínicas adjacentes (Figura 2) (ZHANG, WANG, ZHONG, 2017). A via indireta está associada com a geração de espécies reativas de oxigênio (ERO), como oxigênio singleto ($^1O_2$) que causa danos oxidativos no DNA (JIANG *et al*., 2009).

Figura 2 - Representação esquemática das lesões causada pela radiação ultravioleta em bases pirimidínicas adjacentes.

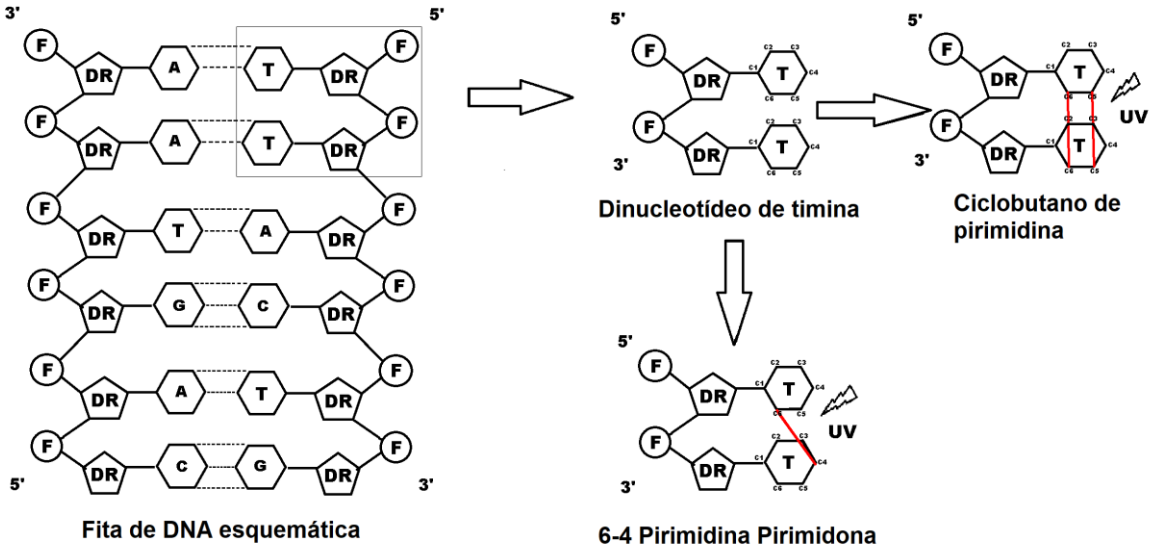

Legenda: Fita esquemática de DNA: F – Fosfato, DR – Desoxirribose, A – Adenina, T – Timina, G – Guanina, C – Citosina; Ciclobutano de pirimidina: Ligações covalentes (linha vermelha) entre os carbonos C5 e C6, UV – Radiação ultravioleta; 6-4 Pirimidina Pirimidona: Ligação covalente cruzada (linha vermelha) entre os carbonos C6 e C4.

Fonte: O autor, 2023.

As enzimas fotoliases apresentam dois cofatores, o dinucleotídeo de flavina e adenina (FAD), que é responsável pelo reparo catalítico dos dímeros de pirimidina induzidos por radiação UV (LIU, WANG, ZHONG, 2015), funcionando também como cromóforo primário e os cromóforos secundários, ou cromóforos antena que absorvem a energia dos fótons incidentes dentro de faixas de comprimento de onda que vão da faixa do UVA (315 nm), passando pelo espectro visível do violeta (400-425 nm), ao azul (425-500 nm) (SANCAR, 2008). Existem diversos cromóforos secundários para as fotoliases, dependendo do tipo de organismo: metil-tetra-hidro-folato (MTHF); 8-hidroxi-7, 8 dimetil-5 deazariboflavina (8-HDF) e 6, 7-dimetil-8- ribitilumazina (DMRL) (TERAI *et al*., 2020).

As fotoliases reconhecem os dímeros de pirimidina na fita de DNA e se associam a estes. O processo de reparo se inicia através da absorção direta da energia dos fótons da radiação incidente pelo cromóforo antena, o que leva a transferência de um elétron para o FAD que assume uma forma instável e reduzida, atingindo um estado energeticamente excitado ($FADH^{-}$*). O elétron é então transferido para as ligações covalentes que formam os dímeros de pirimidina na fita de DNA. Como consequência da transferência de elétron, as ligações covalentes são desfeitas, reestruturando as bases pirimidínicas adjacentes e as ligações de

hidrogênio entre as bases nitrogenadas, resultando na integridade do material genético (Figura 3) (SANCAR, 1993; SANCAR, 2008; LIU, WANG, ZHONG, 2015; TERAI *et al*., 2020).

Figura 3 - Representação esquemática do reparo de dímeros de pirimidina por fotoliases.

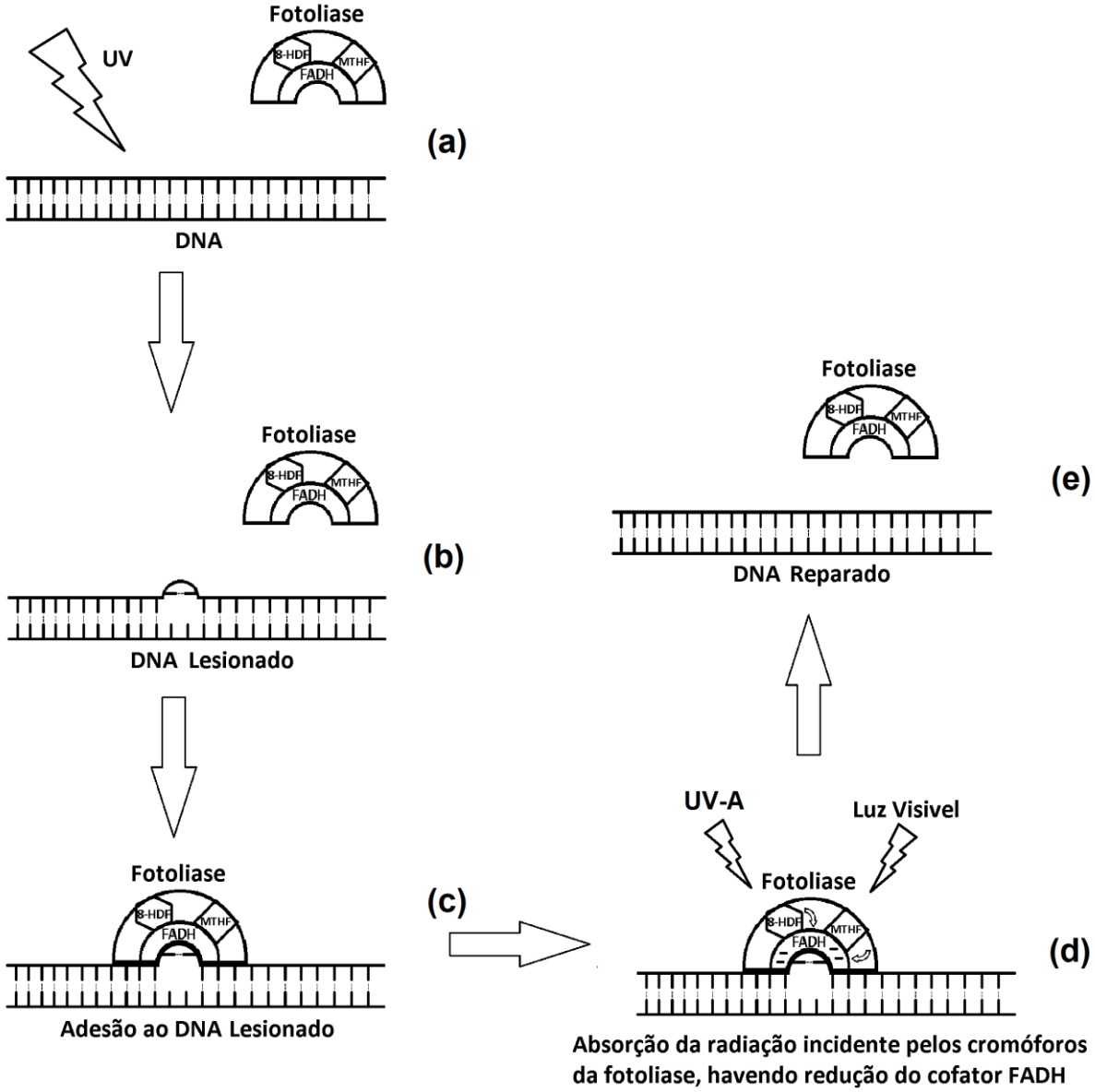

Legenda: incidência da radiação ultravioleta no DNA (a) seguido da formação do dímero de pirimidina que gera uma alteração conformacional na fita de DNA (b) com posterior reconhecimento da enzima fotoliase (c) que absorve radiações na faixa do Ultravioleta A, violeta e azul pelos cromóforos antenas, gerando uma redução do cofator FADH e transferência de um elétron para as ligações covalentes na lesão (d) como resultado, a lesão é desfeita e a fita de DNA é restaurada (e).

Fonte: O autor, 2023.

Por outro lado, tem sido sugerido efeitos bactericidas das radiações violeta e azul. De fato, a luz azul inativa tanto bactérias gram-positivas quanto gram-negativas em altas doses (FUKUI *et al*., 2008; FERRER-ESPADA *et al*., 2019; DOS-ANJOS *et al*., 2020). Os efeitos bactericidas da luz violeta e azul nas bactérias se deve a absorção dos fótons dessas radiações por cromóforos endógenos, como as porfirinas, que leva à produção de espécies reativas de oxigênio (EROs) e ao estresse oxidativo, culminando na morte celular. (ZHANG *et al*, 2013; GOMEZ *et al*, 2015; YOSHIDA *et al*, 2017). Entretanto, apesar das radiações violeta-azul serem propostas como agentes bactericidas, o uso dessas radiações emitidas por LEDs de baixa potência em baixas fluências poderiam aumentar a resistência bacteriana contra a radiação UV devido ao aumento da ação das fotoliases.

1.2.2 Criptocromos

Os criptocromos foram inicialmente identificados em *Arabidopsis thaliana* e a sua função foi associada com o alongamento do hipocótilo, de maneira dependente da luz azul e posteriormente outros estudos demonstraram a presença desse gene em diversas plantas desempenhando diferentes processos de crescimento e desenvolvimento vegetal. (AHMAD, CASHMORE, 1996; CHAVES *et al*., 2011.). Os criptocromos são ortólogos as fotoliases e apresentam em sua estrutura, de forma conservada, o cofator catalítico FAD e o cromóforo antena MTHF, entretanto não apresenta função de reparo do DNA (KAVAKLI *et al*., 2017).

Em animais, incluindo os seres humanos, os criptocromos atuam como repressor transcricional (feedback negativo), regulando o relógio circadiano em nível molecular junto com diversas outras proteínas em *loops* de feedback positivo e negativo ao longo de um período aproximado de 24 horas (SANCAR *et al*., 2010; MASRI, KINOUCHI, SASSONE-CORSI, 2015; KAVAKLI *et al*., 2017). Todas as células de um mamífero apresentam um relógio circadiano próprio que são sincronizados por um "relógio central" ou "relógio mestre". As células que compõe esse "relógio mestre" estão localizadas no núcleo supraquiasmático, estrutura presente na porção anterior do hipotálamo e acima do quiasma óptico, recebendo estímulos de claro e escuro (dia e noite) e assim desencadeando sinais humorais e neurais para sincronizar os relógios periféricos (SANCAR, 2004).

Aproximadamente 50% dos genes de uma célula são expressos ritmicamente, modulando processos fisiológicos e metabólicos, esses genes são designados como "genes

controlados por relógio" (CHAN, LAMIA, 2020). Os genes responsáveis pelo controle circadiano são *BMAL1*, *CLOCK*, *PER1*, *PER2*, *PER3*, *CRY1* e *CRY2*. Os genes *BMAL1* e *CLOCK*, codificam proteínas que formam heterodímeros (BMAL1-CLOCK) que se ligam à promotores (CACGTG) no núcleo atuando como fatores de transcrição de diversos genes estimulando sua expressão, dentre esses genes, estão aqueles que codificam as proteínas período (PER1, PER2 e PER3) e os criptocromos (CRY1 e CRY2). As proteínas período e criptocromos se acumulam no citoplasma onde formam heterodímeros (PER-CRY) que migram para o núcleo e atuam como repressores transcricionais de BMAL1-CLOCK e assim reduzindo a concentração das proteínas controladas por relógio, incluindo as proteínas período e criptocromos até reiniciar todo o ciclo (Figura 4) (KAVAKLI *et al*., 2017; SHAFI, KNUDSEN, 2019; CHAN, LAMIA, 2020).

Figura 4 - Representação esquemática da regulação dos genes circadianos.

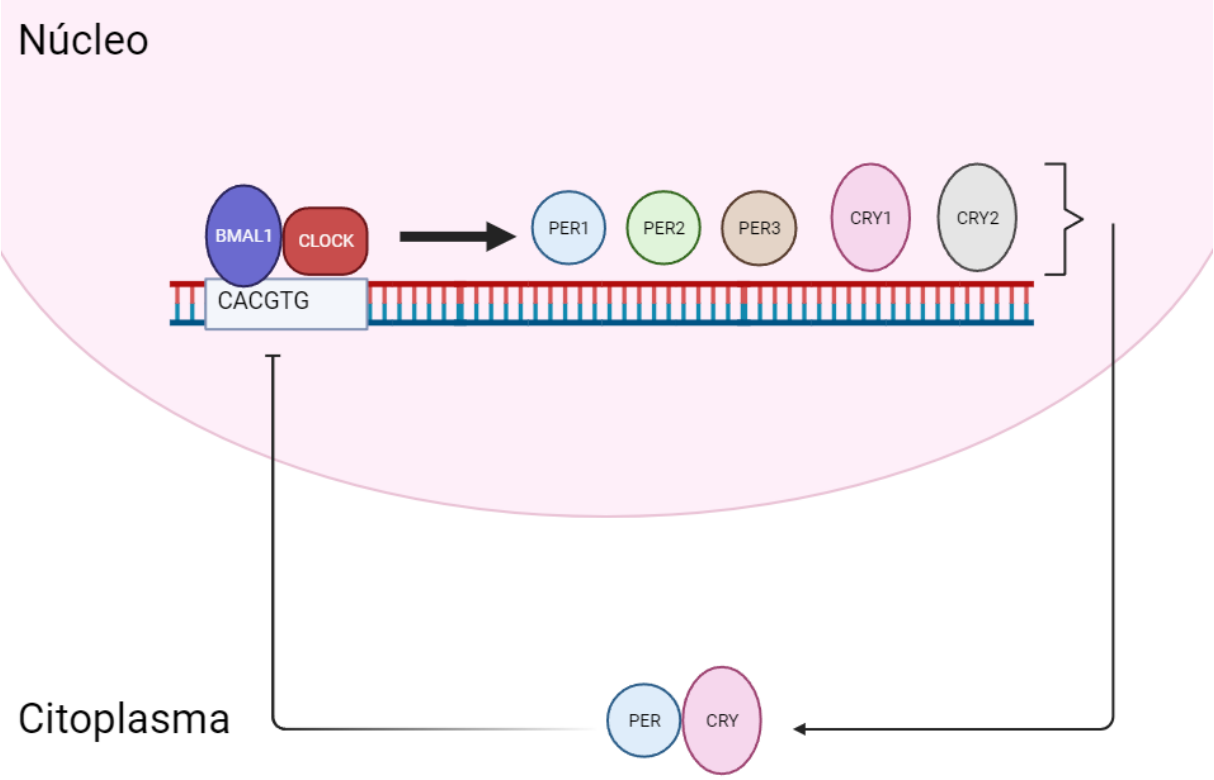

Legenda: As proteínas BMAL1 e CLOCK formam heterodímeros (BMAL1-CLOCK) que se associam a promotores no DNA estimulando a expressão de PER1, PER2, PER3, CRY1 e CRY2. Essas proteínas formam heterodímeros no citoplasma (PER-CRY) que inibem BMAL1-CLOCK reduzindo a expressão de outras proteínas. Até reiniciar o processo.

Fonte: O autor, 2023.

As proteínas período e criptocromos também estão envolvidos em outros processos além da regulação do ritmo circadiano. Essas proteínas também estão associadas fortemente com o reparo de danos no DNA, controle do ciclo celular, em especial em *checkpoints* (G1/S e G2/M), apoptose. Dada a relevância desses genes em diversos processos biológicos, já foi relatado que alterações nesses genes circadianos contribuem para a agressividade de diferentes tumores, tais como: linfomas, gliomas, próstata, mama, ovário e pâncreas (SANCAR *et al*., 2010; MASRI, KINOUCHI, SASSONE-CORSI, 2015; SHAFI, KNUDSEN, 2019).

Embora já esteja bem descrita a função de *CRY1* e *CRY2* como reguladores circadianos, ainda não foram avaliados os efeitos de radiações emitidas por *lasers* e LEDs de baixa potência na expressão desses genes. Por apresentar regiões conservadas em sua estrutura bioquímica como o cromóforo de luz azul FAD e MTHF, essa proteína apresenta a capacidade de absorver fótons na faixa do violeta-azul (400-500 nm) (Figura 5) (LIN, TODO, 2005). Entretanto não há estudos demonstrando se há alteração no perfil de expressão de proteínas circadianas após exposição ao *laser* e LED de baixa potência.

Figura 5 - Estrutura cristalográfica do Criptocromo.

Fonte: NCBI, 2023.

1.2.3 Criptocromos DASH

Os criptocromos DASH (*Drosophila, Arabidopsis, Synechocysstis, human (DASH)-type cryptochrome* (CRY)) também pertencem à família das flavoproteínas, encontrada em bactérias, algas, plantas e animais (BRUDLER *et al*., 2003). Essas proteínas apresentam semelhanças filogenéticas com as fotoliases, sendo inicialmente classificadas como criptocromo pois até então não apresentavam atividade de fotoliases que pudesse ser identificada *in vitro* ou *in vivo* pelo ensaio de complementação de fotoliases (HITOMI *et al*., 2000; WORTHINGTON *et al*., 2003; ASIMGIL, KAVAKLI, 2012). Entretanto, estudos mais recentes demonstram que o CRY-DASH apresenta função de fotoliases através do reparo de dímeros de pirimidina em fitas simples de DNA em vez de fita dupla, sendo designados como fotoliases de fita simples (SELBY, SANCAR, 2006; TAGUA *et al*, 2015).

1.3 **Câncer e os genes circadianos**

Nos últimos anos, evidências crescentes vêm sugerindo uma associação entre genes circadianos e o desenvolvimento e progressão de diversos tipos de tumores (CHEN, *et al*., 2005; OSHIMA *et al*., 2011; RAHMAN *et al*., 2019; DONG *et al*., 2019). Uma das relações dos genes circadianos com o câncer é sua participação em processos de reparo do DNA por excisão de nucleotídeos, onde a expressão da proteína XPA, XPC, TP53, ERCC6 e RPA3 é controlada por genes do relógio circadiano (KANG *et al*., 2010, KORITALA *et al*, 2021) e mutações nesses genes podem desencadear uma instabilidade genômica.

Os genes circadianos também controlam a expressão da proteína c-MYC, responsável por promover a proliferação celular. Em células com os genes *BMAL1* e *PER2* mutantes, há uma super-expressão dessa proteína contribuindo para uma maior incidência em linfomas induzidos por radiação (FU *et al*., 2002). O gene *CDKN1A*, que codifica a proteína p21 também é regulado por BMAL::CLOCK, sendo esse gene importante para a manutenção do *checkpoint* G1/S durante o ciclo celular. A regulação negativa desses genes pode induzir a parada do ciclo celular e apoptose em células tronco de glioblastomas, (GRÉCHEZ-CASSIUAU *et al*., 2008, DONG *et al*, 2019). Estudos reforçaram a hipótese desse mecanismo e sugeriram o *Jetlag* como

agravante no desenvolvimento de adenocarcinoma de pulmão (PAPAGIANNAKOPOULOS *et al*, 2016).

Além da regulação no reparo do DNA e ciclo celular, os genes circadianos também têm sido relacionados a processos apoptóticos, onde as proteínas *CRY1* e *CRY2* participam da via extrínseca da apoptose regulando a síntese de TNFα envolvida no processo inflamatório. A ausência desses genes contribui para uma maior expressão de TNFα (HASHIRAMOTO *et al*., 2010, CHAN, HUBER, LAMIA, 2020).

Em relação ao câncer de mama, estudos demonstraram a relação entre distúrbios nos genes circadianos e a progressão deste tipo de tumor (BLAKEMAN *et al*., 2016). Os genes *PER1* e *PER2* desempenham funções de supressão de tumor. As alterações encontradas para os genes *PER1* e *PER2* foram associados à progressão ciclo celular, aumentando a proliferação e redução da apoptose, aumentando a sobrevivência (GERY, KOEFFLER, 2018). Além das proteínas PER2 e BMAL1 estarem envolvidas na formação dos ácinos mamários (ROSSETTI *et al*., 2012).

Ainda não foi verificado se radiações emitidas por LEDs e *lasers* de baixa potência interferem ou influenciam na expressão de genes circadianos e como isso poderia ocorrer em células tumorais. Além disso, os criptocromos podem participar como potencial alvo em terapias baseadas na fotobiomodulação induzida por estes LEDs e *lasers* devido a sua homologia com as fotoliases que dependem da luz para sua ativação.

Devido as fotoliases e os criptocromos serem ortólogos, pertencentes à mesma família de flavoproteínas e apresentar os fotoaceptores conservados evolutivamente, estas proteínas podem ser alvos para terapias baseadas na fotobiomodulação. O estudo da participação das fotoliases na fotobiomodulação pode ampliar a compreensão dos mecanismos de resistência à radiação ultravioleta em procariotos. Da mesma forma, o estudo da participação dos criptocromos na fotobiomodulação pode ampliar a compreensão deste efeito na apoptose, no ciclo celular e mecanismos de reparo do DNA em células tumorais.

2 **OBJETIVOS**

2.1 **Objetivo geral**

Avaliar os efeitos do *laser* vermelho (658 nm) e LED azul (470 nm) terapêuticos de baixa potência nos genes da família das flavoproteínas através de modelos procarióticos e eucarióticos.

2.2 **Objetivos específicos**

Avaliar os efeitos da radiação emitida por *laser* vermelho e LED azul na(os):

a) Indução de lesões no DNA plasmidial;
b) Viabilidade celular em culturas de *Escherichia coli* expostas à radiação ultravioleta C;
c) Área das colônias de *Escherichia coli* expostas à radiação ultravioleta C;
d) Níveis de mRNA do gene *phr* em células de *Eshcerichia coli*;
e) Viabilidade celular em culturas de células MCF-7 e MDA-MB-231;
f) Níveis de mRNA dos genes *BMAL1*, *CLOCK*, *PER1*, *PER2*, *PER3*, *CRY1* e *CRY2* em células MCF-7 e MDA-MB-231.

3 **MATERIAIS E MÉTODOS**

3.1 **Fontes de radiação**

Foram utilizados um *laser* terapêutico vermelho (658 ± 5 nm) e LED azul (470 ± 10 nm) de baixa potência presentes em um cluster comprado na HTM eletrônica (Fluence, São Paulo, Brasil). O *laser* vermelho se encontra ao centro do cluster e os 3 LEDs ficam posicionados pelo cluster formando um triângulo equilátero. O *laser* foi usado em modo de emissão contínuo com potência de 10 mW nas fluências de 3 e 9 J/cm² correspondente aos tempos de 30 e 90 segundos, respectivamente. Os LEDs azuis também foram usados em modo de emissão contínuo, com potência de 1500 mW nas fluências 160 e 640 J/cm² correspondente aos tempos de 30 e 90 segundos, respectivamente. Também foi utilizado uma lâmpada UVC (Philips, Holanda), com potência de 500 mW na fluência de 50 mJ/cm².

3.2 **Eletroforese do plasmídeo pUC19 após exposição ao *laser* e LEDs de baixa potência**

3.2.1 Eletroforese em gel de agarose

Amostras do plasmídeo pUC19 (New England Biolabs, EUA) (aproximadamente 200 ng) foram expostos ao *laser* vermelho (3 e 9 J/cm²), ao LED azul (160 e 640 J/cm²) e simultaneamente ao *laser* vermelho e ao LED azul (3 + 160 J/cm² e 9 + 640 J/cm²). O cluster *laser*-LED foi posicionado a 7 cm acima das amostras de plasmídeo, de forma que a irradiação incidisse toda a alíquota. Cada amostra de plasmídeo foi misturada com o tampão de carregamento, gelred (Promega, EUA) e água ultrapura, para então ser aplicada no gel de agarose 0,8%, pH 7,4 (Kasvi, Espanha). O marcador de peso molecular utilizado foi o *ladder* (100 pares de bases) (Thermoscientific, Lituânia). O procedimento da eletroforese foi realizado em cuba horizontal contendo TAE 1x (90V, 400 mA, 120W, 70 min).

3.2.2 Fotodocumentação e análise

As formas topológicas do plasmídeo obtidas pela eletroforese foram visualizadas através de um sistema transiluminador de LED azul (Kasvi, Brasil). Os géis foram fotografados (Xiomi redmi note 9, China) e as formas plasmidiais topológicas foram analisadas através da densitometria de bandas utilizando o programa de computador ImageJ (https://imagej.nih.gov/ij/).

3.3 **Cultura bacteriana**

3.3.1 Cepa e cultura bacteriana

Foi utilizada a cepa de *Escherichia coli* C600 (*E. coli* C600), proficiente em mecanismos de reparo do DNA. Os estoques de *E. coli* C600 eram mantidos em freezer (-20°C). Alíquotas de 100 µL foram utilizados para fazer os pernoites em 5 ml de meio nutritivo Luria-Bertani (Kasvi, Brasil) e encaminhados para estufa bacteriológica (De Leo, Brasil) até atingir a fase estacionária de crescimento (37°C, 18 h, 10^{10} células/ml).

3.3.2 Exposição das culturas de *E. coli* ao *laser* e ao LED

Culturas de *E. coli* C600 em fase estacionária de crescimento foram divididos em dois grupos. O primeiro grupo foi exposto de forma individual ao *laser* vermelho (3 e 9 J/cm²), ao LED azul (160 e 640 J/cm²) e simultaneamente ao *laser* vermelho e ao LED azul (3 + 160 J/cm² e 9 + 640 J/cm²). O segundo grupo foi pré-exposto ao *laser* vermelho e ao LED azul nas mesmas condições do primeiro grupo, seguido de uma exposição única à radiação UVC na fluência de 50 mJ/cm² (Figura 6). Como controles, suspensões bacterianas não irradiadas, ou irradiadas somente com UVC. O tempo de exposição ao *laser* e ao LED foi controlado automaticamente

pelo equipamento de acordo com as fluências utilizadas. A fluência da lâmpada de UVC foi mensurada com um radiômetro de ultravioleta (Instrutherm, Brasil), e o tempo de irradiação foi de 100 segundos. O cluster *laser*-LED, assim como a lâmpada de UVC, foi posicionado a 7 cm acima das suspensões bacterianas, de forma que a irradiação incidisse toda a superfície das alíquotas.

Figura 6 - Representação esquemática das irradiações das culturas de *E. coli* C600.

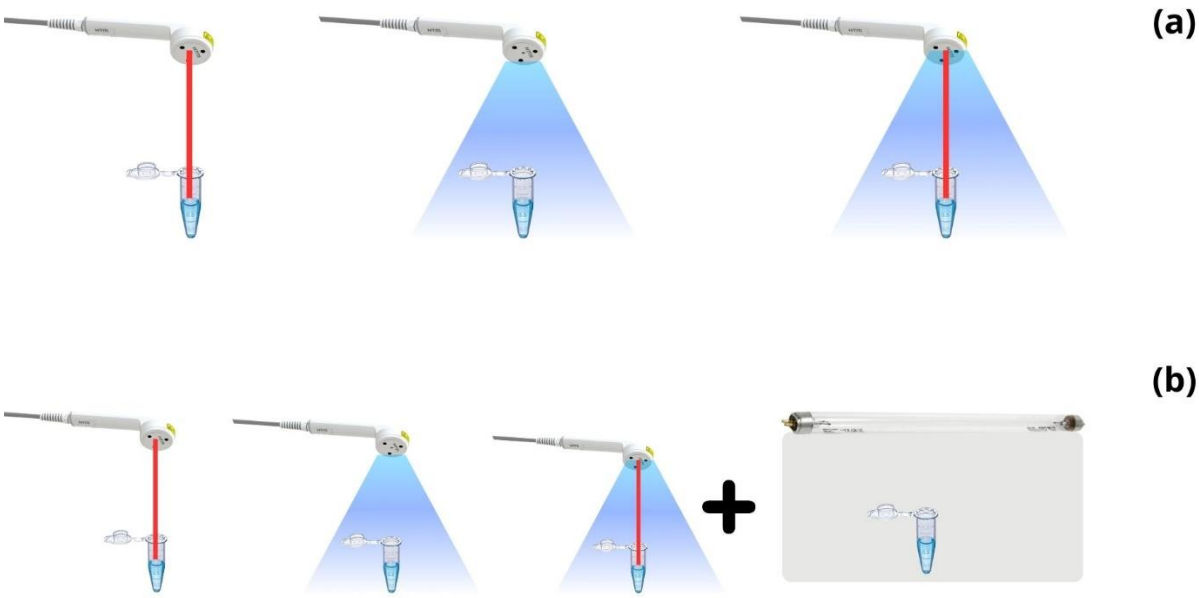

Legenda: Grupo 1: Células de *E. coli* C600 expostas ao *laser* vermelho de baixa potências nas fluências de 3 e 9 J/cm², LED azul de baixa potência nas fluências de 160 e 640 J/cm² e *laser* vermelho e LED azul simultâneos nas fluências 3 + 160 J/cm² e 9 + 640 J/cm² (a). Grupo 2: Células de *E. coli* C600 pré-expostas ao *laser* vermelho, LED azul e *laser* vermelho e LED azul simultâneos nas mesmas fluências do grupo 1, seguido pela exposição a uma dose única de 50 mJ/cm² de radiação ultravioleta C (b). Todas as amostras foram irradiadas a uma distância de 7 cm da saída de radiação do equipamento *laser*/LED.

Fonte: O autor, 2023.

3.4 **Ensaio de viabilidade e proliferação em culturas de *E. coli* C600**

3.4.1 Ensaio de viabilidade e proliferação em culturas de *E. coli* C600

Culturas de *E. coli* C600 em fase estacionária de crescimento (5 ml, n=8) foram centrifugadas (3.000 RPM, 15 min) e suspensas duas vezes em solução salina estéril (NaCl 0,9%). Alíquotas (300 µL) foram divididas de acordo com os grupos de tratamento e então irradiadas. Após o tratamento, as suspensões bacterianas foram diluídas em salina estéril, alíquotas (10 µL) espalhada em placas de *Petri* contendo meio nutritivo Luria-Bertani (Kasvi, Itália) e ágar bacteriológico (HiMedia, Índia) incubados em estufa bacteriológica (37°C, 18h). Após incubação, as placas foram fotografadas (Xiomi redmi note 9, China) para avaliação da sobrevivência e proliferação bacteriana.

3.4.2 Avaliação da viabilidade e proliferação em culturas de *E. coli* C600

As unidades formadoras de colônias (UFC) geradas após o tratamento e incubação foram contadas e a fração de sobrevivência (FS) foi calculada pela razão entre número de colônias viáveis após tratamento e o número de colônias viáveis sem tratamento (controle).

Para avaliação da proliferação bacteriana, a área das colônias (em mm²) foi mensurada pelo programa de computador ImageJ e a fração de área foi calculada pela razão entre a área das colônias das células tratadas e a área das colônias das células não tratadas (controle).

3.5 **Avaliação dos níveis de mRNA do gene *phr***

3.5.1 Procedimento experimental e parâmetros do tratamento

Culturas de *E. coli* C600 em fase estacionária de crescimento (10^{10} células/ml, 18h, 37°C) foram centrifugadas (3000 RPM, 15 min) e suspensas duas vezes em solução salina estéril (NaCl 0,9%). Alíquotas de suspensões bacterianas (400 µL) foram expostas ao *laser* vermelho (9 J/cm²), LED azul (640 J/cm²) e *laser* vermelho + LED azul (9 + 640 J/cm²) a uma distância de 7 cm entre a fonte e as amostras. Como grupo controle, suspensões bacterianas não expostas ao *laser* vermelho e ao LED azul.

3.5.2 Extração de RNA total

Após o tratamento, o RNA total das bactérias foi extraído com kit de extração de mRNA (TRIzol^{tm}, Invitrogen, EUA) e purificado com kit de purificação (kit de purificação de RNA, Invitrogen, EUA). A suspensão bacteriana de cada microtubo foi brevemente incubada com solução de lise celular (200 µL, 95°C, 2 min), em seguida adicionado o reagente TRIzol (1 ml), homogeneizado e incubado (5 min, temperatura ambiente). Foi adicionado clorofórmio (200 µL), homogeneizado, incubado (1 min, temperatura ambiente) e as preparações foram então centrifugadas (13.000 RPM, 15 min, 4°C) para separar a fase orgânica da fase aquosa. Os sobrenadantes foram transferidos para outros tubos e então adicionado isopropanol (500 µL) e incubados (15 min, temperatura ambiente), as preparações foram centrifugadas (13.000 RPM, 30 min, 4°C), o sobrenadante descartado e o precipitado foi lavado com etanol-DEPC (80% etanol, DEPC 0,1% em água) e novamente centrifugado (13.000 RPM, 15 min, 4°C). O sobrenadante foi removido e o RNA total foi suspenso (15 µL) em solução aquosa de DEPC (0,1%) para então ser quantificada. Para determinar a concentração de RNA e pureza, foi usado um espectrofotômetro (Avantor, EUA) para calcular a razão de densidade óptica através da absorbância das preparações nos comprimentos de onda 230, 260 e 280 nm.

3.5.3 Síntese de cDNA e cadeia da polimerase quantitativa em tempo real

A síntese do DNA complementar (cDNA) foi realizada com kit de síntese de cDNA (Promega, EUA) em duas etapas. A primeira etapa consistiu em tratamento com DNAse e a segunda etapa com a transcriptase reversa (GoScript) e outros reagentes (oligoDT, dNTPs e $MgCl_2$) seguindo o protocolo do fabricante. O total da reação gerou um volume de 20 µL de cDNA das culturas bacterianas.

A reação em cadeia da polimerase quantitativa em tempo real (RT-qPCR) foi realizada em um termociclador rotor gene (Qiagen, Holanda) usando 2,5 µL de cDNA e 7,5 µL de mix contendo água livre de RNAse (2 µL), o primer de interesse (0,5 µL) e *sybr green* (5,0 µL) (Promega, USA), totalizando um volume de 10 µL em cada tubo de reação. Como genes de referência foram usados *araC*, *rpoA*, *gyrA* (TEIXEIRA *et al*., 2016). O gene de interesse foi o *phr* (fotoliase de *E. coli*) (Tabela 1).

Tabela 1 - Sequências de primers utilizados para a técnica de RT-qPCR com cDNA das células de *Escherichia coli*.

Gene	**Sequência**	**Tm (°C)**
araC	F: 5’ – CGCTGACAGTACCCAGATTC - 3’	62.8
	R: 5’ – CTCGAAATCGGTGCAGATGA - 3’	66.7
rpoA	F: 5’ - CTTCCAGTTGTTCAGCCAGA - 3’	63.5
	R: 5’ - GTGGAGCGTATTGCCTACAA - 5’	63.1
gyrA	F: 5’ – CAGATTTACCTTTCCCGCCA - 3’	66.2
	R: 5’ – CGTCGTACTGAAATCACCG - 3’	62.3
phr	F: 5’- ACAACCCAGGGCGAGAAATT – 3’	57.2
	R: 5’- TCGCTTCTTTGTGCTCGACT – 3’	56.8

3.6 **Cultura de células de tumor de mama**

3.6.1 Linhagens celulares

Foram utilizadas as linhagens MCF-7 e MDA-MB-231. A linhagem MCF-7 é um tipo de célula epitelial derivada de um adenocarcinoma de mama que apresenta receptores de estrógeno, progesterona e glicocorticoides (CAMARILLO *et al*., 2014; COMSA, CÎMPEAN, RAICA, 2015). A linhagem MDA-MB-231 é um tipo de célula epitelial derivada de um adenocarcinoma de mama em estado metastático. É uma linhagem dita como “triplo negativa” onde ela não apresenta receptores estrógeno, progesterona e HER2 (Receptor do fator de crescimento epidérmico humano, tipo 2) sendo altamente agressiva, invasiva e pouco diferenciada (HUANG, YU, TANG, 2020).

3.6.2 Culturas de MCF-7 e MDA-MB-231

As células das linhagens MCF-7 e MDA-MB-231 foram cultivadas em meio DMEM e RPMI, respectivamente, suplementados com 10% de soro fetal bovino e 1% de

antibiótico/antimicótico (Gibco, EUA) em frascos de cultura celular de 75 cm² com filtro (Corning, EUA) e incubadas em estufa celular (48h, 37°C, 5% CO_2) até atingir uma confluência aproximada de 60-70%.

3.7 **Avaliação da viabilidade celular das culturas de células de tumor de mama**

3.7.1 Procedimento experimental, parâmetros de irradiação e ensaio de WST-1

Culturas de células MCF-7 e MDA-MB-231 cultivadas em frascos de 75 cm² foram lavadas 2 vezes com tampão PBS (*Phosphate buffered* saline), adicionada tripsina (0,25%) e então incubadas em estufa de cultivo celular (37°C, 5% CO_2, 2 min). Para inativar a tripsina, foi adicionado 5 ml de meio DMEM (para MCF-7) e RPMI (para MDA-MB-231) nos frascos e então o conteúdo foi transferido para um tubo falcon (15 ml). O conteúdo foi então centrifugado (3.000 RPM, 3 min) e lavadas duas vezes com tampão PBS e o sobrenadante foi descartado. Em seguida, foi realizada a contagem de células na câmara de Neubauer. As células foram então suspendidas em meio DMEM e RPMI em tubo falcon (15 ml) e aliquotadas 1,8 ml de solução com células em 4 microtubos (2 ml), em seguida centrifugados (3.000 RPM, 3 min). Os 4 microtubos foram referentes aos tratamentos com *laser* vermelho (9 J/cm²), LED azul (640 J/cm²), *laser* vermelho + LED azul (9 + 640 J/cm²) e controle (não irradiado). As fluências foram selecionadas de acordo com resultados preliminares encontrados por outros pesquisadores do mesmo grupo de pesquisa (Dados não publicados). O cluster *laser*-LED, foi posicionado a 7 cm acima das suspensões de células, de forma que a radiação incidisse sobre toda a superfície das alíquotas. Após a centrifugação, o sobrenadante foi descartado e a irradiação realizada. As células foram então suspensas em meio DMEM e RPMI e aliquotadas 150 µL de suspensão celular em 3 poços para cada tratamento, totalizando 12 poços em uma placa de 96 poços. Para cada experimento, foram utilizadas 3 placas referentes aos tempos de avaliação da viabilidade celular (24, 48 e 72 horas). Em seguida, as suspensões de células foram distribuídas nas placas e incubadas em estufa celular (37°C, 5% CO_2).

3.7.2 Aferição da absorbância do reagente

Após a incubação durante os períodos de 24, 48 e 72 horas, foi adicionado o reagente WST-1 aos poços contendo as células e incubadas em estufa de cultivo celular (37°C, 5% CO_2) durante 1-2 horas. Após esse período a placa foi posta em um leitor de ELISA (Celer, Brasil) para aferição da absorbância em 405, 450, 492 e 630 nm e cálculo da viabilidade celular.

3.8 **Avaliação dos níveis relativos de mRNA dos genes circadianos**

3.8.1 Escolha dos genes para estudo

Para esse estudo foram selecionados os genes *BMAL1* (*Basic helix-loop-helix ARNT like 1*), *CLOCK* (*Clock circadian regulator*) que estão relacionados com a expressão dos genes *PER1*, *PER2*, *PER3* (*Period circadian regulator 1, 2 e 3*), bem como, *CRY1* e *CRY2* (*Cryptochrome circadian regulator 1 e 2*). Esses genes fazem parte do relógio circadiano central (MOHAWK, GREEN, TAKAHASHI, 2012) sendo responsáveis pelo controle da expressão de diversos genes associados ao reparo de DNA, apoptose, ciclo celular e metabolismo celular (SHAFI, KNUDSEN, 2019).

3.8.2 Procedimento experimental e parâmetros de irradiação

Culturas de células de MCF-7 e MDA-MB-231 foram realizadas em frascos de 75 cm^2, foram lavadas 2 vezes com tampão PBS 1x (*phosphate buffered* saline), adicionada tripsina (0,25%) e então incubadas em estufa de cultivo celular (37°C, 5% CO_2, 2 min). Para inativar a tripsina, foram adicionados 5 ml de meio DMEM (para MCF-7) e RPMI (para MDA-MB-231) nos frascos e então o conteúdo foi transferido para um tubo falcon (15 ml). O conteúdo foi então centrifugado (3.000 RPM, 3 min) e o sobrenadante foi descartado e os precipitados celulares

foram suspensos duas vezes com tampão PBS. As células foram suspensas em 4 ml de meio DMEM e RPMI e distribuídas para 4 microtubos (1,5 ml) referentes aos tratamentos com *laser* vermelho (9 J/cm²), LED azul (640 J/cm²), *laser* vermelho + LED azul (9 + 640 J/cm²) e controle (não irradiado). As fluências foram selecionadas de acordo com resultados preliminares encontrados por outros pesquisadores do mesmo grupo de pesquisa (Dados não publicados). Para a irradiação, o cluster *laser*-LED foi posicionado a 7 cm acima das suspensões de células, de forma que a radiação incidisse sobre toda a superfície das alíquotas. As suspensões foram centrifugadas (7.200 RPM, 2 min) e o sobrenadante descartado. As células foram irradiadas em seguida adicionado meio DMEM e RPMI (1 ml) e homogeneizado. As células irradiadas foram então transferidas para frascos de cultura de células de 25 cm² contendo o meio das respectivas células (4 ml) e incubadas em estufa de cultivo celular (37°C, 5% CO_2, 48h).

3.8.3 Extração de RNA total

Após a irradiação, o RNA total das células tumorais de mama MCF-7 e MDA-MB-231 foram extraídos com kit de extração de mRNA (TRIzol^{tm}, Invitrogen, EUA). Os meios foram descartados e os frascos de cultura celular, lavadas com tampão PBS. O excedente de PBS foi removido e então adicionado reagente TRIzol (1 ml) nos frascos de cultura celular de 25 cm², homogeneizado e incubado (5 min, temperatura ambiente). Após a lise das células, a solução foi adicionada em um microtubo (1,5 ml) e então centrifugada (13.000 RPM, 10 min, 4°C) e seu sobrenadante transferido para outro microtubo (1,5 ml). Em seguida, foi adicionado clorofórmio (200 µL), homogeneizado e incubado (1 min, temperatura ambiente) e as preparações foram então centrifugadas (13.000 RPM, 15 min, 4°C) para separar a fase orgânica da fase aquosa. Os sobrenadantes foram transferidos para outros microtubos e adicionados isopropanol (500 µL) e incubados (15 min, temperatura ambiente), as preparações foram centrifugadas (13.000 RPM, 30 min, 4°C), o sobrenadante descartado e o precipitado foi lavado com etanol-DEPC (80% etanol, DEPC 0,1% em água) e novamente centrifugado (13.000 RPM, 15 min, 4°C). O sobrenadante foi removido e o RNA total foi suspendido (15 µL) em solução de água tratada com DEPC (0,1%) para então ser quantificada. Para aferir a concentração de RNA e pureza, foi usado um espectrofotômetro (Avantor, EUA) para calcular a razão de

densidade óptica através da absorbância das preparações nos comprimentos de onda 230, 260 e 280.

3.8.4 Síntese de cDNA e RT-qPCR a partir do mRNA das culturas de células MCF-7 e MDA-MB-231

A síntese do DNA complementar (cDNA) foi realizada com kit de síntese de cDNA (Promega, EUA) em duas etapas. A primeira etapa consistiu em tratamento com DNAse e a segunda etapa com a transcriptase reversa (GoScript) e outros reagentes (oligoDT, dNTPs e $MgCl_2$) seguindo o protocolo do fabricante. O total da reação gerou um volume de 20 µL de cDNA das culturas de células tumorais de mama MCF-7 e MDA-MB-231.

A reação em cadeia da polimerase quantitativa em tempo real (RT-qPCR) foi realizada em um termociclador rotor gene (Qiagen, Holanda) usando 2,5 µL de cDNA e 7,5 µL de mix contendo água livre de RNAse (2 µL), os primers de interesse (0,5 µL de cada) e *sybr green* (5,0 µL) (Promega, USA), totalizando um volume de 10 µL em cada tubo de reação. Como gene de referência foi utilizado o ACTB (beta actina) (TEIXEIRA, *et al*., 2017).

Tabela 2 - Sequências de primers utilizados para a técnica de RT-qPCR com cDNA das células MCF-7 e MDA-MB-231.

Gene	**Sequência**	**Tm (°C)**
BMAL1	F: 5’ – GGGCTGGATGAAGACAACGA – 3’	57,3
	R: 5’ – GCTAGAAGGCGATGACCCTC – 3’	57,4
CLOCK	F: 5’ – GGGCACAGTCAGCAAACATC – 3’	56,8
	R: 5’ – GTGACTGAGGGAAGGTGCTC – 3’	57,6
PER1	F: 5’ – GCATGAGTCTAGAGGCGCAT – 3’	57,1
	R: 5’ – CCCAGCAGTTCCATTGCCTA – 3’	57,5
PER2	F: 5’ – TTTCACCTCCCCGTACAAGC – 3’	57,3
	R: 5’ – GCCACGAGAATGAAATCCGC – 3’	56,8
PER3	F: 5’ – TCGGAACCTTGCTGTCTCAC – 3’	57,2
	R: 5’ – GAGGAGGAAAAGTGGGAGGC – 3’	57,7
CRY1	F: 5’ – TGGGAATGGAGGCTTCATGG – 3’	57,4
	R: 5’ – AGTGCCCATGGAGCTTCTTC – 3’	57,5

CRY2	F: 5’ – CCCCACTGAAGGACTTGGTC – 3’	57,7
	R: 5’ – CTACACGGCAGCTACCAACA – 3’	57,2

3.9 **Análise estatística**

Dados sobre as formas plasmidiais, fração de sobrevivência, fração de área, expressão dos níveis relativos de mRNA dos genes *phr*, *BMAL1*, *CLOCK*, *PER1*, *PER2*, *PER3*, *CRY1* e *CRY2* e viabilidade celular das células MCF-7 e MDA-MB-231 foram analisados pelo teste de Kolmogorov-Smirnov para verificar a normalidade. A comparação entre os grupos foi feita pelo teste de Kruskal-Wallis seguido do teste de Dunn como *pos-hoc* teste e $p<0,05$ como menor nível significativo. Os testes estatísticos foram feitos pelo programa InStat GraphPad (GraphPad InStat versão 8.0 para Windows 10, GraphPad Prism Software, San Diego, CA, EUA).

4 **RESULTADOS**

4.1 **Perfil eletroforético do plasmídeo pUC19 após exposição ao *laser* vermelho e ao LED azul de baixa potência**

A figura 7 representa a densitometria de bandas plasmidiais e fotografia representativa de géis de agarose após eletroforese do plasmídeo pUC19 exposto ao LED azul e ao *laser* vermelho em diferentes fluências. Dados nesta figura indicam que a exposição ao LED azul e/ou ao *laser* vermelho não é capaz de alterar a mobilidade do plasmídeo bacteriano pUC19, indicando que não houve quebras do tipo simples e dupla no DNA plasmidial. Esses achados foram confirmados pela quantificação da forma topológica superenrolada do plasmídeo pUC19.

Figura 7 – Porcentagem das formas plasmidiais (a) e fotografia representativa do gel de agarose após exposição ao LED azul e ao *laser* vermelho de baixa potência (b).

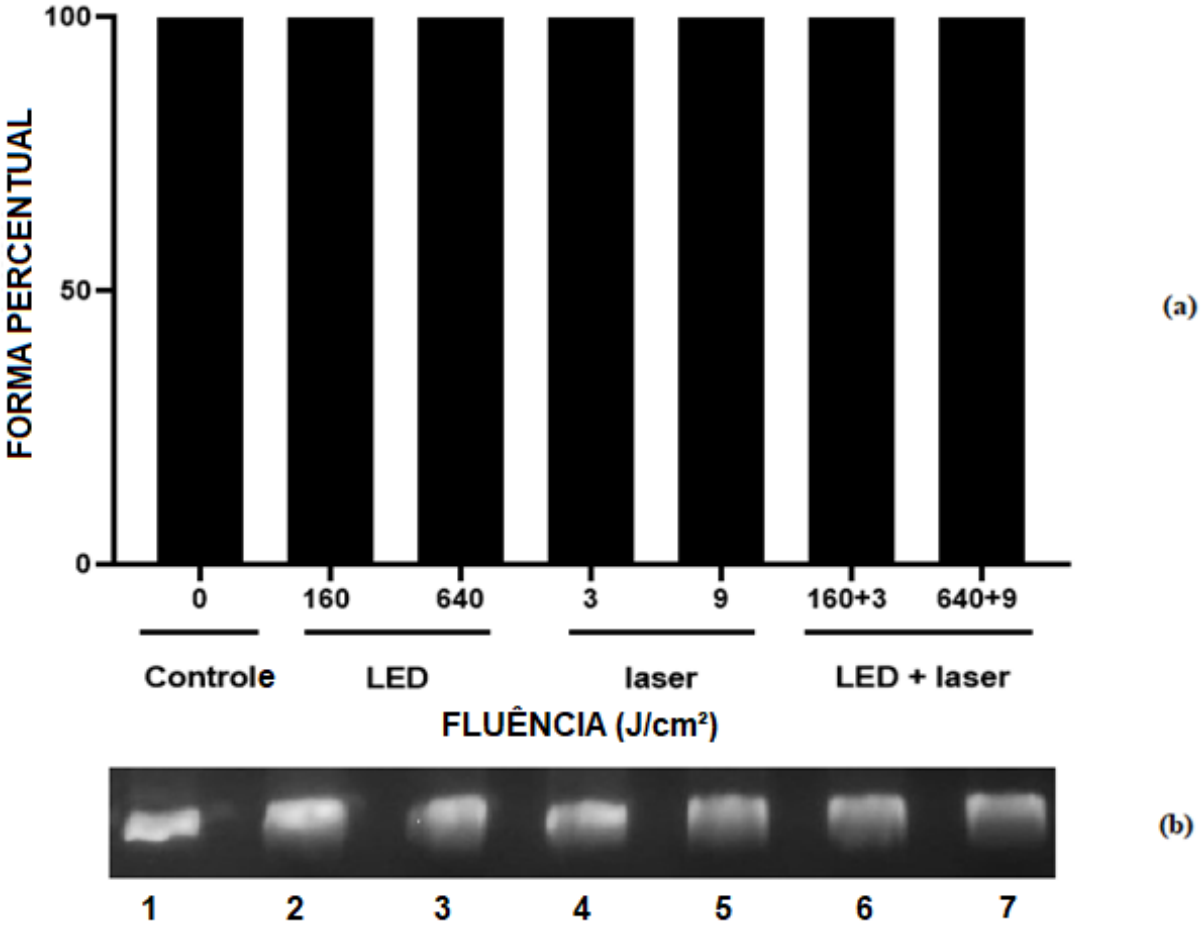

Legenda: Colunas – (1) pUC19 não irradiado, (2) pUC19 + LED azul 160 J/cm², (3) pUC19 + LED azul 640 J/cm², (4) pUC19 + *laser* vermelho 3 J/cm², (5) pUC19 + *laser* vermelho 9 J/cm², (6) pUC19 + LED azul 160 J/cm² + *laser* vermelho 3 J/cm², (7) pUC19 + LED azul 640 J/cm² + *laser* vermelho 9 J/cm².

4.2 **Sobrevivência e proliferação em culturas de *E. coli* C600 após exposição ao LED azul e ao *laser* vermelho de baixa potência**

Na figura 8 estão apresentados os valores da fração de sobrevivência das culturas de *E. coli* C600 expostas ao LED azul e ao *laser* vermelho de baixa potência. Os dados nessa figura sugerem que a exposição aos LED azul e ao *laser* vermelho de baixa potência não alterou significativamente ($p<0,05$) a sobrevivência das culturas de *E. coli* C600 nas fluências avaliadas.

Figura 8 – Frações de sobrevivência das culturas de *E. coli* C600 expostas ao LED azul e ao *laser* vermelho de baixa potência.

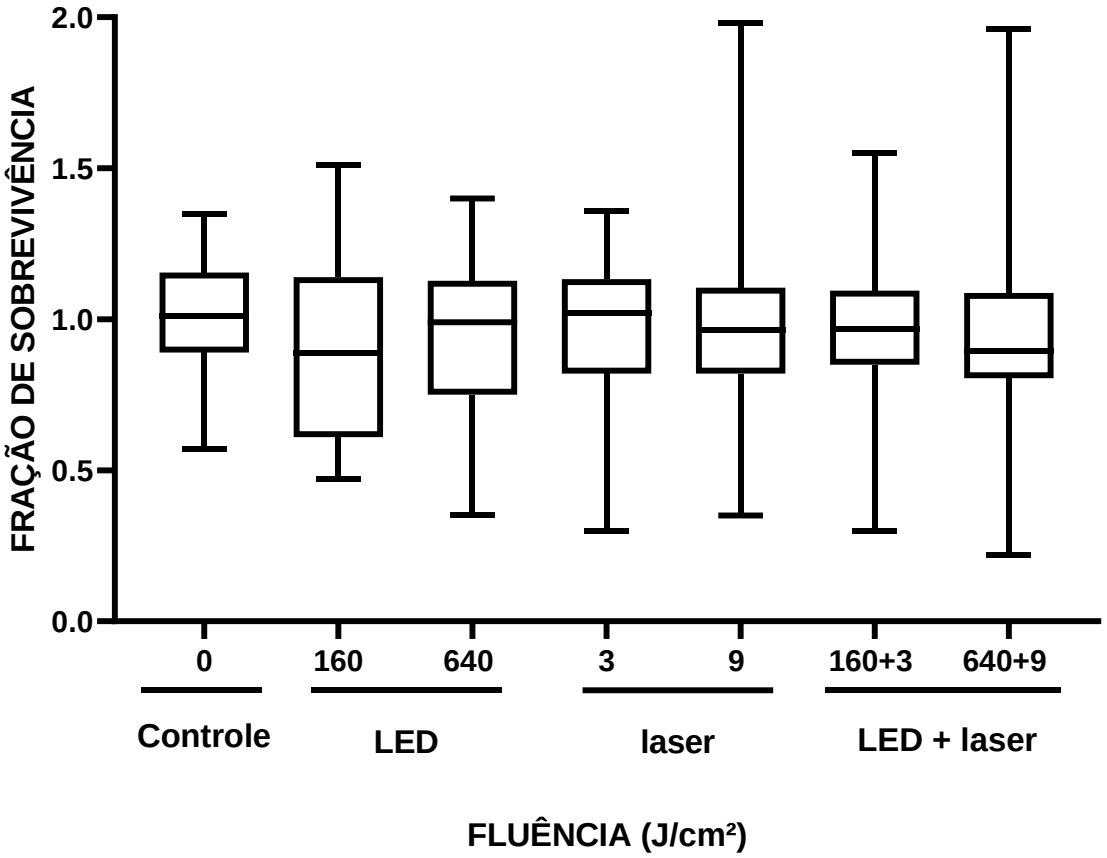

Legenda: N=8. Diagramas de caixa – grupo controle, não irradiado, LED azul 160 J/cm LED azul 640 J/cm², *laser* vermelho 3 J/cm², *laser* vermelho 9 J/cm², LED azul + *laser* vermelho 160 + 3 J/cm², LED azul + *laser* vermelho 640 + 9 J/cm². As barras indicam a amplitude em cada grupo e no gráfico estão as medianas e os quartis.

Na figura 9 estão apresentados a razão de área das colônias das culturas de *E. coli* C600 expostas ao LED azul e ao *laser* vermelho de baixa potência. Na figura 10 estão apresentadas duas fotos representativas de colônias de *E. coli* C600. Os dados nessa figura 9 sugerem que a exposição ao *laser* vermelho nas fluências de 3 e 9 J/cm² reduz significativamente ($p<0,05$) a área das colônias de *E. coli* C600.

Figura 9 – Razão das áreas das colônias das culturas de *E. coli* C600 expostas aos LED azul e ao *laser* vermelho de baixa potência em diferentes fluências

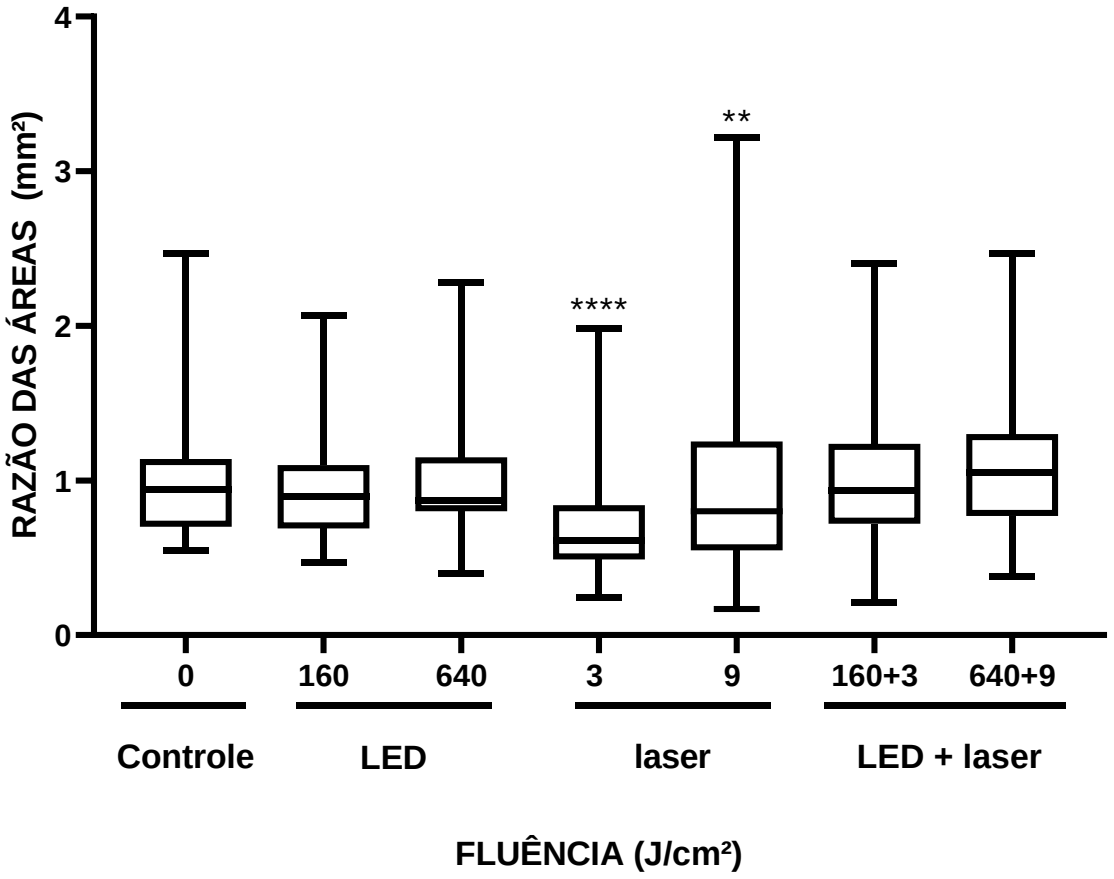

Legenda: N=8. Diagrama de caixa – grupo controle, não irradiado, LED azul 160 J/cm², LED azul 640 J/cm², *laser* vermelho 3 J/cm², *laser* vermelho 9 J/cm², LED azul + *laser* vermelho 160 + 3 J/cm², LED azul + *laser* vermelho 640 + 9 J/cm². As barras indicam a amplitude em cada grupo e no gráfico estão as medianas e os quartis. (****) p<0,0001 quando comparado com a área das colônias do grupo controle (não tratado com LED azul e *laser* vermelho). (**) p<0,001 quando comparado com a área das colônias do grupo controle.

Figura 10 – Fotos representativas das colônias de *E. coli* C600 do grupo controle (a) e grupo irradiado com *laser* na fluência de 3 J/cm² (b).

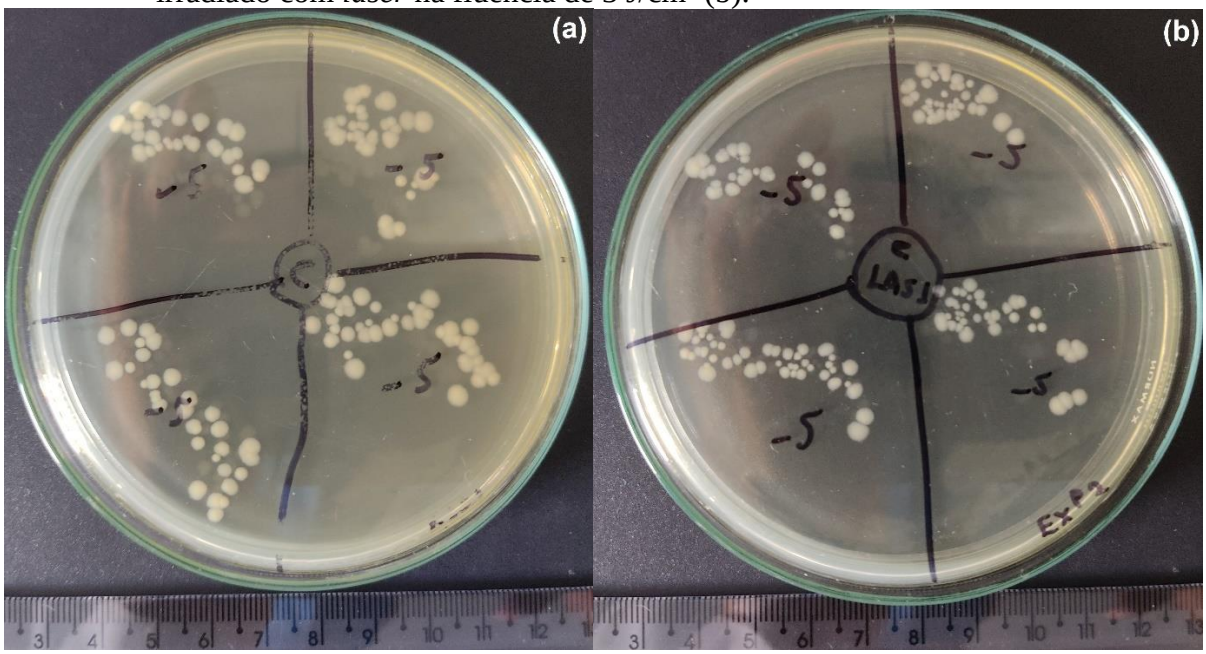

Legenda: Unidades formadoras de colônias de *E. coli* C600 do grupo controle, não expostas as radiações emitidas por *lasers* e LEDs de baixa potências (a) e unidades formadoras de colônias de *E. coli* C600 expostas ao laser vermelho na fluência de 3 J/cm² (b).

Fonte: O autor, 2023.

4.3 **Sobrevivência e proliferação em culturas de *E. coli* C600 após exposição ao LED azul e ao *laser* vermelho de baixa potência seguido pela exposição à radiação UVC**

Na figura 11 estão representados a fração de sobrevivência das culturas de *E. coli* C600 pré-expostas ao LED azul e ao *laser* vermelho de baixa potência, seguido pela exposição à radiação UVC na fluência de 50 mJ/cm². Os dados nessa figura sugerem que a pré-exposição ao *laser* vermelho (9 J/cm²) e ao LED azul + *laser* vermelho aumenta significativamente ($p<0,001$) a sobrevivência das culturas de *E. coli* C600 expostas à radiação UVC.

Figura 11 – Frações de sobrevivência das culturas de *E. coli* C600 pré-expostas aos LED azul e ao *laser* vermelho de baixa potência seguido pela exposição à radiação UVC.

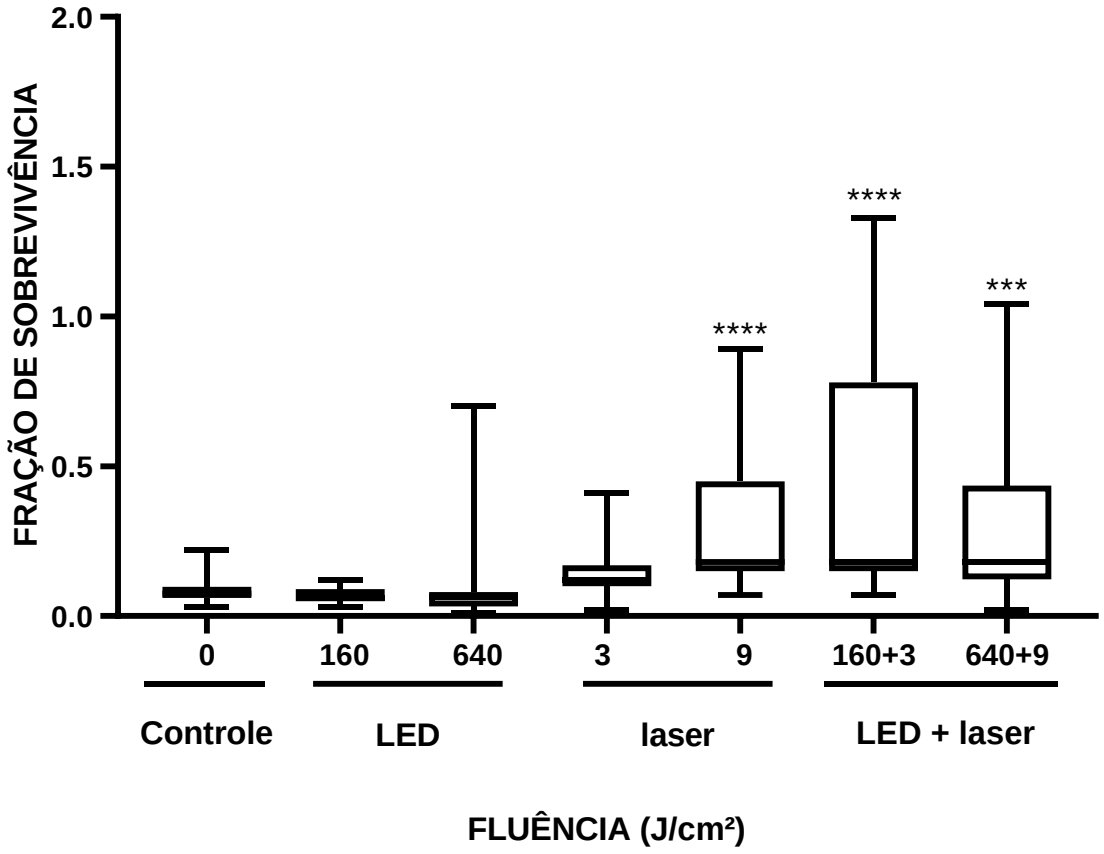

Legenda: N=8. Diagrama de caixa – grupo controle, irradiado somente com UVC, LED azul 160 J/cm², LED azul 640 J/cm², *laser* vermelho 3 J/cm², *laser* vermelho 9 J/cm², LED azul + *laser* vermelho 160 + 3 J/cm², LED azul + *laser* vermelho 640 + 9 J/cm². As barras indicam a amplitude em cada grupo e no gráfico estão as medianas e os quartis. (****) p<0,0001 quando comparado com o grupo controle irradiado somente com 50 mJ/cm² de radiação UVC. (***) p=0,001 quando comparado com o grupo controle.

Na figura 12 estão representados a razão da área das colônias de *E. coli* C600 pré-expostas aos LED azul e ao *laser* vermelho de baixa potência seguido pela exposição à radiação UVC na fluência de 50 mJ/cm². Na figura 13 estão apresentadas duas fotos representativas de colônias de *E. coli* C600. Os dados na figura 12 indicam alteração significativa (p<0,05) nas frações de área das culturas bacterianas expostas ao *laser* vermelho na fluência de 9 J/cm² e ao LED azul + *laser* vermelho na fluência de 160 + 3 J/cm². As culturas bacterianas expostas ao *laser* vermelho (9 J/cm²) apresentaram aumento da sua fração de área (p=0,0009), indicando uma maior taxa de proliferação. Entretanto, as culturas expostas ao LED azul + *laser* vermelho (160 + 3 J/cm²) apresentaram diminuição da fração de área (p<0,0001), indicando menor taxa de proliferação.

Figura 12 – Razão das áreas das colônias das culturas de *E. coli* C600 pré-expostas ao LED azul e ao *laser* vermelho de baixa potência em diferentes fluências, seguido pela exposição à radiação UVC

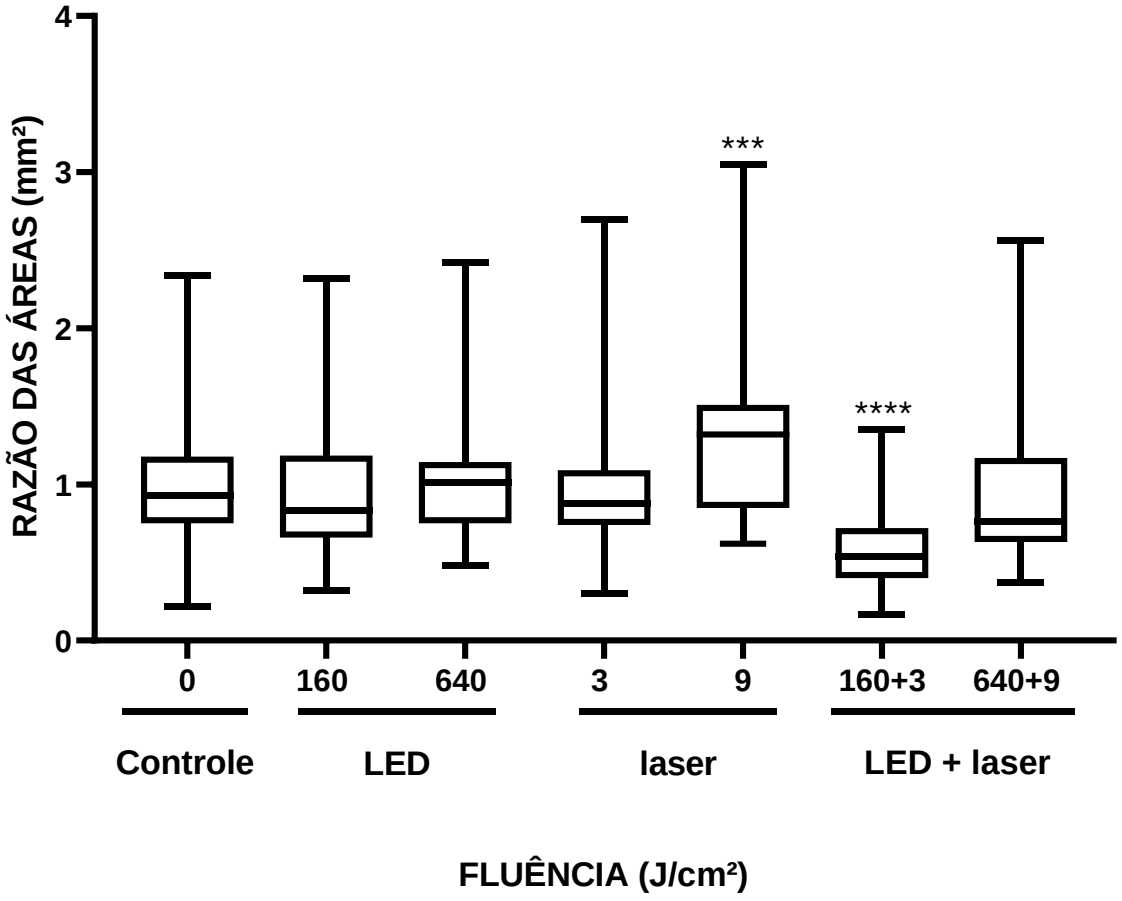

Legenda: N=8. Diagrama de caixa – grupo controle, não irradiado, LED azul 160 J/cm², LED azul 640 J/cm², *laser* vermelho 3 J/cm², *laser* vermelho 9 J/cm², LED azul + *laser* vermelho 160 + 3 J/cm², LED azul + *laser* vermelho 640 + 9 J/cm². As barras indicam a amplitude em cada grupo e no gráfico estão as medianas e os quartis. (****) p<0,0001quando comparado com a área das colônias o grupo controle irradiado somente com 50 mJ/cm² de radiação UVC. (***) p=0,001quando comparado com a área das colônias do grupo controle.

Figura 13 - Fotos representativas das colônias de *E. coli* C600 do grupo controle, irradiado somente com UVC (a) e do grupo *Laser* vermelho + LED azul nas fluências de 3 + 160 J/cm² (b).

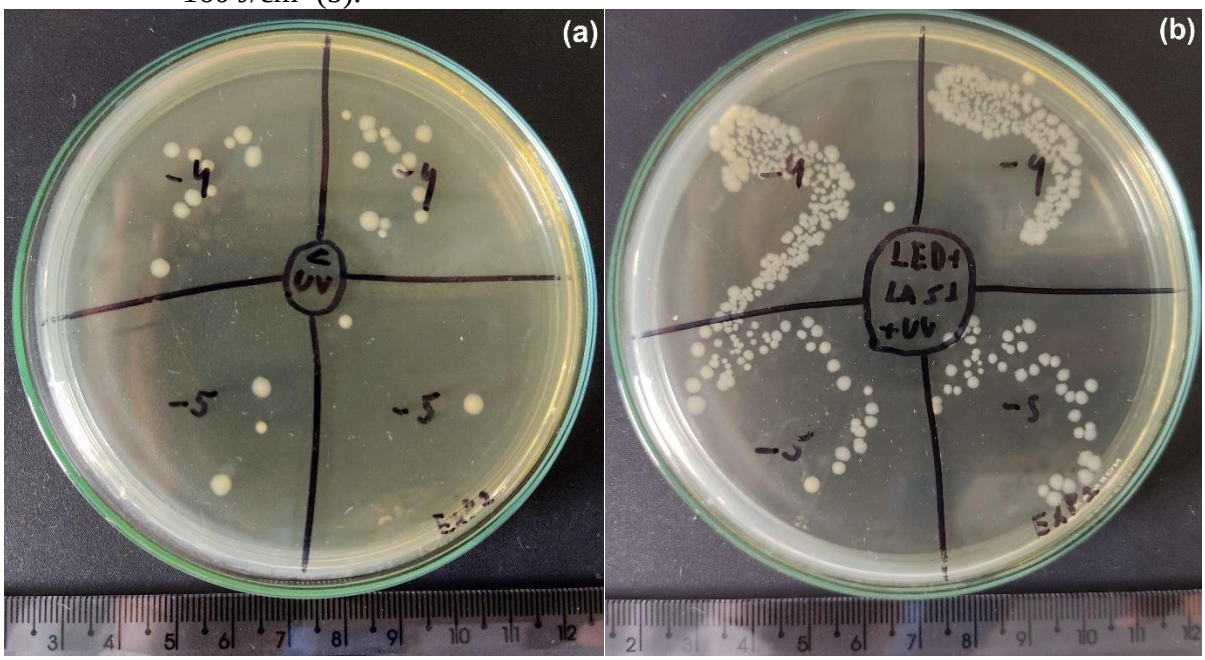

Legenda: Unidades formadoras de colônias de *E. coli* C600 do grupo controle, expostas apenas a radiação ultravioleta C, na fluência de 50 mJ/cm² (a) e unidades formadoras de colônias de *E. coli* C600 pré-expostas ao *laser* vermelho e LED azul de baixa potência na fluência de 3 + 160 J/cm² (b).

Fonte: O autor, 2023.

4.4 **Efeitos nos níveis de RNA mensageiro do gene *phr* em culturas de *E. coli* C600 após exposição ao LED azul e ao *laser* vermelho de baixa potência**

Na figura 14 estão representados os valores dos níveis relativos do mRNA do gene *phr* nas células de *E. coli* C600 após exposição ao LED azul e ao *laser* vermelho de baixa potência. Esses achados indicam que a exposição à essas radiações não alteram significativamente ($p>0,05$) os níveis de mRNA em células de *E. coli* C600.

Figura 14 – N=3. Níveis relativos do mRNA do gene *phr* em células de *E. coli* C600 após exposição ao LED azul e ao *laser* vermelho de baixa potência

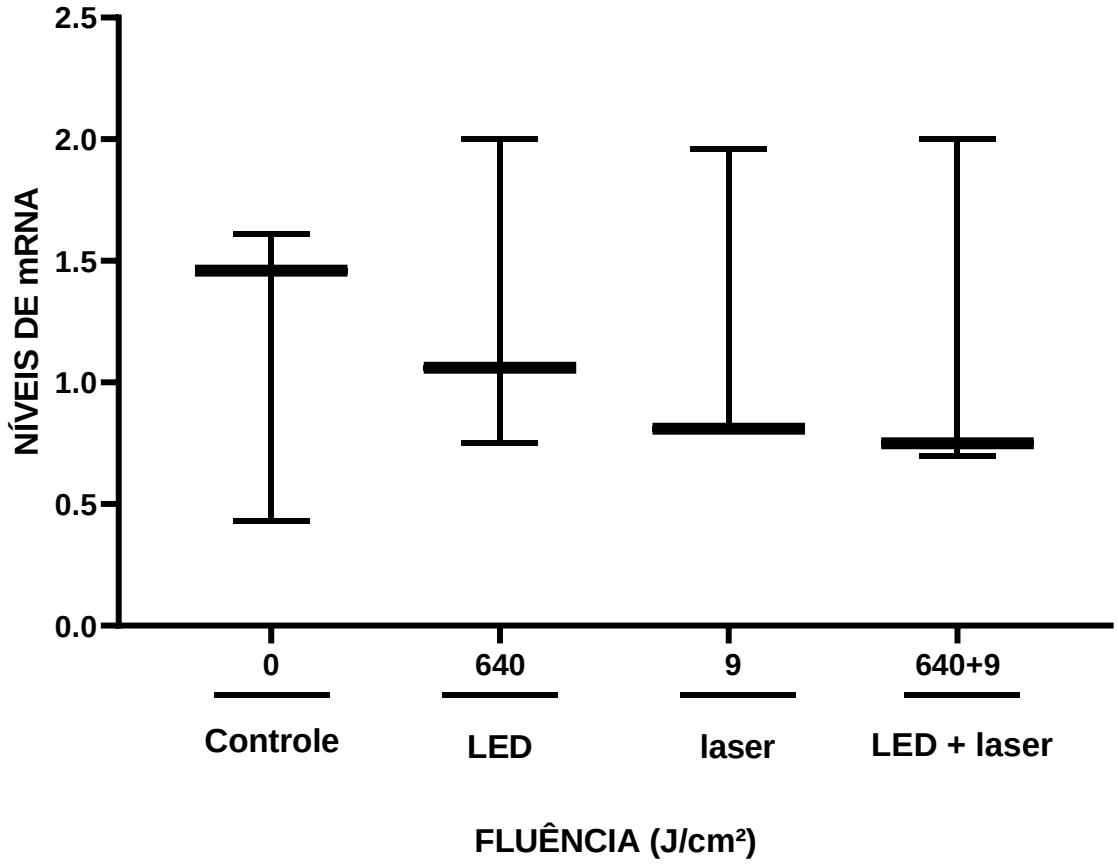

Legenda: N=3. Diagramas de caixa – grupo controle, não irradiado, LED azul 640 J/cm², *laser* vermelho 9 J/cm², LED azul + *laser* vermelho 640 + 9 J/cm². As barras indicam a amplitude em cada grupo e no gráfico estão as medianas e os quartis.

4.5 **Sobrevivência de células de tumor de mama após exposição ao LED azul e ao *laser* vermelho de baixa potência**

Nas figuras 15 e 16 estão apresentados os valores das frações de sobrevivência das células MCF-7 e MDA-MB-231, respectivamente, após 24, 48 e 72 horas de tratamento. Os dados sugerem que a exposição ao LED azul e ao *laser* vermelho de baixa potência não alteram significativamente ($p>0,05$) sua sobrevivência os períodos avaliados.

Figura 15 – Sobrevivência das células MCF-7 após 24, 48 e 72 horas de exposição ao LED azul e ao *laser* vermelho de baixa potência

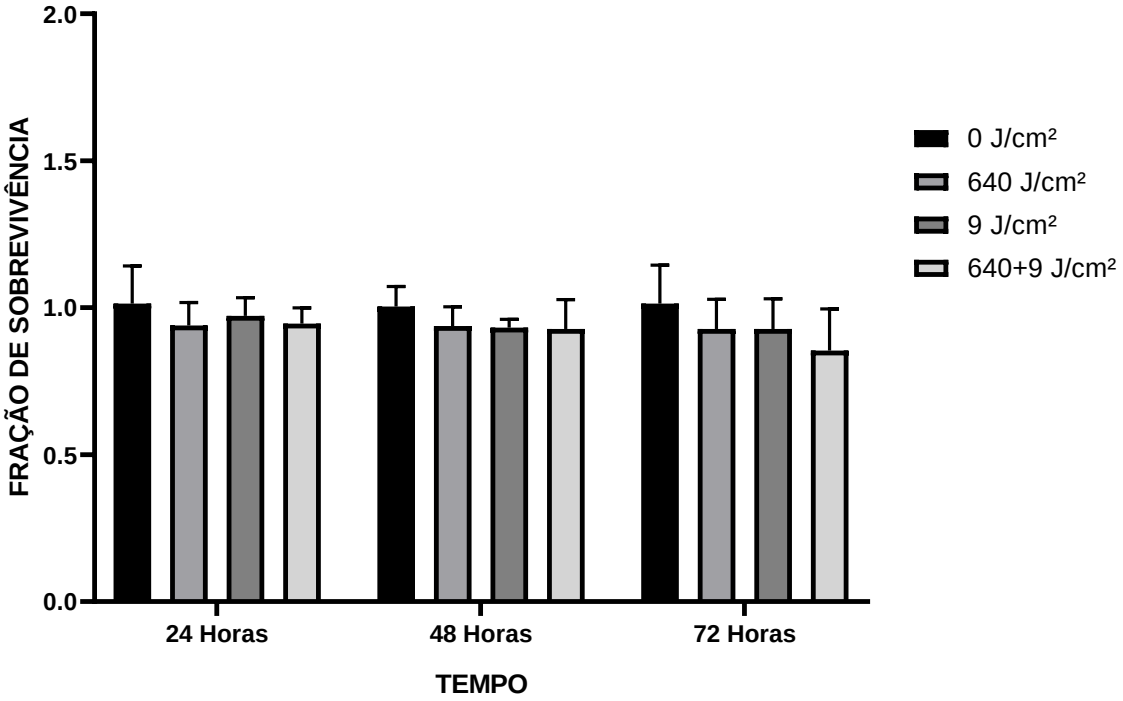

Legenda: N=5. Colunas – grupo controle, não irradiado, LED azul 640 J/cm², *laser* vermelho 9 J/cm², LED azul + *laser* vermelho 640 + 9 J/cm². As barras de erro indicam o desvio padrão da média.

Figura 16 – Sobrevivência das células MDA-MB-231 após 24, 48 e 72 horas de exposição ao LED azul e ao *laser* vermelho de baixa potência

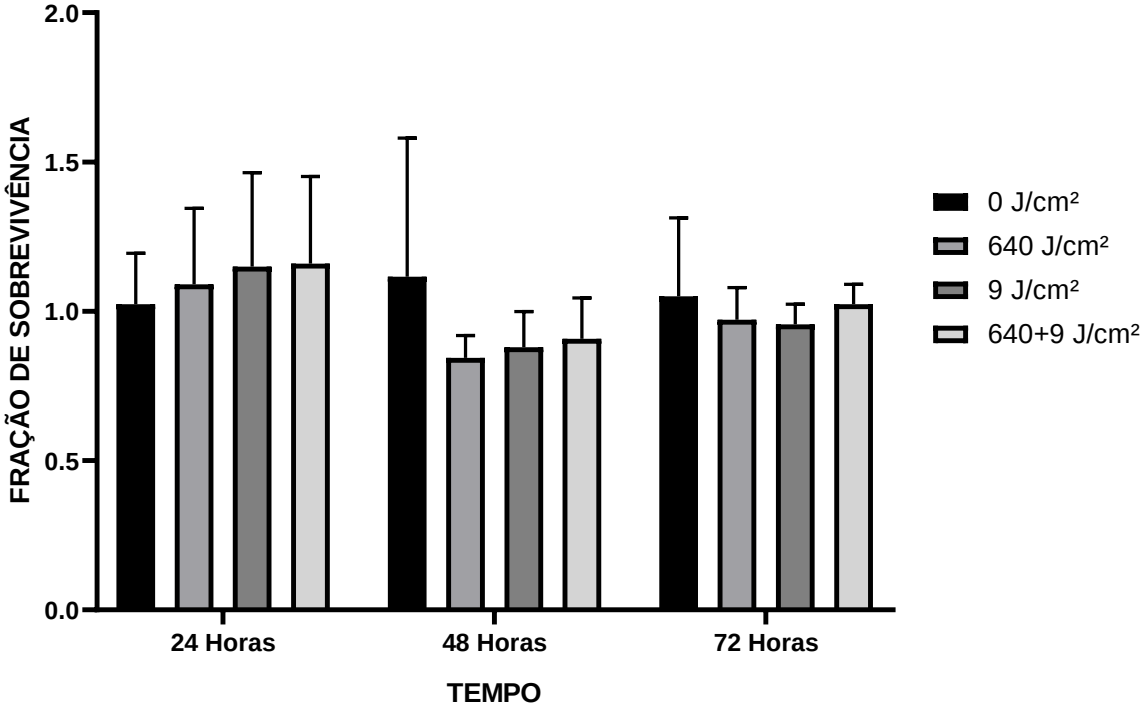

Legenda: N=5. Colunas – grupo controle, não irradiado, LED azul 640 J/cm², *laser* vermelho 9 J/cm², LED azul + *laser* vermelho 640 + 9 J/cm². As barras de erro indicam o desvio padrão da média.

4.6 **Níveis de RNA mensageiro dos genes circadianos em culturas de células de tumor de mama após exposição ao LED azul e *laser* vermelho de baixa potência**

Nas figuras 17 e 18 estão apresentados os valores dos níveis relativos do mRNA do gene *BMAL1* nas células MCF-7 e MDA-MB-231, respectivamente, após exposição ao LED azul e ao *laser* vermelho de baixa potência. Esses achados indicam que a exposição a essas radiações não altera significativamente ($p>0,05$) os níveis de mRNA nas células MCF-7 e MDA-MB-231.

Figura 17 – N=5. Níveis relativos do mRNA do gene *BMAL1* nas células MCF-7 após exposição ao LED azul e ao *laser* vermelho de baixa potência

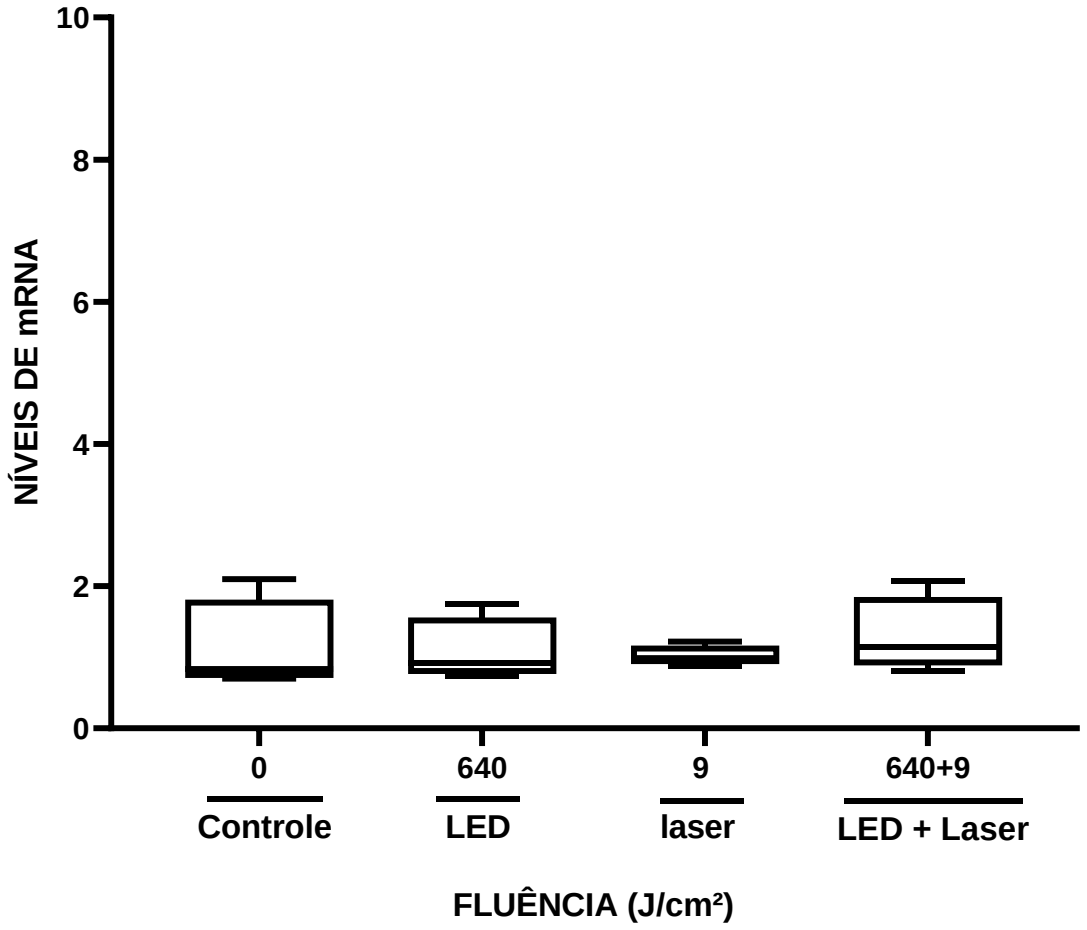

Legenda: N=5. Diagramas de caixa – grupo controle, não irradiado, LED azul 640 J/cm², *laser* vermelho 9 J/cm², LED azul + *laser* vermelho 640 + 9 J/cm². As barras indicam a amplitude em cada grupo e no gráfico estão as medianas e os quartis.

Figura 18 – N=5. Níveis relativos do mRNA do gene *BMAL1* nas células MDA-MB-231 após exposição ao LED azul e ao *laser* vermelho de baixa potência

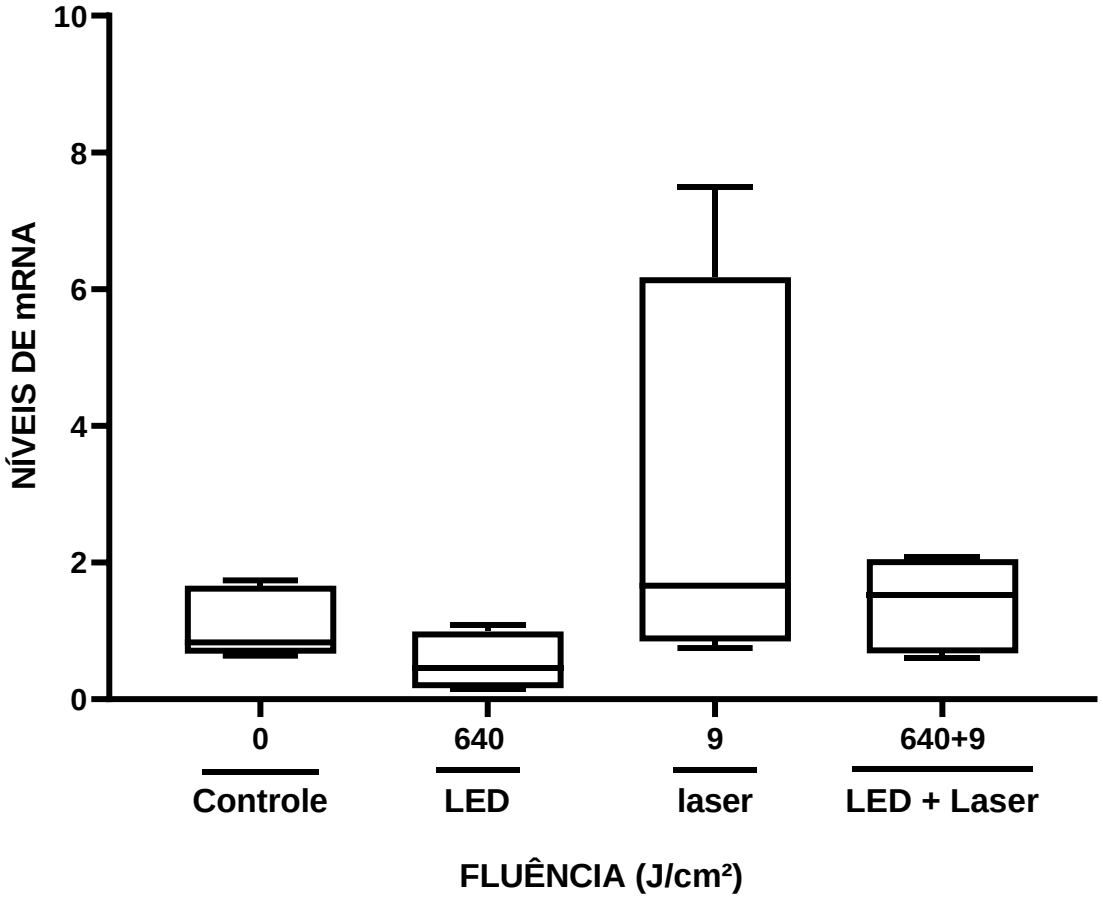

Legenda: N=5. Diagramas de caixa – grupo controle, não irradiado, LED azul 640 J/cm², *laser* vermelho 9 J/cm², LED azul + *laser* vermelho 640 + 9 J/cm². As barras indicam a amplitude em cada grupo e no gráfico estão as medianas e os quartis.

Nas figuras 19 e 20 estão apresentados os valores dos níveis relativos do mRNA do gene *CLOCK* nas células MCF-7 e MDA-MB-231, respectivamente, após exposição ao LED azul e ao *laser* vermelho de baixa potência. Esses achados indicam que a exposição a essas radiações não altera significativamente ($p>0,05$) os níveis de mRNA nas células MCF-7 e MDA-MB-231.

Figura 19 – N=5. Níveis relativos do mRNA do gene *CLOCK* nas células MCF-7 após exposição ao LED azul e ao *laser* vermelho de baixa potência

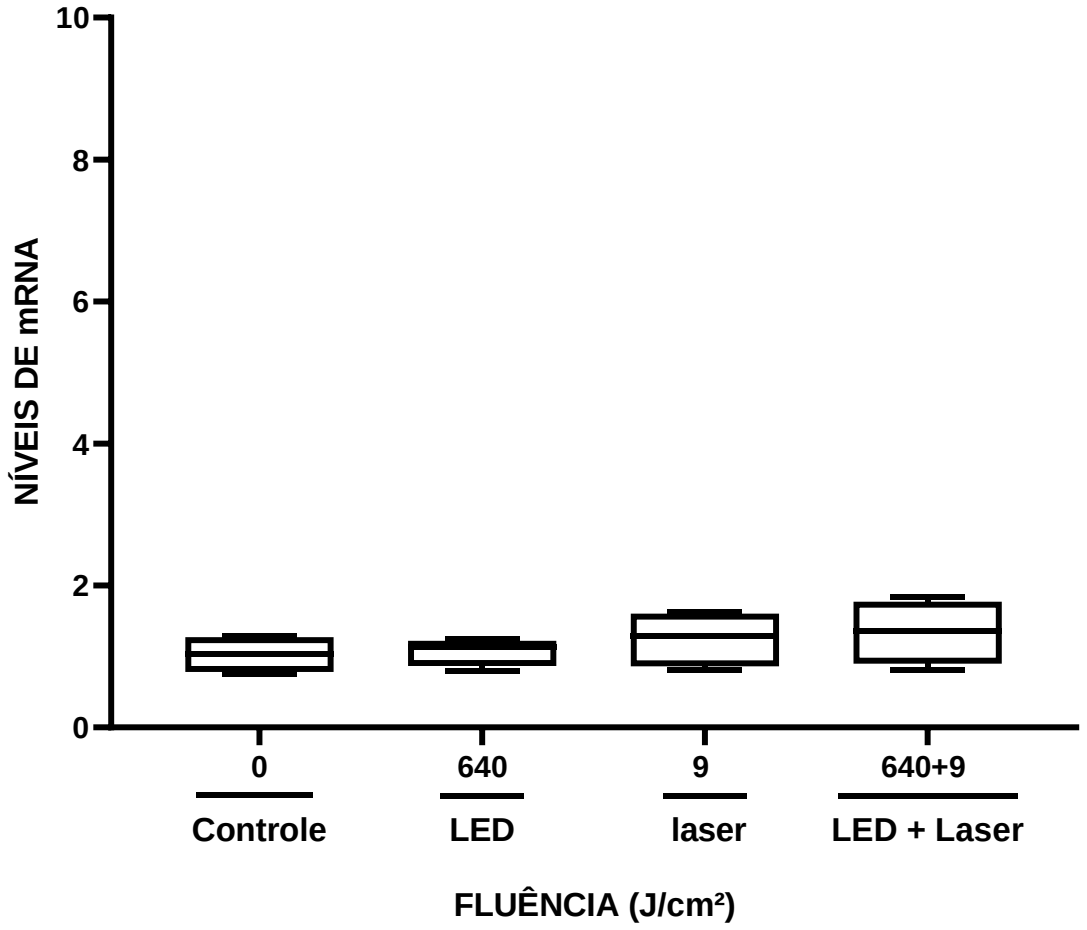

Legenda: N=5. Diagramas de caixa – grupo controle, não irradiado, LED azul 640 J/cm², *laser* vermelho 9 J/cm², LED azul + *laser* vermelho 640 + 9 J/cm². As barras indicam a amplitude em cada grupo e no gráfico estão as medianas e os quartis.

Figura 20 – N=5. Níveis relativos do mRNA do gene *CLOCK* nas células MDA-MB-231 após exposição ao LED azul e ao *laser* vermelho de baixa potência

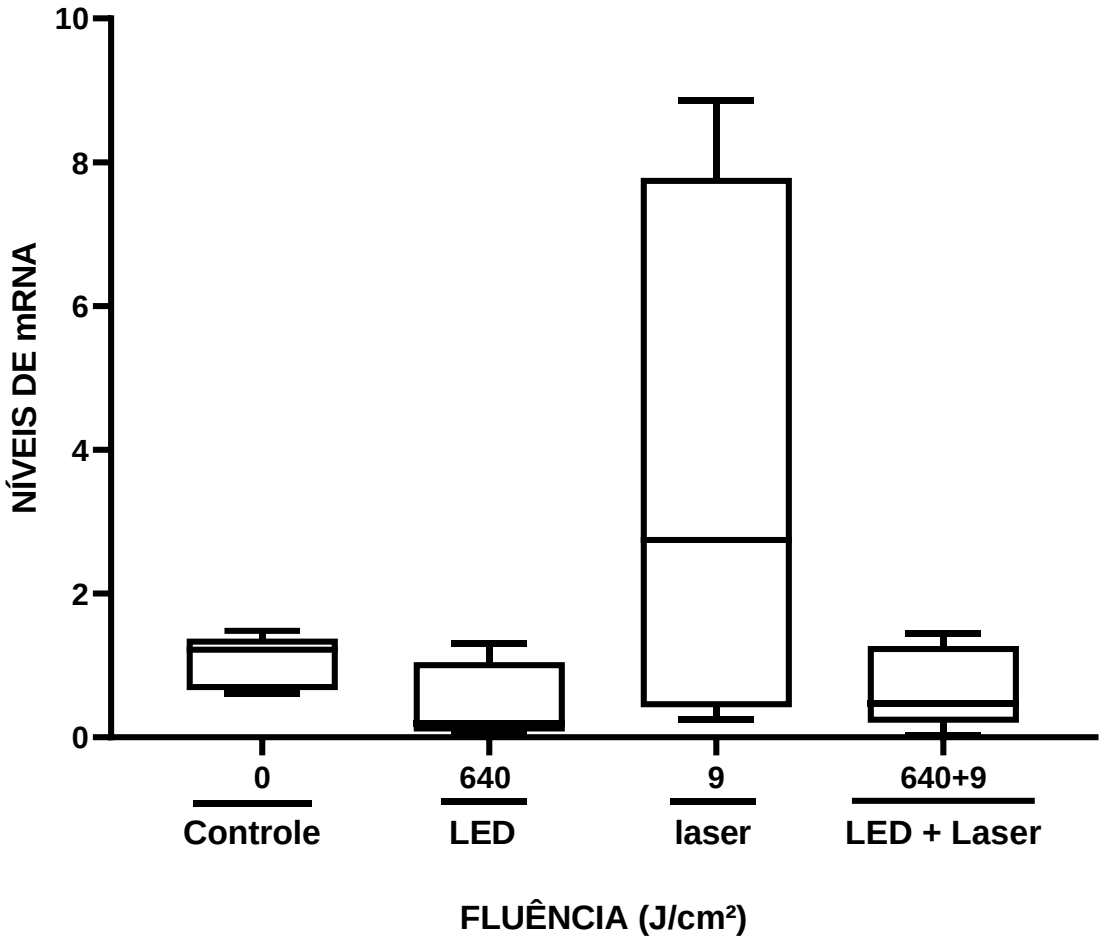

Legenda: N=5. Diagramas de caixa – grupo controle, não irradiado, LED azul 640 J/cm², *laser* vermelho 9 J/cm², LED azul + *laser* vermelho 640 + 9 J/cm². As barras indicam a amplitude em cada grupo e no gráfico estão as medianas e os quartis.

Nas figuras 21 e 22 estão apresentados os valores dos níveis relativos do mRNA do gene *PER1* nas células MCF-7 e MDA-MB-231, respectivamente, após exposição ao LED azul e ao *laser* vermelho de baixa potência. Esses achados indicam que a exposição a essas radiações não altera significativamente ($p>0,05$) os níveis de mRNA nas células MCF-7 e MDA-MB-231.

Figura 21 – N=5. Níveis relativos do mRNA do gene *PER1* nas células MCF-7 após exposição ao LED azul e ao *laser* vermelho de baixa potência

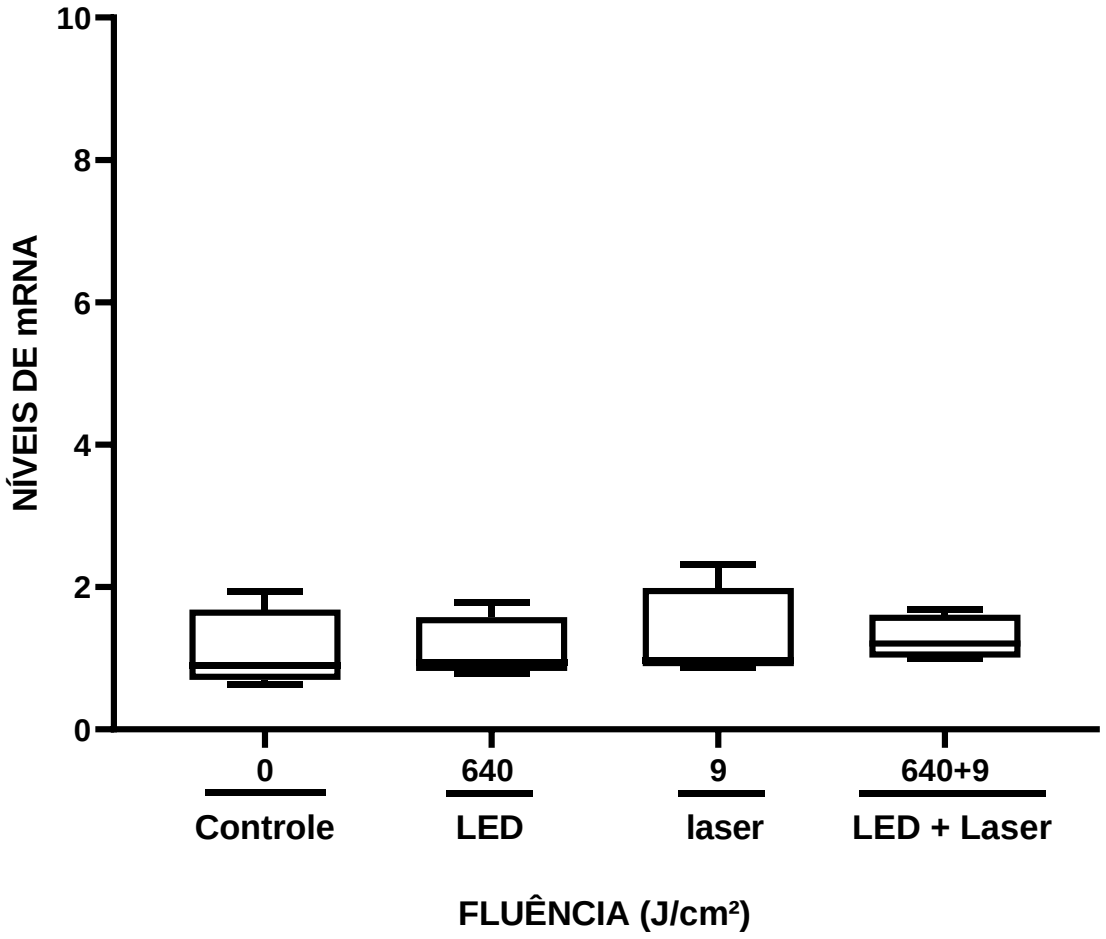

Legenda: N=5. Diagramas de caixa – grupo controle, não irradiado, LED azul 640 J/cm², *laser* vermelho 9 J/cm², LED azul + *laser* vermelho 640 + 9 J/cm². As barras indicam a amplitude em cada grupo e no gráfico estão as medianas e os quartis.

Figura 22 – N=5. Níveis relativos do mRNA do gene *PER1* nas células MDA-MB-231 após exposição ao LED azul e ao *laser* vermelho de baixa potência

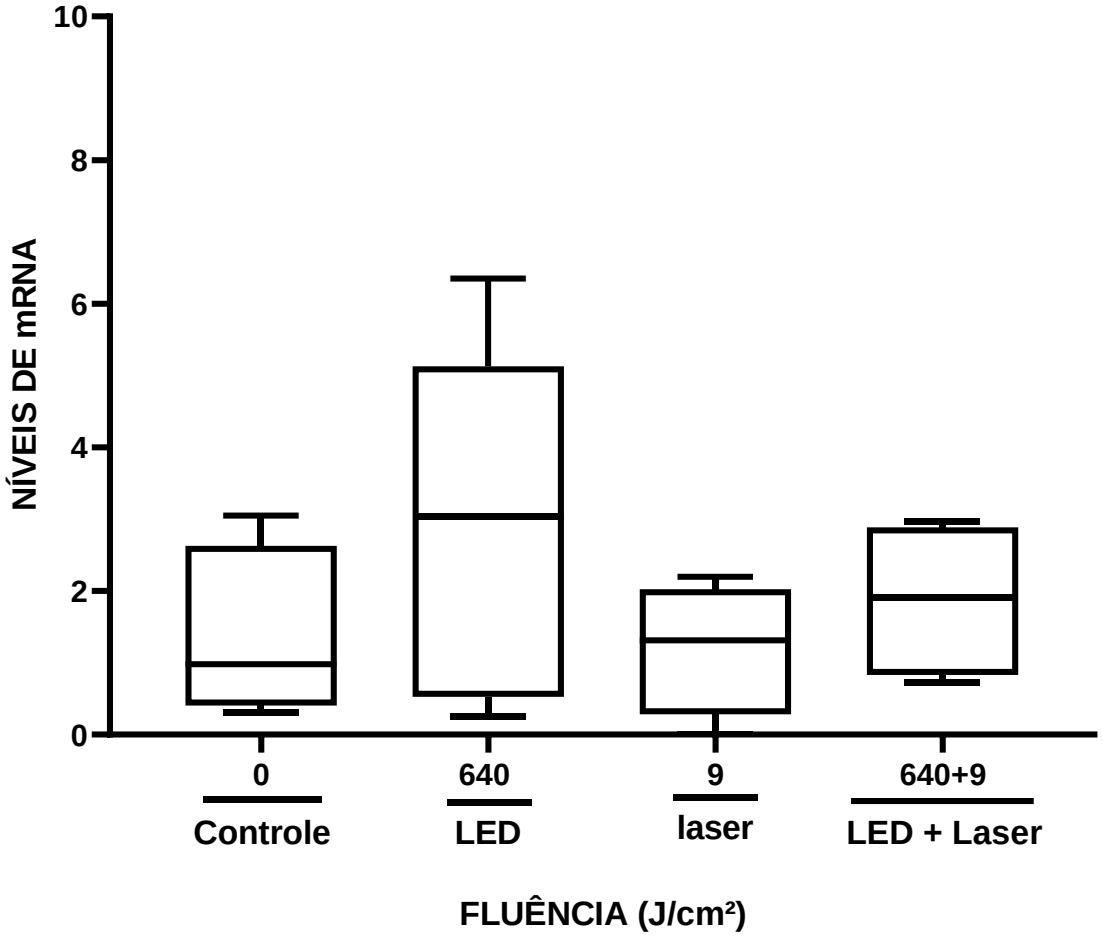

Legenda: N=5. Diagramas de caixa – grupo controle, não irradiado, LED azul 640 J/cm², *laser* vermelho 9 J/cm², LED azul + *laser* vermelho 640 + 9 J/cm². As barras indicam a amplitude em cada grupo e no gráfico estão as medianas e os quartis.

Nas figuras 23 e 24 estão apresentados os valores dos níveis relativos do mRNA do gene *PER2* nas células MCF-7 e MDA-MB-231, respectivamente, após exposição ao LED azul e ao *laser* vermelho de baixa potência. Esses achados indicam que a exposição a essas radiações não altera significativamente ($p>0,05$) os níveis de mRNA nas células MCF-7 e MDA-MB-231.

Figura 23 – N=5. Níveis relativos do mRNA do gene *PER2* nas células MCF-7 após exposição ao LED azul e ao *laser* vermelho de baixa potência

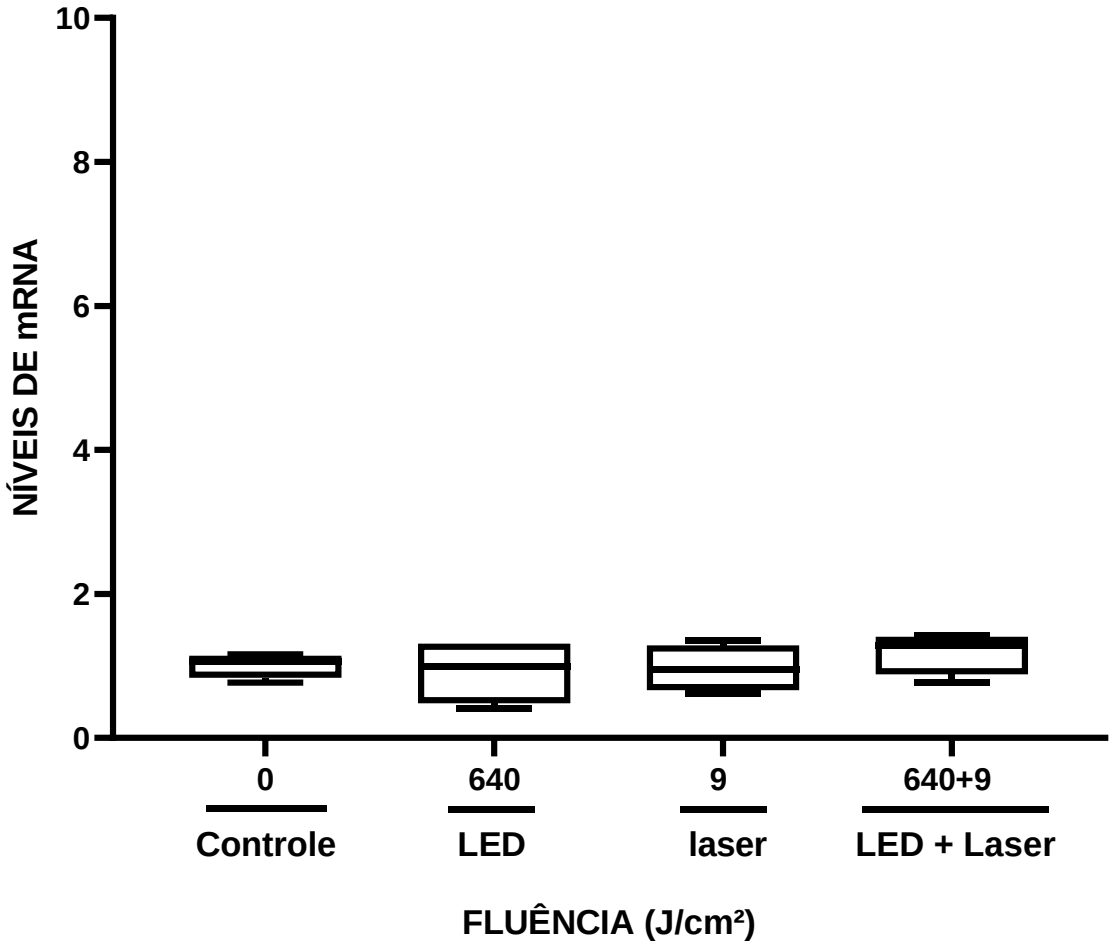

Legenda: N=5. Diagramas de caixa – grupo controle, não irradiado, LED azul 640 J/cm², *laser* vermelho 9 J/cm², LED azul + *laser* vermelho 640 + 9 J/cm². As barras indicam a amplitude em cada grupo e no gráfico estão as medianas e os quartis.

Figura 24 – N=5. Níveis relativos do mRNA do gene *PER2* nas células MDA-MB-231 após exposição ao LED azul e ao *laser* vermelho de baixa potência

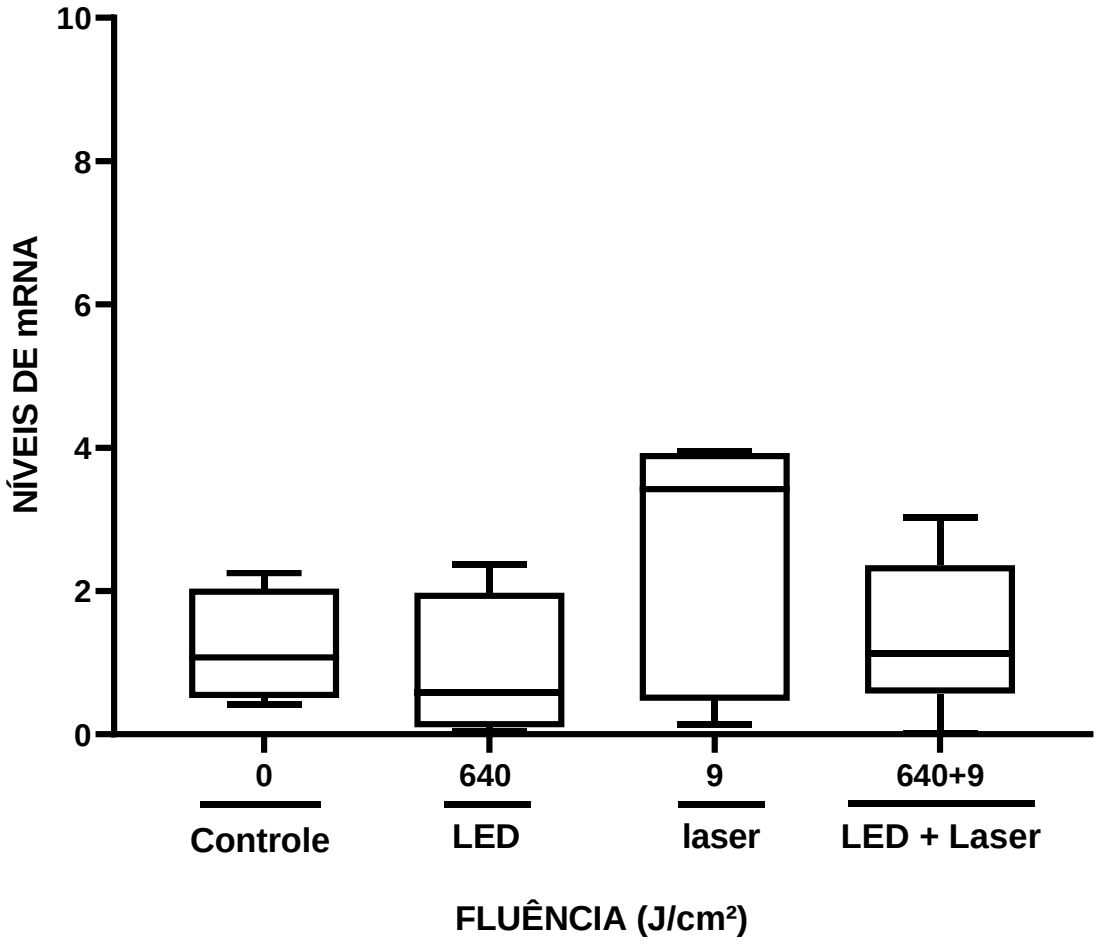

Legenda: N=5. Diagramas de caixa – grupo controle, não irradiado, LED azul 640 J/cm², *laser* vermelho 9 J/cm², LED azul + *laser* vermelho 640 + 9 J/cm². As barras indicam a amplitude em cada grupo e no gráfico estão as medianas e os quartis.

Nas figuras 25 e 26 estão apresentados os valores dos níveis relativos do mRNA do gene *PER3* nas células MCF-7 e MDA-MB-231, respectivamente, após exposição ao LED azul e ao *laser* vermelho de baixa potência. Esses achados indicam que a exposição a essas radiações não altera significativamente ($p>0,05$) os níveis de mRNA nas células MCF-7 e MDA-MB-231.

Figura 25 – N=5. Níveis relativos do mRNA do gene *PER3* nas células MCF-7 após exposição ao LED azul e ao *laser* vermelho de baixa potência

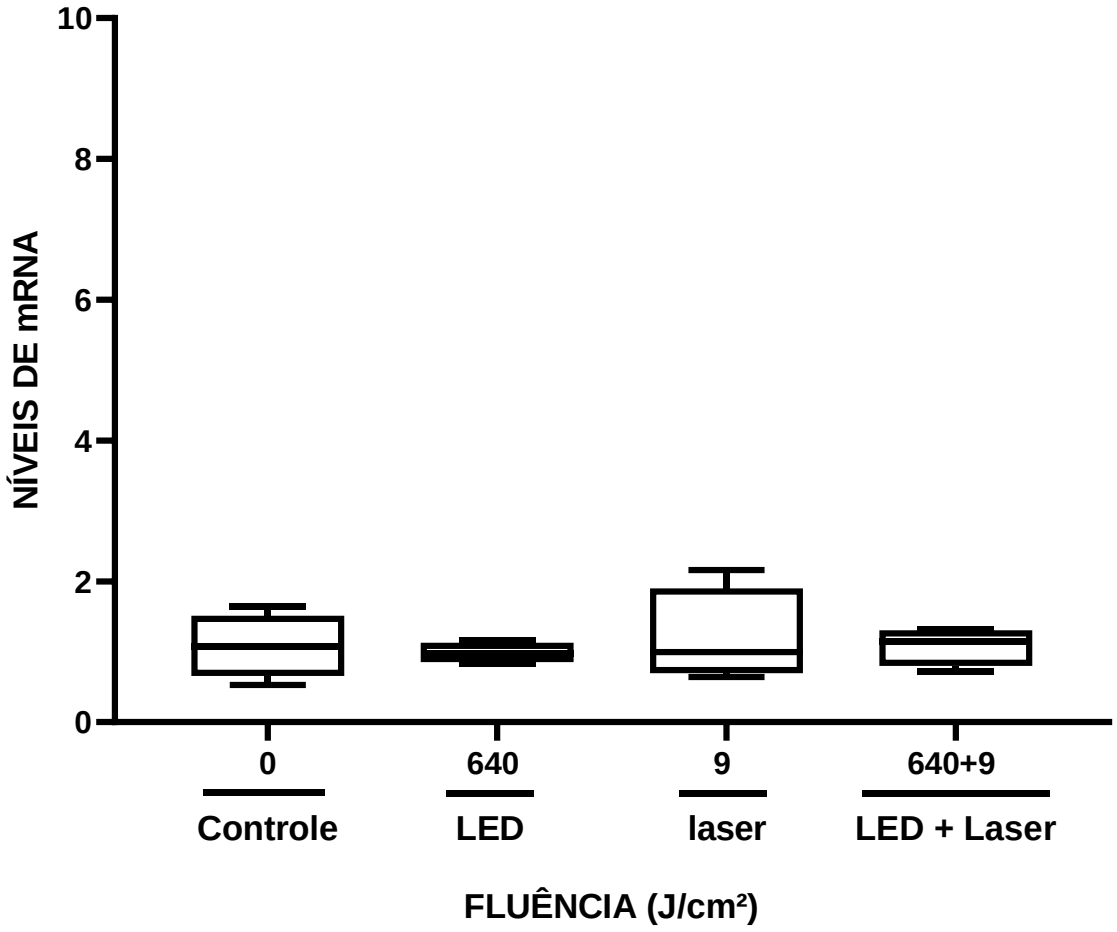

Legenda: Diagramas de caixa – grupo controle, não irradiado, LED azul 640 J/cm², *laser* vermelho 9 J/cm², LED azul + *laser* vermelho 640 + 9 J/cm². As barras indicam a amplitude em cada grupo e no gráfico estão as medianas e os quartis.

Figura 26 – N=5. Níveis relativos do mRNA do gene *PER3* nas células MDA-MB-231 após exposição ao LED azul e ao *laser* vermelho de baixa potência

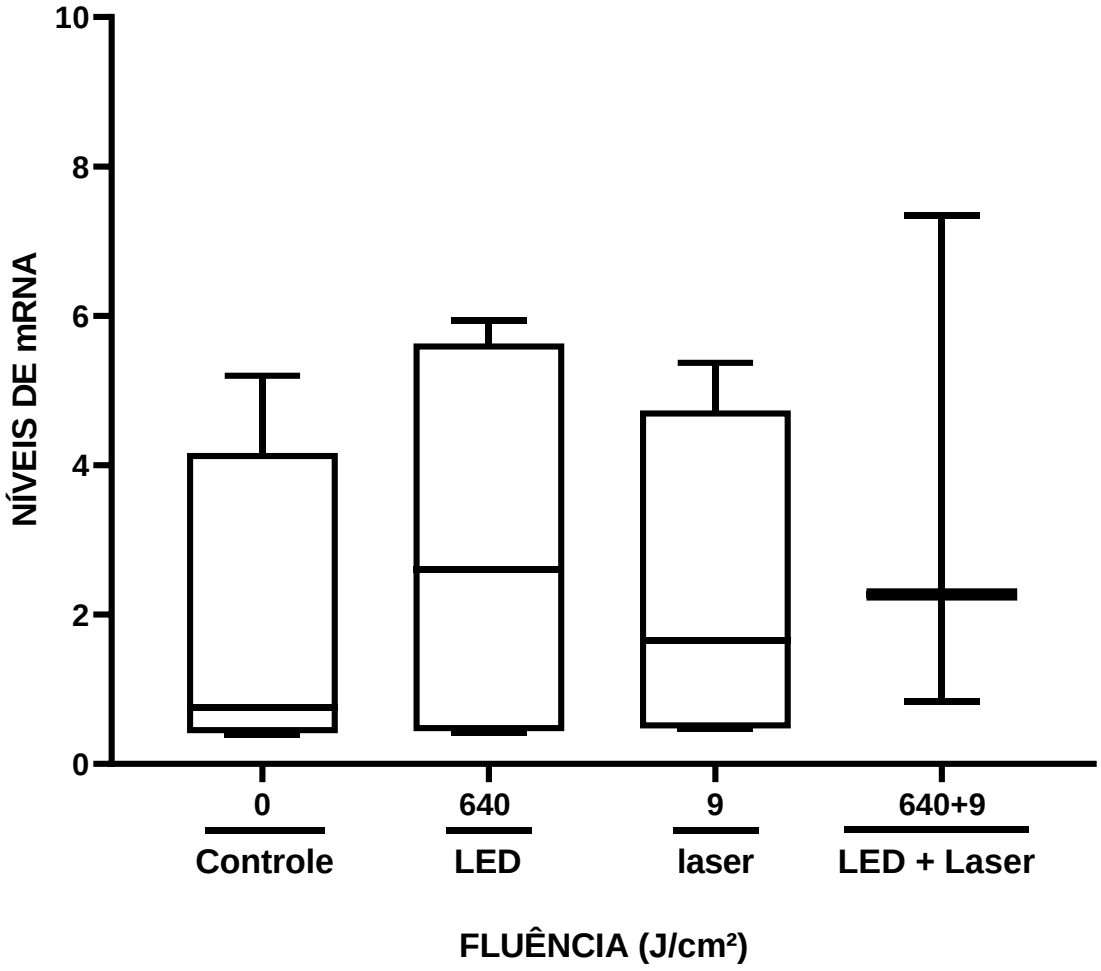

Legenda: Diagramas de caixa – grupo controle, não irradiado, LED azul 640 J/cm², *laser* vermelho 9 J/cm², LED azul + *laser* vermelho 640 + 9 J/cm². As barras indicam a amplitude em cada grupo e no gráfico estão as medianas e os quartis.

Nas figuras 27 e 28 estão apresentados os valores dos níveis relativos do mRNA do gene *CRY1* nas células MCF-7 e MDA-MB-231, respectivamente, após exposição ao LED azul e ao *laser* vermelho de baixa potência. Esses achados indicam que a exposição a essas radiações não altera significativamente ($p>0,05$) os níveis de mRNA nas células MCF-7 e MDA-MB-231.

Figura 27 – N=5. Níveis relativos do mRNA do gene *CRY1* nas células MCF-7 após exposição ao LED azul e ao *laser* vermelho de baixa potência

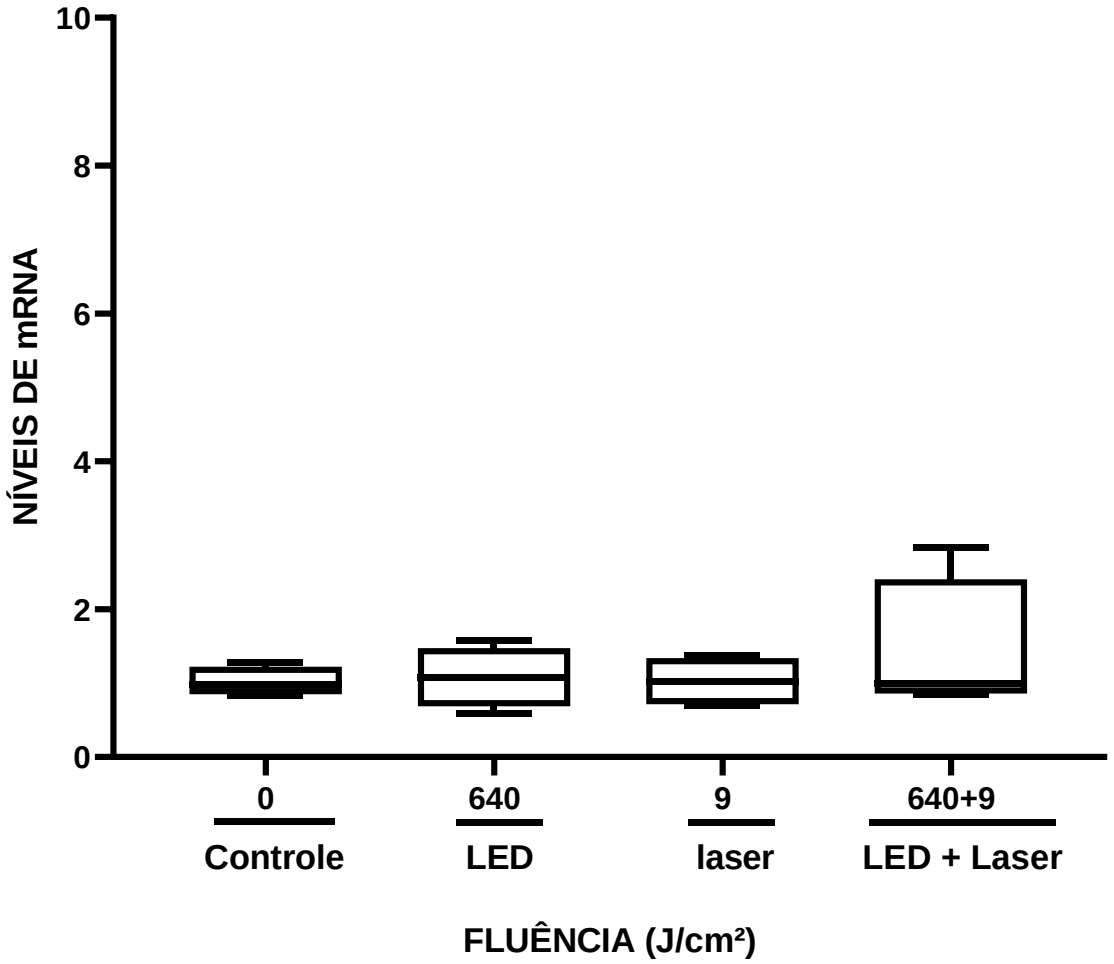

Legenda: Diagramas de caixa – grupo controle, não irradiado, LED azul 640 J/cm², *laser* vermelho 9 J/cm², LED azul + *laser* vermelho 640 + 9 J/cm². As barras indicam a amplitude em cada grupo e no gráfico estão as medianas e os quartis.

Figura 28 – N=5. Níveis relativos do mRNA do gene *CRY1* nas células MDA-MB-231 após exposição ao LED azul e ao *laser* vermelho de baixa potência

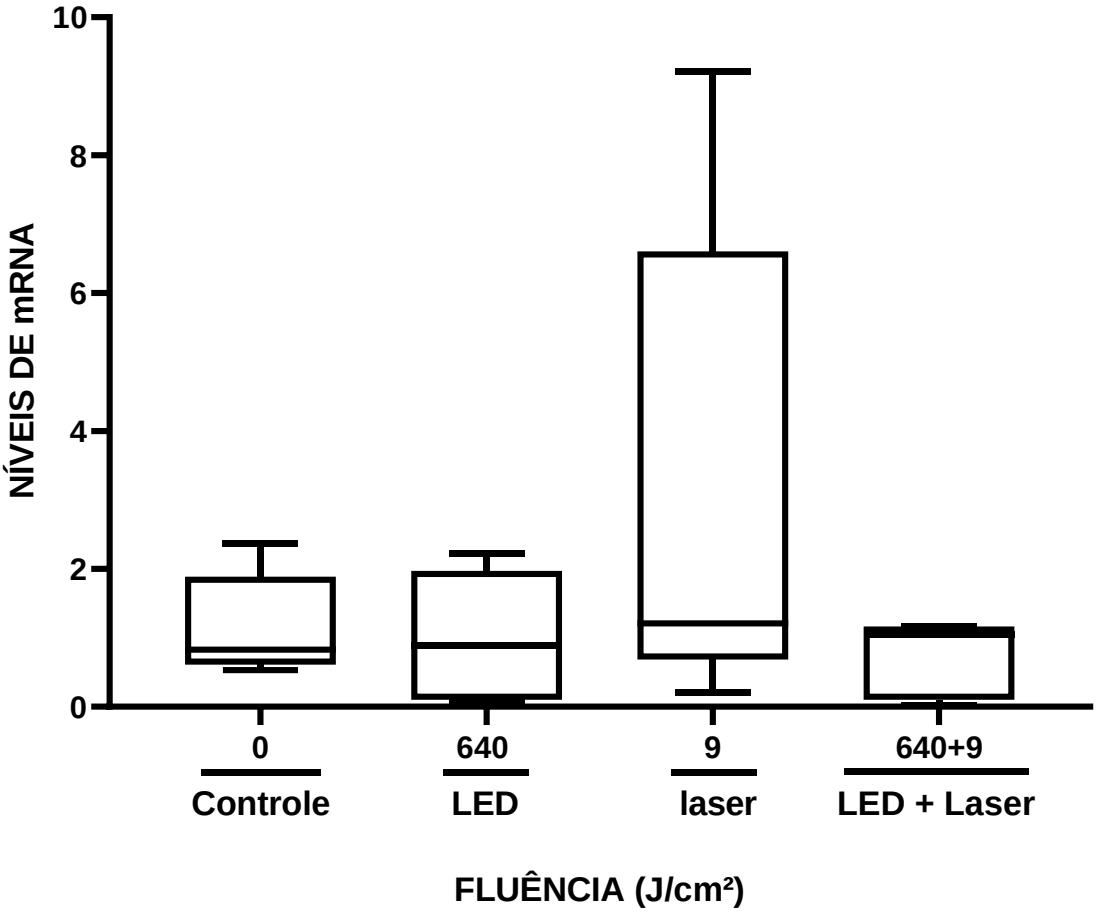

Legenda: Diagramas de caixa – grupo controle, não irradiado, LED azul 640 J/cm², *laser* vermelho 9 J/cm², LED azul + *laser* vermelho 640 + 9 J/cm². As barras indicam a amplitude em cada grupo e no gráfico estão as medianas e os quartis.

Nas figuras 29 e 30 estão apresentados os valores dos níveis relativos do mRNA do gene *CRY2* nas células MCF-7 e MDA-MB-231, respectivamente, após exposição ao LED azul e ao *laser* vermelho de baixa potência. Esses achados indicam que a exposição a essas radiações não altera significativamente ($p>0,05$) os níveis de mRNA nas células MCF-7 e MDA-MB-231.

Figura 29 – N=5. Níveis relativos do mRNA do gene *CRY2* nas células MCF-7 após exposição ao LED azul e ao *laser* vermelho de baixa potência

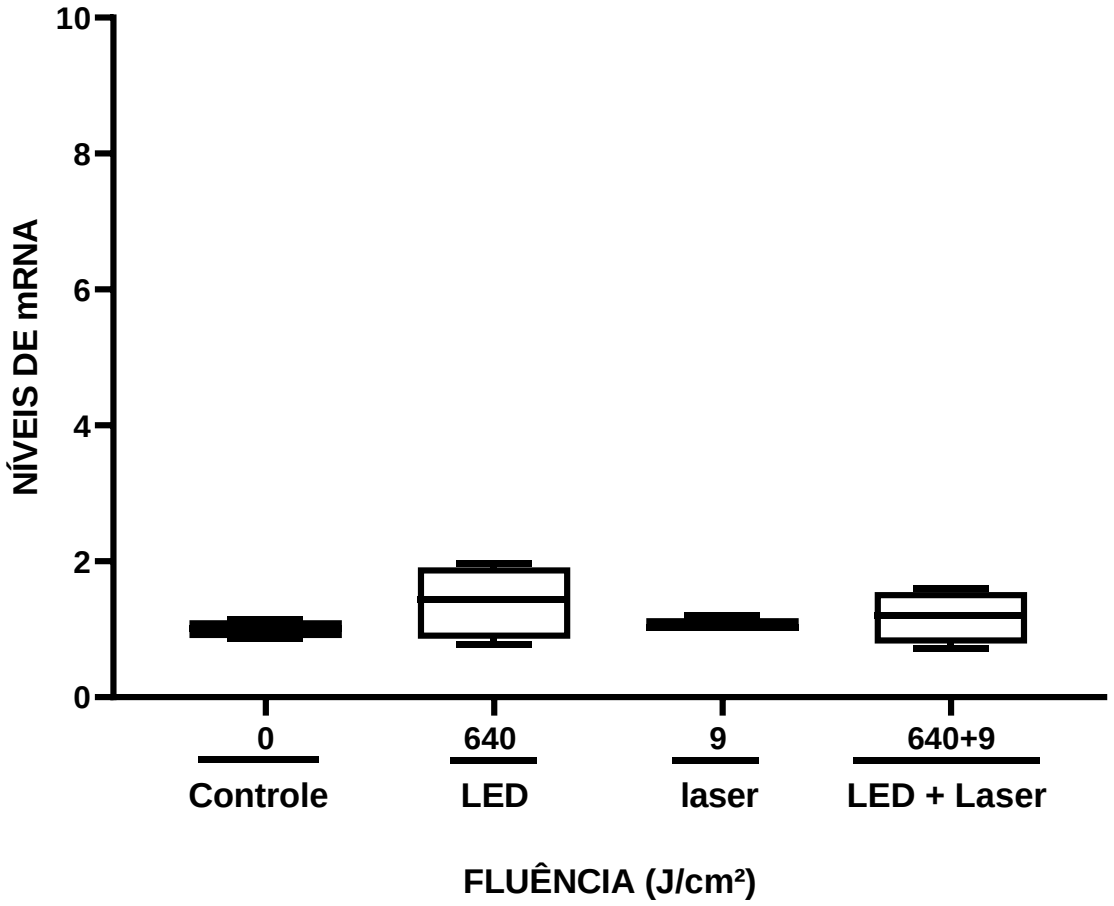

Legenda: Diagramas de caixa – grupo controle, não irradiado, LED azul 640 J/cm², *laser* vermelho 9 J/cm², LED azul + *laser* vermelho 640 + 9 J/cm². As barras indicam a amplitude em cada grupo e no gráfico estão as medianas e os quartis.

Figura 30 – N=5. Níveis relativos do mRNA do gene *CRY2* nas células MDA-MB-231 após exposição ao LED azul e ao *laser* vermelho de baixa potência

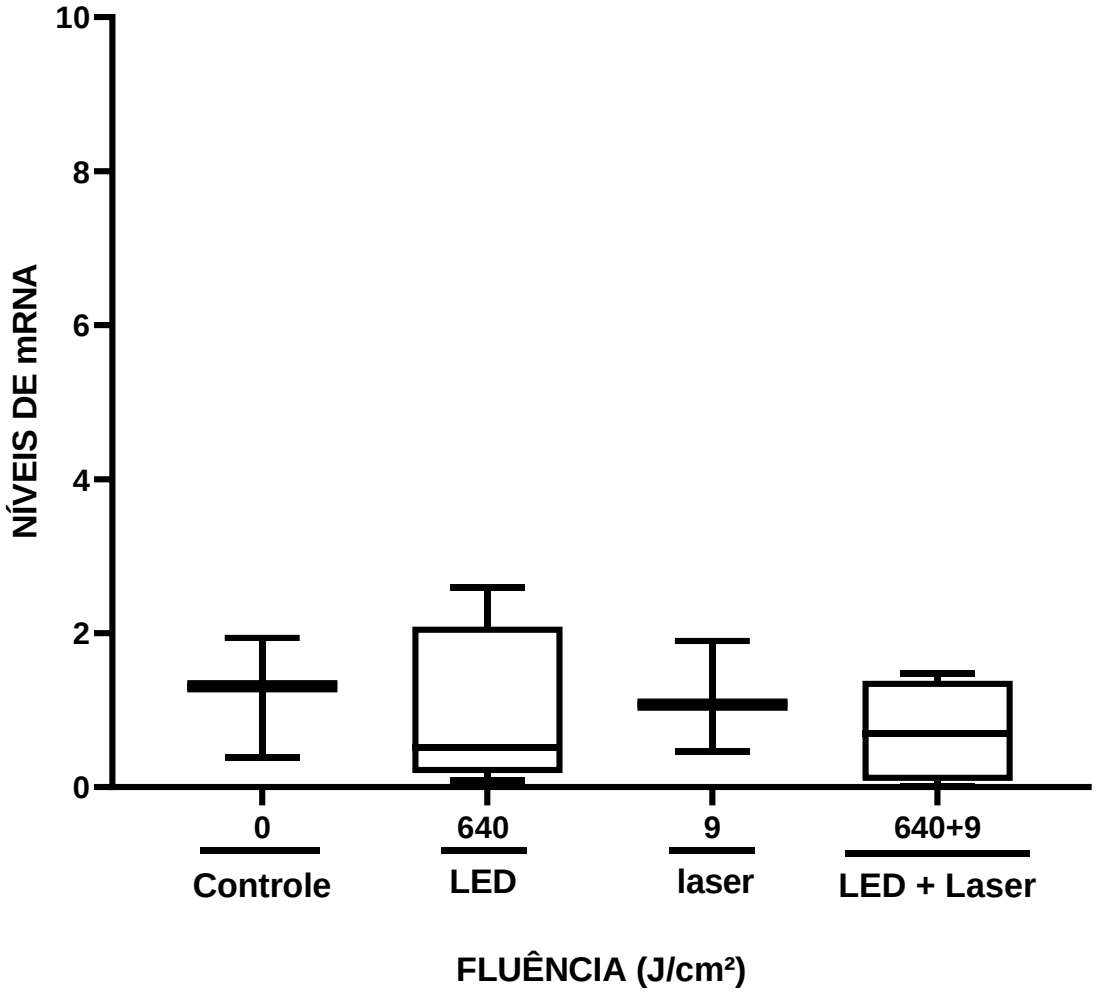

Legenda: Diagramas de caixa – grupo controle, não irradiado, LED azul 640 J/cm², *laser* vermelho 9 J/cm², LED azul + *laser* vermelho 640 + 9 J/cm². As barras indicam a amplitude em cada grupo e no gráfico estão as medianas e os quartis.

5 **DISCUSSÃO**

A densitometria de bandas plasmidiais em géis de agarose após eletroforese tem sido usada para avaliar quebras de fita simples e dupla em moléculas de DNA induzidas por agentes físicos ou químicos (FONSECA *et al.*, 2012). Amostras de plasmídeos pUC19 foram expostas as radiações do LED azul e do *laser* vermelho de baixa potência e foi realizada análise das formas topológicas do plasmídeo (figura 7). Os resultados demonstram ausência de indução de quebras do tipo simples e dupla após exposição ao LED e ao *laser* (sozinhos ou simultâneos). Esses resultados estão de acordo com os relatados por outros autores, que reportaram uma ausência semelhante dos efeitos por *laser* vermelho (658 nm) e infravermelho próximo (830 nm) de baixa potência (FONSECA *et al*., 2010; FONSECA *et al*., 2012). Entretanto, não há dados disponíveis sobre o perfil eletroforético de plasmídeos expostos a radiações emitidas por LEDs azuis de baixa potência.

Ensaios de sobrevivência em células procarióticas têm sido utilizado para avaliar a viabilidade celular após tratamentos com agentes físicos e químicos. Diversos estudos utilizam essa técnica para avaliar os efeitos de fotobiomodulação em células de *E. coli* (FONSECA *et al*., 2010; FONSECA *et al*., 2012; CANUTO *et al*., 2015; KOHLI, GUPTA, 2003; FONSECA 2012; THOMÉ *et al*., 2018). Os resultados encontrados demonstram que o *laser* vermelho de baixa potência na fluência de 9 J/cm² e irradiação simultânea com LED azul na fluência de 160 J/cm² e *laser* vermelho na fluência de 3 J/cm², assim como 640 J/cm² e 9 J/cm² protegem as células de *E. coli* C600 dos efeitos bactericidas da radiação UVC (figura 11). Achados similares foram demonstrados com culturas de *E. coli* AB1157 na fase exponencial de crescimento pré-expostos ao *laser* vermelho (660 nm) de baixa potência na fluência de 8 J/cm² (CANUTO *et al*., 2015). Outro estudo realizado por Kohli e Gupta (2003) demonstrou efeitos de foto-proteção e aumento da sobrevivência bacteriana em culturas de *E. coli* AB1157 expostas à radiação UVC após exposição ao *laser* vermelho (632,8 nm) de baixa potência na fluência de 7 kJ/m² (KOHLI, GUPTA, 2003). Esses resultados sugerem que o *laser* vermelho, assim como, o *laser* vermelho e LED azul simultâneos de baixa potência em fluências terapêuticas aumentam a sobrevivência de culturas de *E. coli* expostas à radiação UVC.

Ensaios de área das colônias pode ser usado para avaliação da proliferação celular de células procarióticas devido ao estímulo dos efeitos proliferativos ou inibitórios da fotobiomodulação (RIBEIRO, *et al*. 2023). As células de *E. coli* C600 foram expostas ao LED azul e *laser* vermelho e de baixa potência em diferentes fluências e os resultados indicam

alterações na proliferação bacteriana em culturas expostas ao *laser* vermelho de baixa potência (figura 9). Os resultados sugerem que o *laser* vermelho na fluência de 3 J/cm² diminui a taxa proliferação das células de *E. coli* C600, mas o *laser* vermelho na fluência de 9 J/cm² aumentou a taxa de proliferação. Além disso, a pré-exposição ao LED azul de baixa potência e ao *laser* vermelho alterou a área das colônias bacterianas de células de *E. coli* C600 expostas à radiação UVC (figura 12). Os resultados indicam que a pré-exposição ao *laser* vermelho na fluência de 9 J/cm² aumenta a proliferação celular, mas a pré-exposição ao LED azul e *laser* vermelho simultaneamente nas fluências de 160 e 9 J/cm², diminuem a proliferação celular. Karu (1994) demonstrou a relação de dose-dependência para estimulação da proliferação de células *E. coli* após da exposição ao *laser* He-Ne (632,8 nm) e indicou que reações bioquímicas que propiciam a estimulação do crescimento ocorrem por duas vias diferentes, sendo um ativado pela dose de irradiação e o outro por um valor crítico do tempo de exposição (KARU *et al*., 1994). Estudos relacionados aos efeitos da luz azul emitida por LEDs têm sugerido a inativação de diversos procariotos, incluindo *E. coli* (MACLEAN *et al*., 2009; DE LUCCA *et al*., 2012; KIM *et al*., 2013). Os resultados demonstraram que a exposição ao LED azul de baixa potência nas fluências de 160 J/cm² e 640 J/cm² não alteraram a taxa de sobrevivência e proliferação das culturas de *E. coli* C600 (figura 8).

As avaliações de RT-qPCR são utilizadas para acessar os níveis relativos de mRNA de genes em células procarióticas e eucarióticas (TRAJANO *et al*., 2014; TEIXEIRA *et al*., 2016; FONSECA *et al*., 2013; FONSECA *et al*., 2014; FONSECA *et al*., 2014). Células de *E. coli* C600 foram expostas ao LED azul e ao *laser* vermelho de baixa potência em diferentes fluências e os níveis relativos de mRNA do gene da fotoliase (*phr*) foi acessado. Os resultados sugerem que a exposição ao LED azul e ao *laser* vermelho não altera os níveis relativos de mRNA do gene *phr* em *E. coli* C600 (figura 14). Essa é a primeira vez que os efeitos de LED azul e *laser* vermelho de baixa potência são avaliados no mecanismo de fotorreativação e expressão do gene *phr*. Esses achados são relevantes pois demonstram a incapacidade da radiação azul emitida por LED terapêutico, na fluência de 640 J/cm², de modular o mecanismo de reparo do DNA dependente de luz azul. Entretanto, estudos têm demonstrado que *lasers* de baixa potência modulam a expressão de genes relacionados a mecanismos de reparo do DNA, como reparo por excisão de bases e reparo por excisão de nucleotídeos em tecidos biológicos (FONSECA *et al*., 2013; FONSECA *et al*., 2014; FONSECA *et al*., 2014).

Estudos sobre fotobiomodulação em procariotos demonstram a capacidade de as radiações desencadearem efeitos em células simples, mas entender como essas radiações geram efeitos em células eucarióticas é fundamental para a compreensão desses efeitos em células

mais complexas. O ensaio de viabilidade celular por WST-1 tem sido utilizado para avaliar a sobrevivência de células eucarióticas após tratamentos com agentes químicos e físicos (TEIXEIRA *et al*., 2018).

Nesse estudo foi demonstrado que o tratamento com LED azul e *laser* vermelho de baixa potência, em diferentes fluências, nas células MCF-7 e MDA-MB-231 não altera a sobrevivência das células mesmo após períodos de 24, 48 e 72 horas (figuras 15 e 16). Estudos sobre os efeitos do LED azul e *laser* vermelho em células da linhagem MCF-7 e MDA-MB 231 já foram realizados (TEIXEIRA *et al*., 2018, ANIOGO, GEORGE, ABRAHAMSE, 2023), entretanto, há escassez de estudos sobre os efeitos das radiações emitidas por esses equipamentos de baixa potência nesses modelos celulares. No estudo de Teixeira e colaboradores (2018) é demonstrado que o LED azul (470 nm) não altera a viabilidade das culturas de MDA-MB-231 nas fluências 160, 320 e 640 J/cm², mas é capaz de potencializar o efeito citotóxico da doxorubicina na fluência de 640 J/cm². Nesse estudo não foi utilizado *laser*. No estudo de Aniogo, George e Abrahamse (2023), foi demonstrado a utilização do *laser* vermelho (681 nm) nas fluências de 20 e 100 J/cm² diminui a viabilidade das células MCF-7 e associado com a Ftalocianina de zinco potencializa o efeito tóxico desse agente fotossensibilizador. Nesse estudo não foi utilizado LED.

As avaliações de RT-qPCR também foram utilizadas nas células da linhagem tumoral de mama MCF-7 e MDA-MB-231, para acessar os níveis relativos de mRNA dos genes circadianos *BMAL1*, *CLOCK*, *PER1*, *PER2*, *PER3*, *CRY1* e *CRY2* após exposição ao LED azul e ao *laser* vermelho de baixa potência em diferentes fluências. Os resultados sugerem que a exposição ao LED azul e ao *laser* vermelho não alteram os níveis relativos de mRNA desses genes circadianos em ambas as linhagens celulares estudadas (figuras 17 a 30). Os genes *BMAL1* e *CLOCK* são reguladores centrais responsáveis por coordenar a expressão de diversos genes entre eles *PER1*, *PER2*, *PER3*, *CRY1* e *CRY2* e também regular processos de supressão de tumor como a parada do ciclo celular através da expressão do gene *WEE1* e inibição da CDK1 permitindo a passagem de fase do ciclo celular (G2/M) e a apoptose através da repressão do regulador anti-apoptótico DEC2. (WU *et al*., 2011; BHATTACHARYA *et al*., 2013; SHAFI, KNUDSEN, 2019; QU *et al*., 2023). Não foram encontradas alterações nos níveis de expressão dos genes *BMAL1* e *CLOCK* após irradiação com LED azul e *laser* vermelho de baixa potência em ambas as células analisadas (figuras 17 a 20)

Os genes *PER1*, *PER2* e *PER3* também têm sido reportados como genes importantes em diversos cânceres em humanos, estando envolvido na tumorigênese e progressão tumoral,

devido sua relação no controle do ciclo celular, respostas a danos no DNA e apoptose (CLIMENT *et al*., 2010; WANG *et al*., 2020; GONG, TANG, YANG, 2021).

A super-expressão de *PER1* está associado a uma supressão de tumor, onde é relatado uma redução da proliferação, migração e invasão, controlando a agressividade das células (YANG *et al*., 2020; LIU *et al*., 2021). O tratamento com LED azul e *laser* vermelho de baixa potência não alteraram o perfil de expressão do gene *PER1* das células MCF-7 e MDA-MB-231 (figuras 21 e 22). Já foi relatado que a expressão desse gene é significativamente reduzida em tumores de mama (LIU *et al*., 2021). Entretanto a relação entre *PER1* e a patogênese do câncer de mama permanece incerto. O mecanismo está relacionado com uma expressão alterada de proteínas envolvidas na progressão do ciclo celular, entre elas ATM e CHK2 permitindo a passagem do ciclo celular (G1/S) e aumentando a proliferação (BLAKEMAN *et al*., 2016; SHAFI, KNUDSEN, 2019).

O gene *PER2* também tem sido reportado como gene envolvido no ciclo celular e apoptose (MITCHELL, ENGELBRECHT, 2016; BLAKEMAN *et al*., 2016; SHAFI, KNUDSEN, 2019). A expressão normal dessa proteína está associada com a parada do ciclo celular e controle da proliferação. Ambas as células analisadas nesse estudo apresentavam expressão do *PER2* (figuras 23 e 24), mas o tratamento com LED azul e *laser* vermelho de baixa potência não alteraram o perfil de expressão do gene nas células analisadas. A expressão deficiente dessa proteína está relacionada com a maior incidência de tumores, devido a sua relação com instabilidade genômica e maior sensibilidade à radiação através da ativação do mediador pró-apoptótico c-MYC (FU *et al*., 2002; SHAFI, KNUDSEN, 2019).

O gene *PER3* é um forte candidato à maior risco de surgimento de tumores, entretanto, o mecanismo exato de atuação ainda permanece incerto, mas há estudos correlacionando deleções ou mutações do *PER3* com a recorrência de câncer de mama positivo para receptores estrógeno (CHEN *et al*., 2005; CLIMENT *et al*., 2010). Nesse estudo, as células MCF-7 e MDA-MB-231 apresentaram expressão do gene *PER3* (figura 25 e 26). O tratamento com LED azul e *laser* vermelho de baixa potência não alteraram o perfil de expressão do gene *PER3* das células MCF-7 e MDA-MB-231.

Os genes *CRY1* e *CRY2* também estão associados em vias de regulação do ciclo celular, onde em camundongos deficientes nessas proteínas apresentavam desregulação na expressão de proteínas WEE-1 e Ciclina D1, levando a distúrbios na regulação do ciclo celular (MATSUO, 2003). Há também estudos demonstrando a atuação das proteínas CRY1 e CRY2 na resposta a danos no DNA em fibroblastos "*Knockout*" onde tornava essas células mais sensíveis a radiação ionizante aumentando a mortalidade (GAUGER, SANCAR, 2005; FU *et*

al., 2002). Os níveis relativos de mRNA dos genes *CRY1* e *CRY2* foram avaliados nas células MCF-7 e MDA-MB-231 pela técnica de RT-qPCR, (figura 27 a 30). A exposição ao LED azul e *laser* vermelho de baixa potência não alterou os níveis relativos das proteínas CRY1 e CRY2 apesar destas proteínas possuírem cromóforos para luz azul em sua estrutura, que possui homologia com as fotoliases (KAVAKLI *et al*, 2017; MICHAEL *et al*. 2017).

CONCLUSÃO

Os resultados encontrados no presente trabalho sugerem que a exposição as radiações emitidas pelo LED azul e *laser* vermelho de baixa potência:

a) Não causam quebras na fita de DNA do plasmídeo bacteriano pUC19
b) Aumenta a sobrevivência de células de *E. coli*, quando expostas a radiação ultravioleta C, dependendo da fluência do LED e do *laser*.
c) Aumenta a proliferação das células de *E. coli* quando expostos a radiação ultravioleta C, dependendo da fluência do LED e do *laser*.
d) Não altera os níveis de mRNA do gene da fotoliase (*phr*) em células de *E. coli*
e) Não altera a viabilidade celular nas células MCF-7 e MDA-MB-231.
f) Não alteram os níveis de mRNA dos genes relacionados com o ciclo circadiano *BMAL1*, *CLOCK*, *PER1*, *PER2*, *PER3*, *CRY1* e *CRY2*.

REFERÊNCIAS

AHMAD, M.; CASHMORE, A. R. HY4 gene of *A. thaliana* encodes a protein with characteristics of a blue-light photoreceptor. **Nature**, v. 366, n. 6451, p. 162-166, 11 nov. 1993.

ANIOGO, E. C.; GEORGE, B. P.; ABRAHAMSE, H. Photobiomodulation Improves Anti-Tumor Efficacy of Photodynamic Therapy against Resistant MCF-7 Cancer Cells. **Biomedicines**. v. 11, n. 6, p. 1547, 26 mai. 2023.

ANTIPA, C. *et al*. Low-power coherent and noncoherent light in clinical practice. **Proc. SPIE**, v. 2929, p. 119-123, 25 nov. 1996.

ASIMGIL, H.; KAVAKLI, I. H. Purification and characterization of five members of photolyase/cryptochrome family from *Cyanidioschyzon merolae*. **Plant Sci**., v. 185-186, p. 190-198, Abr. 2012.

BHATTACHARYA, A. *et al*. Regulation of cell cycle checkpoint kinase WEE1 by miR-195 in malignant melanoma. **Oncogene**, v. 15, n. 26, p. 3175-3183, 27 jun. 2013.

BIRNGRUBER, R. *Laser* output characteristics. **Health phys**. v. 56, n. 5, p. 605-611, 1989.

BLAKEMAN, V. *et al*. Circacian clocks and breast cancer. **Breast Cancer Res**, v. 18, n. 1, p. 1-9, 2 set. 2016.

BRUDLER, R. *et al*. Identification of a new cryptochrome class: Structure, function, and evolution. **Mol. Cell**, v. 11, n. 1, p. 59-67, jan. 2003.

CANUTO, K. S. *et al*. Low-level red laser therapy alters effects of ultravioleta C radiation on *Escherichia coli* cells. **Braz. J. Med. Biol. Res.**, v. 48, n. 10, p. 939-944, out. 2015.

CHAN, A. B.; HUBER, A-L.; LAMIA, K. A. Cryptochromes modulate E2F Family transcription factors. **Sci. Rep.** v. 10, n. 1, p. 4077, 5 mar. 2020.

CHAN, A. B.; LAMIA, K. A. Cancer, hear my battle CRY. **J. Pineal Res.**, v. 69, n. 1:e12658, ago. 2020.

CHAVES, I. *et al*. The cryptochromes: Blue light photoreceptors in plants and animals. **Annu, Rev. Plant Biol**., v. 62, p. 335-364, 2011.

CHEN, S-T. *et al*. Deregulated expression of the PER1, PER2 and PER3 genes in breast cancers. **Carcinogenesis**, v. 26, n. 7, p. 1241-1246, jul. 2005.

CLIMENT, J. *et al*. Deletion of the PER3 Gene on Chromosome 1p36 in Recurrent ER-Positive Breast Cancer. **J. Clin. Oncol.**, v. 28, n. 23, p. 3770-3778, 10 ago. 2010.

COM**S**A, S.; CÎMPEAN, A. M.; RAICA, M. The Story of MCF-7 Breast Cancer Cell Line: 40 Years of Experience in Research. **Anticancer Res.**, v. 35, n. 6, p. 3147-3154, jun. 2015.

COURTLAND, R. **Nobel for the Father of the LED**. IEEE Spectrum. 2014.

CRONSHAW, M. *et al*. Photobiomodulation and Oral Mucositis: A Systematic Review. **Dent. J. (basel).**, v. 8, n. 3, p. 87, 5 Ago. 2020.

DANTAS, R. V. F. Uso do Laser de Alta Intensidade como Alternativa à Cirurgia Convencional de Melanoplastia: Uma Revisão Sistemática. **Arch. Healt Invest.** v. 11, n. 2, p. 201-209, 2022.

DONG, Z. *et al*. Targeting Glioblastoma Steam Cells through Disruption of the Circadian Clock. **Cancer Discov**., v. 9, n. 11, p. 1556-1573, nov. 2019.

DOS-ANJOS, C. *et al*. Antimicrobial blue light inactivation of international clones of multidrug-resistant *Escherichia coli* ST10, ST131 and ST648. **Photodiagnosis. Photodyn. Ther.**, v. 27, p. 51-53, set. 2019.
EUROPEAN COLLECTION OF AUTHENTICATED CELL CULTURES. ECACC General Cell Collection: MDA-MB-231 cell line profile.

EINSTEIN, A. Zur quantum Theories der Strahlung. **Physiol Z**., p. 121-128. 1917.

ENWEMEKA, C. S. The place of coherence in light induced tissue repair and pain modulation. **Photomed. Laser Surg.**, v. 24, n. 4, p. 457, ago. 2006.

FERRER-ESPADA, R. *et al*. Antimicrobial Blue Light Inactivation of Microbial Isolates in Biofilms. **Lasers Surg. Med.**, v. 52, n. 6, p. 472-478, jun. 2020.

FONSECA, A. S. *et al*. Effect of Laser Therapy on DNA Damage. **Lasers Surg. Med.**, v. 42, n. 6, p. 481-488, ago. 2010.

FONSECA, A. S. *et al*. Low-level infrared laser effect on plasmid DNA. **Lasers Med. Sci.**, v. 27, n. 1, pag. 121-130, jan. 2012.

FONSECA, A. S. *et al*. DNA repair gene expression in biological tissues exposed to low-intensity infrared laser. **Lasers Med. Sci.**, v. 28, n. 4, p. 1077-1084, jul. 2013.

FONSECA, A. S. *et al*. Low-intensity red and infrared lasers on XPA and XPC gene expression. **Laser Phys. Lett.**, v. 11, n. 9, p. 1-6, jul. 2014.

FONSECA, A. S. *et al*. Low intensity infrared laser affects expression of oxidative DNA repair genes in mitochondria and nucleus. **Laser Phys,**, v. 24, n. 11, p. 1-6, set. 2014.

FONSECA, A. S. *et al*. Low Intensity Infrared Laser Effects on *Escherichia coli* Cultures and Plasmid DNA. **Braz. J. Med. Biol. Res.**, v. 48, n. 10, p. 929-938, out. 2015.

FUKUI, M. *et al*. Specific-wavelenghts visible light irradiation inhibits bacterial growth of *Porphiromonas gingivalis*. **J. Periodont. Res.**, v. 43, p. 174-178, 2008.

FU, L. *et al*. The circadian gene Period2 plays an important role in tumor suppression and DNA damage response *in vivo*. **Cell**, v. 111, n. 1, p. 41-50, 4 out. 2002.

GAUGER, M. A.; SANCAR, A. Cryptochrome, circadian cycle, cell cycle, checkpoints and cancer. **Cancer Res.**, v. 65, n. 15, p. 6828-6834, 1 ago. 2005.

GERY, S.; KOEFFLER, H. P. Circadian rhythms and cancer. **Cell Cycle.**, v. 9, n. 6, p. 1097-1103, 15 mar. 2010.

GOMEZ, G. F. et al. Photo Inactivation of *Streptococcus mutans* Biofilm by Violet-Blue light. **Curr. Microbiol.** v. 73, n. 3, p. 426-433, set. 2016.

GONG, X.; TANG, H.; YANG, K. PER1 suppresses glycolysis and cell proliferation in oral squamous cell carcinoma via the PER1/ RACK1/PI3K signaling complex. **Cell Death Dis.**, v. 12, n. 3, p. 276, 15 mar. 2021.

GRÉCHEZ-CASSIAU, A. *et al*. The circadian clock componente BMAL1 is a critical regulator of p21WAF1/CIP1 expression and hepatocyte proliferation. **J. Biol. Chem.**, v. 283, n. 8, p. 4535-4542, 22 fev. 2008.

HAMBLIN, M. R.; NELSON, S. T.; STRAHAN, J. R. Photobiomodulation and Cancer: What is the truth? **Photomed. Laser Surg.**, v. 36, n. 5, p. 241-245, 1 mai. 2018.

HASHIRAMOTO, A. *et al*. Mammalian clock gene Cryptochrome regulates arthritis via Proinflammatory cytokine TNF-alpha. **J. Immunol.**, v. 184, n. 3, p. 1560-1565, 1 fev. 2010.

HEISKANEN, V.; HAMBLIN, M. R. Photobiomodulation: lasers vs. light emitting diodes? **Photochem. Photobiol. Sci.**, v. 17, n. 8, p. 1003-1017, 8 ago. 2018.

HITOMI, K. *et al*. Bacterial cryptochrome and photolyase: Characterization of two photolyase-like genes of *Synechocystis* sp. PCC6803. **Nucleic Acids Res**., v. 28, n. 12, p. 2353-2362, 15 jun. 2000.

HUANG, Z.; YU, P.; TANG, J. Characterization of Triple-Negative Breast Cancer MDA-MB-231 Cell Spheroid Model. **Onco. Targets Ther.** v. 13, p. 5395-5405, 11 jun. 2020.

IGNACIO, G. C. *et al*. low and high voltage electrochemotherapy for breast cancer: an in vitro model study. **Electroporation-based Therapies for cancer**. p. 55-102, dez. 2014.

JORI, G.; KARU, T. Effects of Low-Power Light on Biological Systems II. **Proc. SPIE.**, v. 2929, 25, nov. 1996.

KANG, T-H.; *et al*. Circadian control of XPA and excision repair of cisplatin-DNA damage by cryptochrome and HERC2 ubiquitin ligase. **Proc. Natl. Acad. Sci. USA.**, v. 107, n. 11, p. 4890-4895, 16 mar. 2010.

KARU, T.; PYATIBRAT, L. V.; KALENDO, G. S. Photobiological modulation of cell attachment via cytochrome c oxidase. **Photochem. Photobiol. Sci.**, v. 3, n. 2, p. 211-216, fev. 2004.

KARU, T. *et al*. Two different mechanisms of low-intensity laser photobiological effects on *Escherichia coli*. **J. Photochem. Photobiol. B.**, v. 24, n. 3, p. 155-161, ago. 1994.

KAVAKLI, I. H. *et al*. The Photolyase/Cryptochrome Family of Proteins as DNA Repair Enzymes and Transcriptional Repressors. **Photochem. Photobiol**. v. 93, n. 1, p. 93-103, jan. 2017.

KIM, S. *et al*. In vitro bactericidal effects of 625, 525 and 425 nm wavelength (red, green and blue) light-emitting diode irradiation. **Photomed. Laser Surg.**, v. 31, n. 11, p. 554-562, nov. 2013.

KOHLI, R.; GUPTA, P. K. Irradiance dependence of the He-Ne laser-induced protection against UVC radiation in *E. coli* strains**. J. Photochem. Photobiol. B.**, v. 69, n. 3, p. 161-167, mar. 2003.

KORITALA, B. S. C. *et al*. Night shift schedule causes circadian dysregulation of DNA repair genes and elevated DNA damage in humans. **J. Pineal Res.** v. 70, n. 3, p. e12726, abr. 2021.
LIN, C.; TODO, T. The cryptochromes. **Genome Biol.** v. 6, n. 5, p. 220, 29 abr. 2005.

LIU, Y. *et al*. PER_1 as a Tumor Suppressor Attenuated in the Malignant Phenotypes of Breast Cancer Cells. **Int. J. Gen. Med.**, v. 14, p. 7077-7087, 22 out. 2021.

LIU, Z.; WANG, L.; ZHONG, D. Dynamics and mechanisms of DNA repair by photolyase. **Phys. Chem. Chem. Phys.**, v. 17, n. 18, p. 11933-11949, 29 abr. 2015.

DE-LUCCA, A. J. *et al*. Blue light (470 nm) effectively inhibits bacterial and fungal growth. **Lett. Appl. Microbiol.**, v. 55, n. 6, p. 460-466, dez. 2012.

MACLEAN M. *et al*. Inactivation of bacterial pathogens following exposure to light from 405-nanometer light-emitting diode array. **Appl. Environ. Microbiol.**, v. 75, n. 7, p. 1932-1937, abr. 2009.

MAIMAN, T. H. Stimulated Optical Radiation in Ruby. **Nature**. v. 187, p. 493-494, 6 ago. 1960.

MARTINS, A. P.; PAULA, M. R.; SIMÕES, N. P. Efeitos fisiológicos e terapêuticos da luz intensa pulsada. **Fisioter. Bras.** v. 18, n. 5, p. 632-641, 2017.

MASRI, S.; KINOUCHI, K.; SASSONE-CORSI, P. Circadian clocks, epigenetics, and cancer. **Curr. Opin. Oncol.**, v. 27, n. 1, p. 50-60, jan. 2015.

MASSEY V, The chemical and biological versatility of riboflavin. **Biochem. Sco. Trans**. V. 27, n. 4, p. 283-296, 2000.

MATSUO, T. *et al*. Control mechanism of the circadian clock for timing of cell division *in vivo*. **Science.**, v. 302, n. 5643, p. 255-259, 10 out. 2003.

MCGUFF, P. E.; *et al*. The laser treatment of experimental malignant tumors. **Canad. Med. Ass. J.**, v. 91, n. 21, p. 1089-1095, 21 nov. 1964.

MENG, Q. *et al*. Circadian regulator BMAL1::CLOCK promotes cell proliferation in hepatocellular carcinoma by controlling apoptosis and cell cycle. **Proc. Natl Acad. Sci. USA.**, v. 120, n. 2:e2214829120, 10 jan. 2023.

MESTER, A.; MESTER, A. The history of photobiomodulation: Endre Mester (1903-1984). **Photomed. Laser Surg.**, v. 35, n. 8, p. 393-394, 35 ago. 2017.

MESTER, E. *et al*. Experimentelle intersuchungen uber derlaserstrahlen auf die wundheilung. **Z Expert Chirs Forsch.**, v. 2, n. 94, 1969.

MICHAEL, A. K. *et al*. Animal Cryptochromes: Divergent Roles in Light Perception, Circadian Timekeeping and Beyond. **Photochem. Photobiol.** v. 93, n. 1, p. 128-140, Jan. 2017.

MITCHELL, M. I.; ENGELBRECHT, A-M. Circadian Rhytms and Breast Cancer: The Role of Per2 in Doxorubicin-Induced Cell Death. **J. Toxicol**. 2015:392360.

MOHAWK, J. A.; GREEN, C. B.; TAKAHASHI, J. S. Central and Peripheral circadian clocks in mammals. **Annu. Rev. Neurosci.**, v. 35, p. 445-462, 2012.

OLIVEIRA, G. B. Remoção de tatuagens com laser: revisão de literatura. **Surg. Cosmet. Dermatol.** v. 5, n. 4, p. 289-295, 2013.

OSHIMA, T. *et al*. Expression of circadian genes correlates with liver metastasis and outcomes in colorectal cancer. **Oncol. Rep.**, v. 25, n. 5, p. 1439-1446, mai. 2011.

PAPAGIANNAKOUPOULOS, T. Circadian Rhythm Disruption Promotes Lung Tumorigenesis. **Cell Metab**. v. 24, n. 2, p. 324-331, ago. 2016.

RAHMAN, S. *et al*. Circadian (De) regulation in Head and Neck Squamous Cell Carcinoma. **Int. J. Mol. Sci.**, v. 20, n. 11, p. 2662, mai. 2019.

RENK, K. F. **Basics of Laser Physics**. 2. ed. Springer International Publishing. 2017. 676 p.
RIBEIRO, M. S. *et al*. Laser em Baixa Intensidade. In: *Técnicas e procedimentos terapêuticos*. Cap 66, p. 945-953.

RIBEIRO, R. S. *et al*. Low-power blue LED and red laser effects on plasmid DNA, survival, and photolyase mRNA levels in Escherichia coli cultures. **Laser Phys. Lett**. v. 20, n. 8, p. 085601, 29 jun. 2023.

ROSSETTI, S. *et al*. Identification of an estrogen-regulated circadian mechanism necessary for breast acinar morphogenesis. **Cell Cycle.**, v. 11, n. 19, p. 3691-3700, 1 out. 2012.

SANCAR, A. Structure and function of DNA photolyase. **Biochemistry**., v. 33, n. 1, p. 2-9, 11 jan. 1994.

SANCAR, A. Regulation of the mammalian circadian clock by cryptochrome. **J. Biol. Chem.**, v. 279, n. 33, p. 34079-34082, 13 ago. 2004.

SANCAR, A. Structure and function of photolyase and *in vivo* enzymology: 50th anniversary. **J. Biol. Chem.**, v. 283, n. 47, p. 32153-32157, 21 nov. 2008.

SANCAR, A. *et al*. Circadian clock control of the cellular response to DNA damage. **FEBS Lett.**, v. 584, n. 12, p. 2618-2625, 18 jun. 2010.

SELBY, C. P.; SANCAR, A. cryptochrome/photolyase class of enzymes with single-stranded DNA-specific photolyase activity. **Proc. Natl. Acad. Sci. USA.**, v. 103, n. 47, p. 17696-17700, 21 nov. 2006.

SHAFI, A. A.; KNUDSEN, K. E. Cancer and the circadian clock. **Cancer Res.**, v. 79, n. 15, p. 3806-3814, 1 ago. 2019.

SILVA, T. G. *et al*. Photobiomodulation at molecular, cellular, and systemic levels. **Lasers Med. Sci.** v. 38, n. 1, p. 136, 13 jun. 2023.

SINHA, R. P.; HÄDER, D. P. UV-induced DNA damage and repair: a review. **Photochem. Photobiol. Sci.**, v. 1, n. 4, p. 225-236, abr. 2002.

STRAIGHT, R. C. Leon Goldman: Dermatologist & surgeon; pioneer and leader in laser surgery and medicine (1905-1997). **Lasers Surg. Med.**, v. 48, n. 10, p. 911, dez. 2016.

TEIXEIRA, A. F. *et al*. Low-level lasers and mRNA levels of reference genes used in *Escherichia coli*. **Laser Phys. Lett.**, v. 13, n. 11, p. 115602, 13 out. 2016.

TEIXEIRA, A. F. *et al.* Low power blue LED exposure increases effects of doxorubicin on MDA-MB-231 breast cancer cells. **Photodiagnosis Photodyn. Ther.**, v. 24, p. 250-255, dez. 2018.

TEIXEIRA, A. F. *et al.* Low-level lasers alter mRNA levels from traditional reference genes used in breast cancer cell lines. **Laser phys.**, v. 27, n. 7, p. 075601, jul. 2017.

TERAI, Y. *et al*. Enhanced DNA repair by DNA photolyase bearing an artificial light-harvesting chromophore. **Nucleic Acids Res**., v. 48, n. 18, p. 10076-10086, 9 set. 2020.

THOMÉ, A. M. C. *et al*. Dichromatic and monochromatic laser radiation effects on antibiotic resistance, biofilm formation, and division rate of *Pantoea agglomerans*. **Laser Phys.**, v. 28, n. 6, p. 065606, 3 mai. 2018.

TRAJANO, E. T. L. *et al*. Expression of DNA repair genes in burned skin exposed to low-level red laser. **Lasers Med. Sci.**, v. 29, n. 6, p. 1953-1957, nov. 2014.

WANG, Z. *et al*. Associated analysis of PER1/ $TUBB_2B$ with endometrial cancer development caused by circadian rhythm disorders. **Med. Oncol.**, v. 37, n. 10, p. 90, 14 set. 2020.

WORTHINGTON, E. N. *et al*. Purification and characterization of three members of the photolyase/cryptochrome family blue-light photoreceptors from *Vibrio cholera*. **J. Biol. Chem.**, v. 278, n. 40, p. 39143-39154, 3 out. 2003.

WU, Y. *et al*. Basic helix-loop-helix transcription factors DEC_1 and DEC_2 regulate the paclitaxel- induced apoptotic pathway of MCF-7 human breast cancer cells. **Int. J. Mol. Med.**, v. 27, n. 4, p. 491-495, abr. 2011.

YANG, B. *et al*. Effectiveness of Er: YAG Laser Combined with Photobiomodulation on Periodontitis based on 3-month Observation. **Oral Health Prev. Dent.** v. 20, n. 1, p. 193-198, 27 abr. 2022.

YANG, G. *et al*. Loss of the clock gene Per_1 promotes oral squamous cell carcinoma progression via the AKT/ mTOR pathway. **Cancer Sci.**, v. 111, n. 5, p. 1542-1554, mai. 2020.

YOSHIDA, A. *et al*. Antimicrobial effect of blue light using Porphyromonas gingivalis pigment. **Sci. Rep.** v. 7, n. 1, p. 5225, 12 jul. 2017.

YU, S.; LAN, C-C. E.; YU, H-S. Mechanisms of repigmentation induced by photobiomodulation therapy in vitiligo. **Exp. Dermatol.** v. 28, p. 10-14, 28 fev. 2019.

ZHANG, M.; WANG, L.; ZHONG, L. Photolyase: Dynamics and Mechanisms of repair of sun-induced DNA Damage. **Photochem. Photobiol.**, v. 93, n. 1, p. 78-92, jan. 2017.

ZHANG, M.; WANG, L.; ZHONG, L. P. Photolyase: Dynamics and Electron-Transfer Mechanisms of DNA repair. **Arch. Biochem. Biophys.**, v. 632, p. 158-174, 15 out. 2017.

ZHANG, Y. *et al*. Antimicrobial Blue Light Therapy for Multidrug-Resistant Acinetobacter baumanii Infection in a Mouse Burn Model: Implications for Prophylaxis and Treatment of Combat-related Wound Infections. **J. Infect. Dis.** v. 209, n. 12, p. 1963-1971, 15 jun. 2014.

APÊNDICE A – Low-power blue LED and red laser effects on plasmid DNA, survival, and photolyase mRNA levels in *Escherichia coli* cultures (artigo publicado)

IOP Publishing | Astro Ltd Laser Physics Letters
Laser Phys. Lett. **20** (2023) 085601 (9pp) https://doi.org/10.1088/1612-202X/ace0b1

Letter

Low-power blue LED and red laser effects on plasmid DNA, survival, and photolyase mRNA levels in *Escherichia coli* cultures

Rickson Souza Ribeiro[1], Juliana Alves Rodrigues[1], Andre Luiz Mencalha[1] and Adenilson de Souza da Fonseca[1,2,3,*]

[1] Departamento de Biofísica e Biometria, Instituto de Biologia Roberto Alcantara Gomes, Universidade do Estado do Rio de Janeiro, Boulevard Vinte e Oito de Setembro, 87, Vila Isabel, Rio de Janeiro 20551030, Brazil
[2] Departamento de Ciências Fisiológicas, Instituto Biomédico, Universidade Federal do Estado do Rio de Janeiro, Rua Frei Caneca, 94, Rio de Janeiro 20211040, Brazil
[3] Centro de Ciências da Saúde, Centro Universitário Serra dos Órgãos, Avenida Alberto Torres, 111, Teresópolis, Rio de Janeiro 25964004, Brazil

E-mail: adnfonseca@yahoo.com.br

Received 21 April 2023
Accepted for publication 9 June 2023
Published 29 June 2023

Abstract

Low-power lasers and light-emitting diodes (LEDs) are used for photobiomodulation therapy, but the photobiological effects on DNA repair mechanisms in bacteria cells are disputed yet. This work aimed to evaluate the induction of DNA damages in plasmids, bacterial survival and proliferation, and photolyase mRNA levels in *E. coli* cultures exposed to low-power blue LED and red laser, followed by ultraviolet c (UVC) radiation. Aliquots of pUC19 plasmids and *E. coli* C600 cultures were exposed to low-power blue LED (470 nm) and red laser (658 nm) at different fluences. Other *E. coli* C600 cultures were exposed to UVC radiation after exposure to low-power blue LED and red laser. After irradiations, plasmids were submitted to agarose gel electrophoresis to evaluate DNA damage, bacterial cultures were spread onto Petri dishes content rich medium and incubated to evaluate bacterial survival and proliferation, and photolyase mRNA levels in bacterial cells were evaluated by reverse transcription-quantitative polymerase chain reaction. The results suggest that exposure to blue and red lights emitted from low-power LEDs and lasers does not cause DNA strand breaks in bacterial plasmids and does not alter the survival and mRNA levels from photolyase gene in *E. coli* cells, but increases bacterial survival and proliferation in *E. coli* cultures exposed to UVC radiation depending on LED and laser fluences.

Keywords: photobiomodulation, DNA damage, bacterial survival

(Some figures may appear in colour only in the online journal)

* Author to whom any correspondence should be addressed.

1. Introduction

Low-power lasers and light-emitting diodes (LEDs) devices are used as non-ionizing radiation sources for different purposes, such as wound healing, anti-inflammatory effects, pain reduction, and acne treatment [1–3]. Low-power laser devices emit monochromatic, collimated, and coherent radiations, and low-power LEDs emit quasi-monochromatic, non-collimated, and non-coherent radiations [4]. Photobiomodulation (PBM) is the basis for therapeutic applications of these devices at low-power densities and doses, in the so-called therapeutic window (400–1100 nm) [5, 6].

The PBM action mechanism is under investigation yet, but it established that the non-ionizing radiations are absorbed by endogenous cellular molecules (chromophores, or photoacceptors), such as cytochrome *bd* in prokaryotes cells and cytochrome c oxidase in mammalian cells [7, 8]. After absorbing radiations at specific wavelengths, biochemical changes are generated, which trigger transduction signal pathways and transform the primary photo signal into amplified signals [7, 8]. The result is an increase in deoxyribonucleic acid (DNA), ribonucleic acid (RNA), protein, and adenosine triphosphate (ATP) synthesis, as well as an increase in reactive oxygen species levels [7, 8]. In prokaryotic cells and eukaryotic cells, radiation can stimulate the generation of free radicals, which can induce oxidative DNA damage [1, 6].

To repair DNA damage, the eukaryotic and prokaryotic cells present different mechanisms able to repair DNA, such as excision base repair, nucleotide excision repair, homologous recombination, and mismatch repair [9]. The specific mechanism of repair of lesions caused by ultraviolet c (UVC) radiation in prokaryotic cells is the photoreactivation mechanism, which is mediated by the photolyase enzyme [10–12]. Photolyase is a direct repair enzyme responsible for repairing injuries, such as pyrimidine cyclobutanes and photoproducts of 6–4 pyrimidine pyrimidone [12]. To repair UVC-induced DNA damage, the photolyase depends on the absorption of energy photons. This process changes the redox state of the molecule, acquiring the reduced character, which leads to electron transport events that revert UVC-induced DNA damage and restore the neutral redox state of the enzyme [12].

Due to the UVC-induced bactericidal effect, several disinfection methods are based on UVC LED and UVC lamp treatment systems [13]. Disinfection based on UVC systems helps inactivate pathogens in food, water, and beverages [13–15]. In healthcare and hospital settings, UVC has been used on room surfaces to inactivate pathogens that can cause infections by multidrug-resistant bacteria [16].

Although the mechanism of action of photolyases has been well described, it has not yet been verified whether the radiation contained by low-power devices influences the modulation of the expression of this enzyme, which is directly associated with direct DNA repair and increasing bacterial survival. Thus, this work aims to evaluate induction DNA damages, bacterial survival and proliferation, and photolyase phr messenger ribonucleic acid (mRNA) levels in *E. coli* cultures exposed to low-power blue LED and red laser, and to UVC radiation.

2. Materials and methods

2.1. Radiation sources

A cluster containing a therapeutic low-power red laser and blue LED was purchased from HTM Eletrônica (Fluence, São Paulo, Brazil). The low-power red laser (AlGaInP, 10 mW), with emission at 658 ± 5 nm and laser output at the cluster's center. The therapeutic low-power blue LED (1500 mW), with emission at 470 ± 10 nm, and constituted of three LEDs positioned as the vertices of an equilateral triangle in the cluster. The UVC source was a germicidal lamp (Philips, Netherlands).

2.2. Electrophoresis of pUC19 plasmids after exposure to blue LED and red laser

Samples of pUC19 plasmids (approximately 200 ng) were exposed to low-power red laser (3 and 9 J $^{-1}$ cm^2), low-power blue LED (160 and 640 J cm^{-2}), and simultaneous low-power red laser and blue LED (3 J cm^{-2} red laser and 160 J cm^{-2} blue LED, 9 J cm^{-2} red laser and 640 J cm^{-2} blue LED). Each plasmid sample was mixed with a loading buffer and applied on 0.8% neutral agarose gel. The electrophoresis procedure was performed in a horizontal chamber containing a tris-acetate-ethylenediamine tetraacetic acid (EDTA) buffer. The topological plasmid forms were visualized under fluorescence using a blue LED trans-illumination system (Kasvi, Brazil). The gels were photographed and the plasmid topological forms were quantified using the ImageJ software.

2.3. Evaluation of low-power blue LED and red laser exposure on survival in E. coli cultures and bacterial proliferation

Cultures of *E. coli* C600 (wild-type) in the stationary growth phase were divided into two groups (300 μl, $n = 8$, for each fluence). The first group was exposed to a low-power red laser (3 and 9 J $^{-1}$ cm^2), low-power blue LED (160 and 640 J cm^{-2}), and simultaneous low-power red laser and blue LED (3 J cm^{-2} red laser and 160 J cm^{-2} blue LED, 9 J cm^{-2} red laser and 640 J cm^{-2} blue LED). The second group was pre-exposed to the low-power red laser and a blue LED at the same conditions as the first group, followed by a single exposure to 50 mJ cm^{-2} of UVC. Bacterial cultures not exposed to the blue LED, and red laser and bacterial cultures exposed to UVC alone were used as controls. The cluster device controlled laser fluence, LED fluence, and irradiation time. UVC fluence was measured by an ultraviolet radiometer (Instrutherm, Brazil), and irradiation time at 100 s. The cluster device was positioned 7 cm above the bacterial suspension aliquots covering the entire surface. *E. coli* C600, DNA repair wild type, from frozen stocks were used to prepare bacterial cultures in Luria-Bertani nutritive medium up to reach stationary growth phase (10^{10} cells ml^{-1}, 18 h, 37 °C). Bacteria cultures were centrifuged (3.000 RPM, 15 min, clinical centrifuge) and suspended twice in sterile saline (0.9% NaCl). Bacterial suspensions were diluted in saline and spread 10 μl onto Petri dishes containing

rich medium. Colony forming unit (CFU) from irradiation incubation (37 °C, 18 h) were counted, and the survival fractions were calculated by the ratio between the numbers of viable cells from irradiation cultures and the numbers of viable cells from non-irradiated cultures. For the evaluation of bacterial proliferation, bacterial colony areas were measured by an ImageJ software and the area fractions were calculated by the ratio between the bacterial colony areas from irradiated cultures and the bacterial colony areas from non-irradiated cultures.

2.4. Evaluation of photolyase mRNA levels

2.4.1. Total RNA extraction. Bacterial suspensions of *E. coli* C600 in the stationary growth phase (10^{10} cells ml^{-1}, 18 h, 37 °C) were centrifuged (3000 RPM, 15 min, clinical centrifuge) and suspended twice in saline (400 μl, 0.9% NaCl). The bacterial suspensions were divided into 100 μl in 4 microtubes (for each fluence: control, LED 640 J cm^{-2}, laser 9 J cm^{-2}, and LED 640 J cm^{-2} + laser 9 J cm^{-2}). After irradiation, bacterial total RNA was extracted by a bacterial mRNA extraction kit (TRIzol^{lm} plus RNA purification kit, Invitrogen, USA). Briefly, bacterial suspension (100 μl) was incubated with a cell lysis solution (200 μl, 95 °C, 2 min), TRIzol was added (1 ml), homogenized, and incubated (5 min, room temperature). After that, chloroform (200 μl) was added, homogenized, and incubated (room temperature, 1 min) and the preparations were centrifuged (13.000 RPM, 15 min, 4 °C) to separate the organic phase from the aqueous phase. Supernatants were transferred to other tubes and isopropanol (1 ml) was added. After incubation (room temperature, 15 min), preparations were centrifuged again (13.000 RPM, 15 min, 4 °C), supernatants were discarded, and precipitates were washed with ethanol-diethyl pyrocarbonate (DEPC) (80% ethanol, DEPC 0.1% in water). After centrifugation (13.000 RPM, 5 min, 4 °C), supernatants were withdrawn, and total RNA was suspended in water-DEPC (0,1%) solution and stored (at −20 °C) until complementary DNA synthesis procedure.

2.4.2. Complementary DNA (cDNA) synthesis. cDNA synthesis was carried out using a two-step cDNA synthesis kit (Promega, USA). One microgram of RNA was reverse transcribed into cDNA using GoScipt reverse transcriptase according to the manufacturer's protocol using a total reaction of 20 μl. To determine the RNA concentration and purity was used a spectrophotometer for calculating the ratio of optical density at a wavelength ratio of 260/280 nm.

2.4.3. Real-time quantitative polymerase chain reaction (RT-qPCR). The RT-qPCRs were performed in Rotor-gene Q (Qiagen, Netherlands) using 2.5 μl of cDNA and 7.5 μl of mix containing free RNAse water (2 μl), the primer of interest (0.5 μl) and sybr green (5.0 μl) (Promega, USA) totalizing 10 μl in each reaction tube. Such reference genes were used araC, rpoA, and gyrA [17]. The interest gene was phr (*E. coli* photolyase).

2.5. Statistical analysis

Data of percentage of supercoiled plasmid forms, survival fraction, area ratio, and phr relative mRNA levels were analyzed by Kolmogorov–Smirnov test to verify normality. Comparison between the groups was done by the Kruskal–Wallis test followed by the Dunn test as a post hoc test with $p < 0.05$ as the less significant level. Statistical tests were performed by InStat GraphPad software (GraphPad InStat version 8.0 for Windows 10, GraphPad Prism Software, San Diego, CA, USA).

3. Results

3.1. Electrophoretic profile of plasmid DNA after exposure to low-power red laser and/or blue LED radiations

Figure 1 shows the quantification of the electrophoretic profile and the photograph of agarose gel electrophoresis of bacterial plasmid pUC19 exposed to low-power blue LED and/or red laser at different fluences. Data on this figure indicate that exposure to blue LED and/or red laser is not capable to alter the mobility of bacterial plasmid pUC19 indicating that there were no single and double-strand breaks in plasmid DNA. These findings were confirmed by quantification of supercoiled pUC19 plasmid topological forms.

3.2. Survival in E. coli C600 cultures after exposure to low-power blue LED and red laser radiations

Figure 2 shows survival fractions for *E. coli* C600 cultures exposed to low-power blue LED and red laser. Data on this figure suggest that exposure to low-power blue LED and the red laser did not significantly ($p > 0.05$) alter the bacterial survival at fluences evaluated.

3.3. Survival in E. coli C600 culture pre-exposed to low-power blue LED and red laser radiations followed by exposure to UVC

Figure 3 shows the survival fraction for pre-exposure to low-power blue LED and red laser radiation on *E. coli* C600 cells followed by exposure to 50 mJ cm^{-2} of UVC radiation. Data on this figure suggest that pre-exposure to red laser alone and simultaneous red laser and blue LED increase significantly ($p < 0.001$) the survival of *E. coli* C600 cultures exposed to UVC.

3.4. Evaluation of E. coli C600 colony areas after exposure to low-power blue LED and red laser radiations

Figure 4 shows the area ratios of *E. coli* C600 colonies from bacterial cultures exposed to low-power red laser and blue

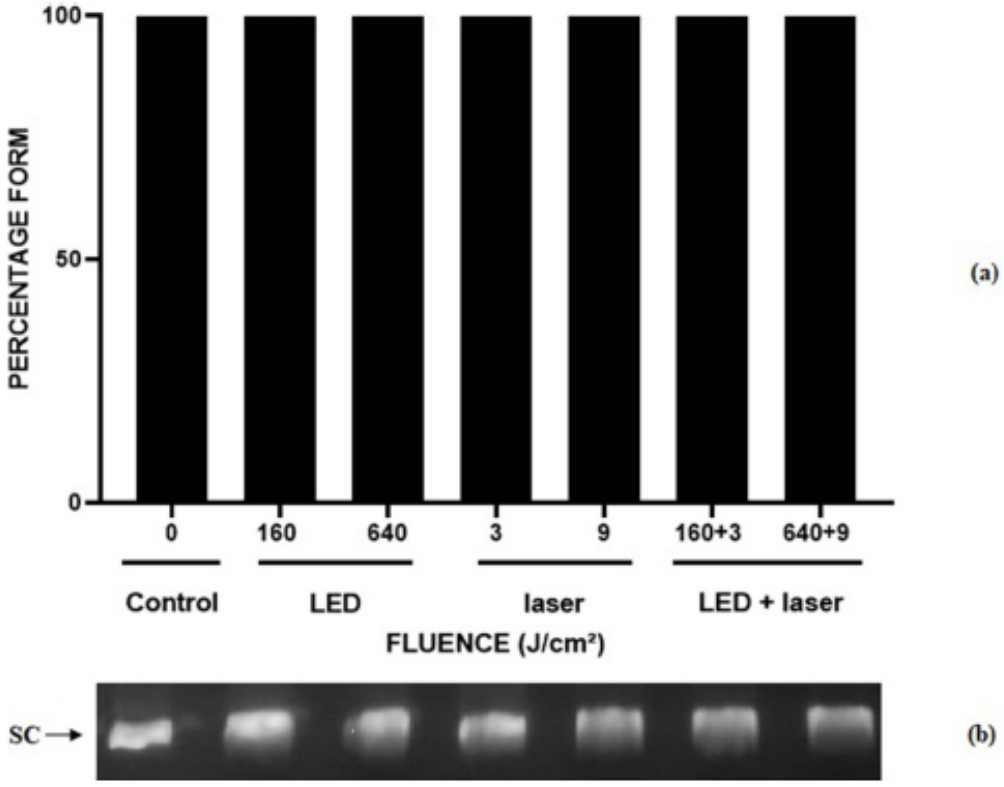

Figure 1. Percentages of plasmid forms (a) and photography of a representative agarose gel after exposure to low-power blue LED and red laser (b). Samples of pUC19 plasmids were exposed to a low-power red laser and a blue LED at different fluences, incubated with a loading buffer, and applied on 0.8% neutral agarose gel. The electrophoresis procedure was performed in a horizontal chamber containing tris-acetate-EDTA buffer. The topological plasmid forms were visualized under fluorescence using a blue LED trans-illumination system. Lanes: (1) pUC19 non-irradiated, (2) pUC19 + blue LED 160 J cm^{-2}, (3) pUC19 + blue LED 640 J cm^{-2}, (4) pUC19 + red laser 3 J cm^{-2}, (5) pUC19 + red laser 9 J cm^{-2}, (6) pUC19 + blue LED 160 J cm^{-2} + red laser 3 J cm^{-2}, (7) pUC19 + blue LED 640 J cm^{-2} + red laser 9 J cm^{-2}.

LED radiations. Data on this figure suggest that exposure to red laser at 3 and 9 J cm^{-2} significantly ($p < 0.05$) reduced the bacterial area ratio.

3.5. *Evaluation of E. coli C600 colonies areas pre-exposed to low-power blue LED and red laser radiations followed by exposure to UVC*

Figure 5 shows the colony area ratios for *E. coli* C600 pre-exposed to low-power blue LED and red laser radiation followed by exposure to UVC radiation at 50 mJ cm^{-2}. Data on this figure indicate significant ($p < 0.05$) alteration in the area ratios from bacterial cultures exposed to laser at 9 J^{-1} cm^2 and simultaneous blue LED and red laser at 160 + 3 J cm^{-2}. Bacterial cultures exposed at 9 J cm^{-2} increase the area ratio, indicating a higher proliferation rate while bacterial cultures exposed at 160 + 3 J cm^{-2} decrease their area, indicating a lower proliferation rate.

3.6. *Evaluation of phr mRNA relative levels in E. coli C600 cells after exposure to low-power blue LED and red laser radiations*

Figure 6 shows the phr mRNA relative levels in *E. coli* C 600 cells after exposure to low-power blue LED and red laser radiations. These findings indicate that exposure to these radiations did not significantly ($p > 0.05$) alter the phr mRNA levels in *E. coli* cells.

4. Discussion

Quantification of supercoiling and open circular forms of bacterial plasmids in agarose gels after electrophoresis has been used to evaluate single and double-strand breaks in DNA molecules induced by physical or chemical agents [18]. Bacterial plasmid pUC19 samples were exposed to low-power blue LED and red laser radiations and plasmid topological

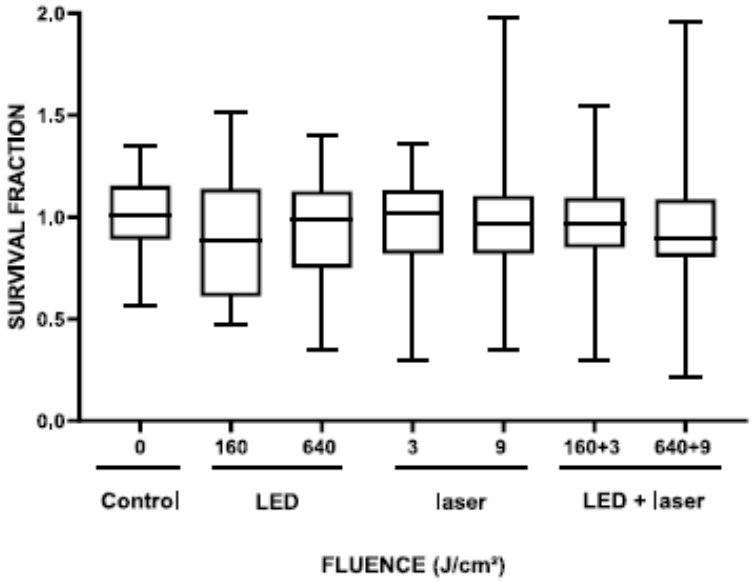

Figure 2. Survival in *E. coli* C600 cultures exposed to low-power blue LED and red laser. Bacterial cultures were exposed to low-power blue LED at 160 and 640 J cm^{-2}, low-power red laser at 3 and 9 J cm^{-2}, and simultaneous low-power blue LED and red laser at 160 + 3 J cm^{-2}, and 640 + 9 J cm^{-2}. Aliquots of bacterial cultures were diluted in saline (0.9% NaCl), spread onto Petri dishes containing nutritive medium, incubated (37 °C, 18 h), and colony forming unit (CFU) were counted to calculate survival fractions.

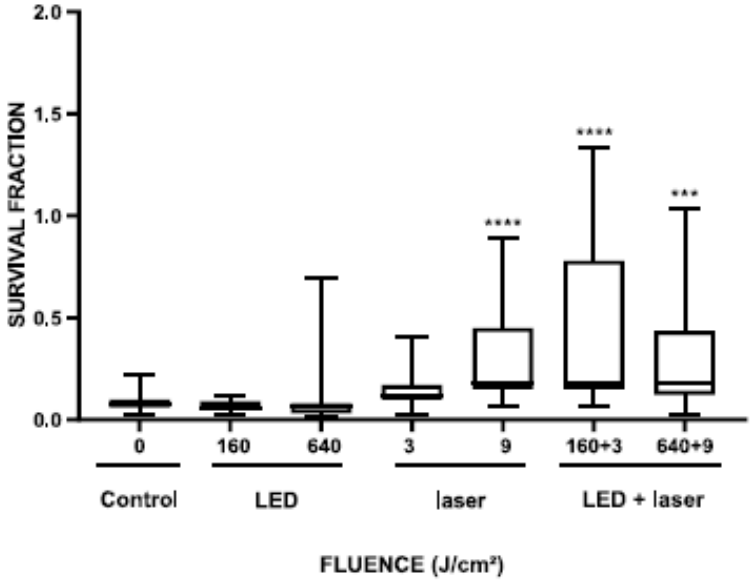

Figure 3. Survival in *E. coli* C600 cultures pre-exposed to low-power blue LED and red laser followed by exposure to 50 mJ cm^{-2} UVC radiation. Bacterial cultures were exposed to low-power blue LED at 160 and 640 J cm^{-2}, low-power red laser at 3 and 9 J cm^{-2} and simultaneous low-power blue LED and red laser at 160 + 3 J cm^{-2}, and 640 + 9 J cm^{-2} followed by a single exposure to 50 mJ cm^{-2} of UVC radiation. Aliquots of bacterial cultures were diluted in saline (0.9% NaCl), spread onto Petri dishes containing nutritive medium, incubated (37 °C, 18 h), and colony forming unit (CFU) were counted to calculate survival fractions. (****) $p < 0.0001$ when compared to the control group (exposed to UVC alone). (***) $p < 0.001$ when compared to the control group.

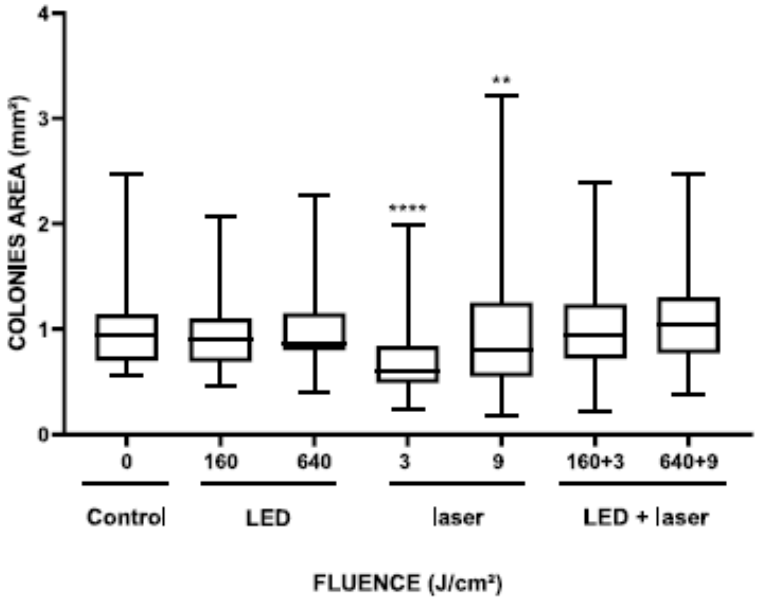

Figure 4. Colonies areas of *E. coli* C600 cultures exposed to low-power blue LED and red laser radiations at different fluences. Bacterial cultures were exposed to low-power blue LED at 160 and 640 J cm^{-2}, low-power red laser at 3 and 9 J cm^{-2} and simultaneous low-power blue LED and red laser at 160 + 3 J cm^{-2}, and 640 + 9 J cm^{-2}. Aliquots of bacterial cultures were diluted in saline (0.9% NaCl), spread onto Petri dishes containing nutritive medium, and incubated (37 °C, 18 h), and units forming colonies were measured by ImageJ Pro plus software for area measurement. (****) $p < 0.0001$ when compared to the colony area ratio of the control group (not exposed to red laser and blue LED). (**) $p < 0.001$ when compared to the colony area ratio of the control group.

forms analysis was carried out (figure 1). Results demonstrated the absence of induction of single or double-strand breaks exposed to such laser and LED (alone or simultaneously). These results agree with those reported by other authors, who reported a similar absence of effects by low-power red laser (658 nm) and near-infrared (830 nm) lasers at similar fluences [19, 20]. However, there are no available data about the electrophoretic profile of plasmids exposed to radiation emitted from the low-power blue LED.

Survival assays of prokaryotic cells have been used to evaluate the viability of cells after treatments with physical and chemical agents. Several studies used such a technique to evaluate the PBM effects on *E. coli* cells [18–23]. Our research demonstrated that a low-power red laser at 9 J cm^{-2} and simultaneous low-power red laser at 3 J cm^{-2} and a blue LED at 160 J cm^{-2} as well as at 9 J cm^{-2} and 640 J cm^{-2} protects the *E. coli* C600 cells from the bactericidal effect of UVC radiation (figure 3). Similar finds were reported in *E. coli* AB1157 cultures in the exponential growth phase pre-exposed to low-power red laser (660 nm) at 8 J cm^{-2} [18]. Another study carried out by Kohli and Gupta (2003) reports photoprotection and an increase in bacterial survival in *E. coli* AB1157 exposed to UVC after exposure to low-power red (632.8 nm) laser at 7 kJ m^{-2} [21]. This suggests that a low-power red laser as well as simultaneous low-power red laser and a blue LED at therapeutic fluence increases survival in *E. coli* cultures exposed to UVC.

Colonies area assays could be used for the evaluation of cell proliferation of prokaryotic cells to estimate the PBM-induced proliferative or inhibitory effects [24]. The *E. coli* C600 cells were exposed to low-power blue LED and red laser at different fluences and the results indicated alterations of bacterial proliferation in cultures exposed to low-power red laser (figure 4). The results suggested that a low-power red laser at 3 J cm^{-2} decreases the proliferation rate of *E. coli* C600 cells, but a low-power red laser at 9 J cm^{-2} increases the proliferation rate. Also, pre-exposure to low-power blue LED and red laser altered the bacterial colony area of *E. coli* C600 cells exposed to UVC radiation (figure 5). The results suggest that pre-exposure to low-power red laser at 9 J cm^{-2} increases cell proliferation, but simultaneous pre-exposure to low-power blue LED and red laser at 160 and 9 J cm^{-2}, respectively, decreases cell proliferation. Karu (1994) demonstrated the dose dependence for stimulation of *E. coli* proliferation by He–Ne laser (632.8 nm) and indicated that the biochemical reactions providing for growth stimulation occur by two different channels, one being activated by irradiation dose and the other by a critical value of the exposure time [24]. Studies related to the blue light effects emitted from LEDs have suggested the inactivation of several prokaryotes, including *E. coli* [25–27]. Results demonstrated that exposure to low-power blue LED at 160 J cm^{-2} and 640 J cm^{-2} did not alter the survival and proliferation of *E. coli* C600 cultures (figures 2 and 4).

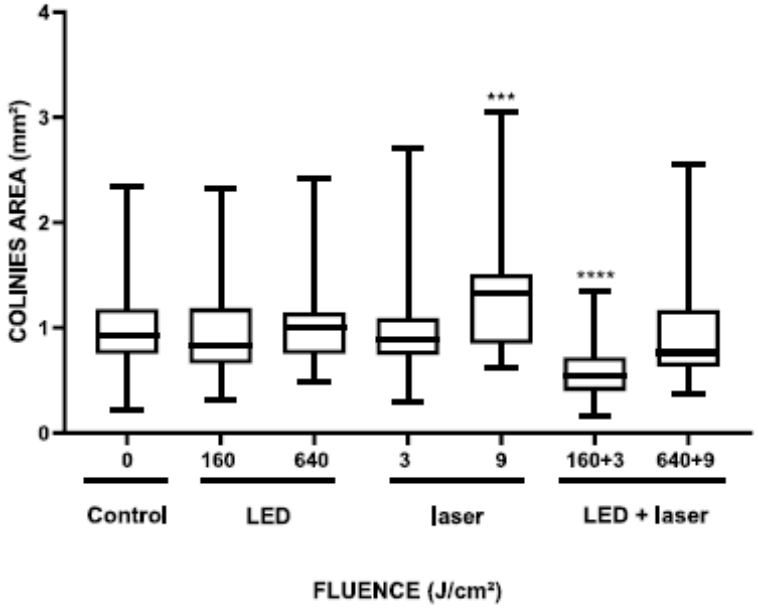

Figure 5. Colony area ratios from *E. coli* C600 cultures pre-exposed to low-power blue LED and red laser radiations at different fluences followed by exposure to UVC radiation. *E. coli* C600 cultures were exposed to low-power blue LED at 160 and 640 J cm^{-2}, low-power red laser at 3 and 9 J cm^{-2}, and simultaneous low-power blue LED and red laser at 160 + 3 J cm^{-2}, and 640 + 9 J cm^{-2}. Aliquots of bacterial cultures were diluted in saline (0.9% NaCl), spread onto Petri dishes containing nutritive medium, incubated (37 °C, 18 h), and colony forming unit (CFU) were measured by ImageJ Pro plus software for area measurement. (****) $p < 0.0001$ when compared to the colonies area of the control group. (***) $p = 0.001$ when compared to the colonies area of the control group.

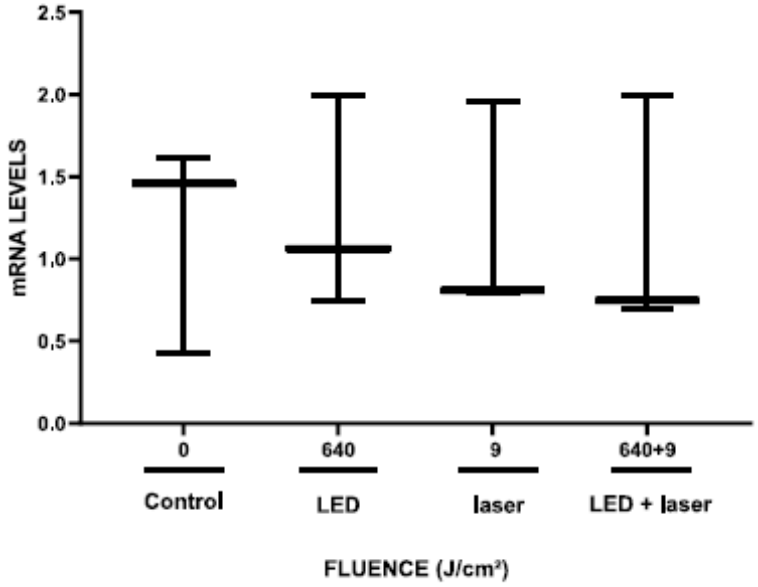

Figure 6. Phr relative mRNA levels in *E. coli* C600 cells after exposure to low-power red laser and blue LED. Aliquots of *E. coli* C600 were exposed to low-power blue LED at 640 J cm^{-2}, low-power red laser at 9 J cm^{-2}, and simultaneous low-power blue LED and red laser (640 and 9 J cm^{-2}, respectively). Total RNA extraction was performed to cDNA synthesis and quantification of relative phr mRNA levels by reverse transcription-quantitative polymerase chain reaction.

RT-qPCR measurements are used to assess mRNA relative levels from genes in prokaryotic and eukaryotic cells [1, 17, 28–30]. *E. coli* C600 cells were exposed to low-power blue LED and red laser at different fluences and the mRNA relative levels from the photolyase gene (phr) were assessed. The results suggested that exposure to low-power blue LED and the red laser does not alter phr mRNA relative levels in *E. coli* C600 (figure 6). This is the first time the effects of low-power blue LED and a red laser on phr gene involved in the photoreactivation mechanism have been evaluated. These findings are relevant due to the inability of blue radiation to modulate the DNA repair mechanism dependent on blue light. However, studies have shown that low-power lasers modulate the gene expression related to DNA repair mechanisms, such as base excision repair and nucleotide excision repair, in biological tissues [28–30].

5. Conclusion

Our research suggests that exposure to blue and red lights emitted from low-power LEDs and lasers does not cause DNA strand breaks in bacterial plasmid and does not alter the survival and mRNA levels from photolyase gene in *E. coli*, but increases bacterial and proliferation in *E. coli* cultures exposed to UVC radiation depending on LED and laser fluences.

Acknowledgments

This research was supported by Fundação de Amparo à Pesquisa do Estado do Rio de Janeiro (FAPERJ), Conselho Nacional de Desenvolvimento Científico e Tecnológico (CNPq), and Universidade do Estado do Rio de Janeiro (UERJ).

Conflict of interest

The authors declare that they have no conflict of interest.

References

[1] Trajano E T, Mencalha A L, Costa A M, Pôrto L C and Fonseca A S 2014 Expression of DNA repair genes in burned skin exposed to low-level red laser *Lasers Med. Sci.* **29** 1953–7

[2] Peplow P V, Chung T Y and Baxter G D 2010 Laser photobiomodulation of wound healing: a review of experimental studies in mouse and rat animal models *Photomed. Laser Surg.* **28** 291–35

[3] Diogo M L G *et al* 2021 Effect of blue light on acne vulgaris: a systematic review *Sensors* **21** 1–13

[4] Heiskanen V and Hamblin M R 2018 Photobiomodulation: lasers vs light emitting diodes? *Photochem. Photobiol. Sci.* **17** 1003–17

[5] Dai T, Gupta A, Murray C K, Vrahas M S, Tegos G P and Hamblin M R 2012 Blue light for infectious diseases: *Propionibacterium acnes, Helicobacter pylori*, and beyond? *Drug Resist. Update* **14** 223–36

[6] Martins W A, Polignano G A C, Guimarães O R, Geller M, Paoli F and Fonseca A F 2015 Dichromatic laser radiation effects on DNA of *Escherichia coli* and plasmids *Laser Phys. Lett.* **25** 045603

[7] Karu T 2000 Mechanisms of low-power laser light action on cellular level *Proc. SPIE* **4159** 1–17

[8] Karu T I, Pyatibrat L V and Kalendo G S 2004 Photobiological modulation of cell attachment via cytochrome c oxidase *Photochem. Photobiol. Sci.* **3** 211–6

[9] Chatterjee N and Walker G C 2017 Mechanisms of DNA damage, repair and mutagenesis *Photochem. Photobiol.* **58** 235–63

[10] Portero L R, Alonso D, Zannier F, Vazquez M P, Fárias M E, Gärtner W and Albarracín V H 2018 Photolyases and cryptochromes in UV-resistant bacteria from high-altitude Andean Lakes *Photochem. Photobiol.* **95** 315–30

[11] Kavakli I H *et al* 2017 The photolyase/cryptochrome family of proteins as DNA repair and transcriptional repressors *Photochem. Photobiol.* **93** 93–103

[12] Zhang M, Wang L and Zhong D 2017 Photolyase: dynamics and mechanisms of repair of sun-induced DNA damage *Photochem. Photobiol.* **93** 78–92

[13] Li X, Cai M, Wang L, Niu F, Yang D and Zhang G 2019 Evaluation survey of microbial disinfection methods in UV-LED water treatments systems *Sci. Total Environ.* **659** 1415–27

[14] Beck S E, Ryu H, Boczek L A, Cashdollar J L, Jeanis K M, Rosenblum J S, Lawal O R and Linden K G 2017 Evaluating UV-C LED disinfection performance and investigating potential dual-wavelengths synergy *Water Res.* **109** 207–16

[15] Nicolau T, Filho N G, Padrão J and Zille A 2022 A comprehensive analysis of the UVC LEDs applications and decontamination capability *Materials* **15** 1–31

[16] Yang J H, Wu U I, Huei-Min S and Sheng W H 2019 Effectiveness of an ultraviolet-C disinfection system for reduction of healthcare-associated pathogens *J. Microbiol. Immunol. Infect.* **52** 487–93

[17] Teixeira A F, Machado Y L E C, Fonseca A D and Mencalha A L 2016 Low-level lasers and mRNA levels of reference genes used in *Escherichia coli Laser Phys. Lett.* **13** 115602

[18] Canuto K S, Sergio L P S, Guimarães O R, Geller M and Fonseca A S 2015 Low-level red laser therapy alters effects of ultraviolet C radiation on *Escherichia coli* cells *Braz. J. Med. Biol. Res.* **48** 939–44

[19] Fonseca A S, Moreira T O, Paixão D L, Farias F M, Guimarães O R, Paoli S, Geller M and Paoli F 2010 Effect of laser therapy on DNA damage *Lasers Surg. Med.* **42** 481–8

[20] Fonseca A S, Geller M, Filho M B, Valença S S and Paoli F 2012 Low-level infrared laser effect on plasmid DNA *Lasers Med. Sci.* **27** 121–30

[21] Kohli R and Gupta P K 2003 Irradiance dependence of the He-Ne laser-induced protection against UVC radiation in *E. coli* strains *J. Photochem. Photobiol.* B **69** 161–7

[22] Fonseca A S, Teixeira A F, Presta G A, Geller M, Valença S S and Paoli F 2012 Low intensity infrared laser effects on *Escherichia coli* cultures and plasmid DNA *Laser Phys.* **22** 1635–41

[23] Thomé A M C, Souza B P, Mendes J P M, Cardoso A F R, Soares L C, Trajano E T L and Fonseca A S 2018 Dichromatic and monochromatic laser radiation effects on antibiotic resistance, biofilm formation, and division rate of *Pantoea agglomerans Laser Phys. Lett.* **28** 065606

[24] Karu T, Tiphlova O, Esenaliev R and Letokhov V 1994 Two different mechanisms of low-intensity laser photobiological effects on *Escherichia coli J. Photochem. Photobiol.* **27** 155–61

[25] Lucca J, Carter- W, Williamsn K A and Bhatnagar D 2012 Blue light (470 nm) effectively inhibits bacterial and fungal growth *Lett. Appl. Microbiol.* **55** 460–6

[26] Kim S, Kim J, Lim W, Jeon S, Kim O, Koh J T, Kim C S, Choi H and Kim O 2013 *In vitro* bactericidal effects of 625, 525 and 425 nm wavelength (red, green and blue) light-emitting diode irradiation *Lasers Surg. Med.* **31** 554–62

[27] Maclean M, MacGregor S J, Anderson J G and Woolsey G 2009 Inactivation of bacterial pathogens following exposure to light from 405-nanometer light emitting diode array *Appl. Environ. Microbiol.* **75** 1932–7

[28] Fonseca A S, Mencalha A L, Campos V M A, Samara C F, Peregrino A A F, Geller M and Paoli F 2013 DNA repair gene expression in biological tissues exposed to low-intensity infrared laser *Lasers Med. Sci.* **28** 1077–84

[29] Fonseca A S, Magalhães L A G, Mencalha A L, Ferreira-Machado S C, Geller M and Paoli F 2014 Low-intensity red and infrared lasers on XPA and XPC gene expression *Laser Phys. Lett.* **11** 095601

[30] Fonseca A S, Magalhães L A G, Mencalha A L, Geller M and Paoli F 2014 Low intensity infrared laser affects expression of oxidative DNA repair genes in mitochondria and nucleus *Laser Phys.* **24** 115605

APÊNDICE B – Low-power red laser and blue LED on circadian gene mRNA levels in human breast cancer cells (artigo publicado)

IOP Publishing | Astro Ltd Laser Physics
Laser Phys. 33 (2023) 115602 (7pp) https://doi.org/10.1088/1555-6611/acfd9b

Low-power red laser and blue LED on circadian gene mRNA levels in human breast cancer cells

Rickson Souza Ribeiro[1], Juliana Alves Rodrigues[1], Márcia dos Santos Soares[1], Andre Luiz Mencalha[1] and Adenilson de Souza da Fonseca[1,2,3,*]

[1] Departamento de Biofísica e Biometria, Instituto de Biologia Roberto Alcantara Gomes, Universidade do Estado do Rio de Janeiro, Boulevard 28 de setembro, 87, Vila Isabel, Rio de Janeiro 20551030, Brazil
[2] Departamento de Ciências Fisiológicas, Instituto Biomédico, Universidade Federal do Estado do Rio de Janeiro, Rua Frei Caneca, 94, Rio de Janeiro 20211040, Brazil
[3] Centro de Ciências da Saúde, Centro Universitário Serra dos Órgãos, Avenida Alberto Torres, 111, Teresópolis, Rio de Janeiro 25964004, Brazil

E-mail: adnfonseca@yahoo.com.br

Received 8 September 2023
Accepted for publication 21 September 2023
Published 6 October 2023

Abstract

Low-power blue light-emitting diode (LED) and red laser have been used for therapeutic proposals based on photobiomodulation (PBM). This effect is trigged after absorption of radiation by photoacceptors, which lead to molecular, cellular and systemic responses. Cryptochromes are involved in circadian cycle control, and associated with development and progression of tumors. Despite such proteins are able to absorb violet-blue lights, there are few data on their participation in PBM. Thus, this work aims to evaluate the effects of radiations emitted by low-power blue LED (470 nm) and red laser (658 nm) on mRNA levels from cryptochromes genes as well as those from involved in their regulation in human breast cancer cells. The MCF-7 and MDA-MB-231 cells were exposed to low-power blue LED (470 nm, 640 J cm^{-2}) and red laser (660 nm, 9 J cm^{-2}), and relative mRNA levels from CRY1, CRY2, PER2, BMAL1 and CLOCK genes were evaluated by reverse transcription-quantitative polymerase chain reaction. The results suggested that exposure to low-power blue LED and red laser do not alter the mRNA levels from cryptochromes genes, and those involved in their regulation, in MCF-7 and MDA-MB-231 human breast cancer cells.

Keywords: cryptochromes, laser, LED, mRNA levels, photobiomodulation

1. Introduction

Low-power light-emitting diodes (LEDs) and lasers are devices that emitted radiations with clinical applications, such as pain relief, wound healing, treatment of acne and anti-inflammatory activity based on the photobiomodulation (PBM) process [1–4]. Lasers are able to emit monochromatic, coherent, and collimated radiation, and LEDs emit quasi-monochromatic, non-coherent, and non-collimated radiations [5, 6]. The wavelength, coherence, and collimation are some of key factors for PBM effect, which is the base for clinical protocols based on low-power radiation sources, as LEDs and lasers (Fonseca, 2020). PBM occurs as a consequence of photon-photoacceptor interactions, which lead to the production of trigger molecules capable of inducing signaling, effector molecules, and transcription factors, which are responsible for cellular effects, which in turn are responsible for systemic effects [5, 7].

* Author to whom any correspondence should be addressed.

Cytochrome C oxidase is able to absorb photons belong red and near-infrared (600 up to 1100 nm) range of electromagnetic spectrum, and in consequence ATP, DNA and RNA synthesis is increased [8]. Cryptochromes are intracellular proteins that present a dinucleotide of flavin and adenine in their structure, which is able to absorb radiations in violet-blue (400 up to 500 nm) range of electromagnetic spectrum [9]. The cryptochromes are involved in the control of circadian rhythm, acting as a transcriptional repressor, and their activity oscillates during periods of 24 h [10–12]. Approximately 50% of genes are on influence of the circadian clock, these genes are so-called clock-controlled genes [13]. The circadian clock is controlled by loops of positive and negative feedback of proteins CRY1, CRY2, BMAL1, CLOCK, PER1, PER2, and PER3. The BMAL1 (basic helix-loop-helix ARNT like 1) and CLOCK (clock circadian regulator) genes are positive regulators (positive feedback) and form heterodimers (BMAL1::CLOCK) in the cytoplasm that move to nucleus, and bind at gene promotors (CACGTG) in DNA to stimulate the expression of the period proteins (PER1, PER2 and PER3) and cryptochromes (CRY1 and CRY2). The PER and CRY are negative regulators (negative feedback), and form heterodimers (PER::CRY) in cytoplasm to act in the nucleus to inhibit BMAL1::CLOCK, and to reduce the expression of clock-controlled genes, including PER and CRY proteins, which restarting the cycle [12–14].

A relationship between circadian genes and the development of several types of tumors has been proposed [15, 16], and studies have demonstrated the participation of circadian genes on DNA repair mechanisms, cell cycle, apoptosis, and metabolism [15–19]. Despite the cryptochromes (CRY1 and CRY2) absorb violet-blue lights, there are few data on their participation in PBM. Thus, this work aims to evaluate the effects of radiations emitted by low-power blue LED (470 nm) and red laser (658 nm) on mRNA levels from cryptochromes genes as well as those from involved in their regulation in human breast cancer cells.

2. Material and methods

2.1. Low-power red laser and blue LED source

The cluster containing a therapeutic low-power red laser and blue LED was purchased from HTM Eletrônica (Fluence, São Paulo, Brazil). The low-power red laser (AlGaInP, 10 mW), which emission at 658 ± 5 nm and laser exit point at the cluster center. The therapeutic low-power blue LED (1500 mW) was constituted of three LEDs positioned as the vertices of an equilateral triangle, which emission at 470 ± 10 nm in the cluster.

2.2. Cell culture conditions, low-power red laser, and blue LED exposure on MCF-7 and MDA-MB 231 cultures

The MCF-7 and MDA-MB 231 breast cancer cells cultures were maintained in DMEM and RPMI medium (Sigma-Aldrich, USA), respectively, supplemented with 10% bovine fetal serum FBS (Sigma-Aldrich, USA) and 1% penicillin-streptomycin (Life Technologies, USA) and sustained in a humidified atmosphere at 37 °C and 5% CO_2 until reaching 60%–70% confluence. Cells were washed in phosphate-buffered saline (PBS) twice, trypsinized, centrifuged (1500 RPM, 5 min), and suspended in 4 ml of DMEM or RPMI medium supplemented with 10% fetal bovine serum. Aliquots (1 ml) were separated in 4 microtubes (Eppendorf, 1.5 ml), centrifuged (7200 RPM, 2 min) and the supernatant was removed and added 50 μl of PBS. Each cell suspension aliquot in the microtubes was exposed to a low-power source, being: (i) control, (ii) blue LED (640 J cm^{-2}), (iii) red laser (9 J cm^{-2}) and (iv) simultaneous blue led and red laser (640 J cm^{-2} + 9 J cm^{-2}). The control group was the not exposed cell suspension aliquot. The cluster device was positioned 7 cm above the cell suspension aliquots covering the entire surface. After exposure, the cells were suspended in 1 ml of DMEM or RPMI medium supplemented and incubated in t-flasks of 25 cm^2 during 48 h in a humidified atmosphere at 37 °C and 5% CO_2.

2.3. Evaluation of CRY1, CRY2, PER2, BMAL1, and CLOCK mRNA levels

2.3.1. Total RNA extraction. After incubation, the t-flask was washed twice with PBS and added TRIzol (1 ml), homogenized, incubated (5 min, room temperature), and centrifuged (13 000 RPM, 10 min, 4 °C). After that, the supernatant was transferred to other microtubes, added chloroform (200 μl), homogenized, and incubated (1 min, room temperature), and the preparations were centrifuged (13 000 RPM, 15 min, 4 °C) to separate the organic phase from the aqueous phase. Supernatants were transferred to other tubes and isopropanol (1 ml) was added. After incubation (room temperature, 15 min), preparations were centrifuged again (13 000 RPM, 15 min, 4 °C), supernatants were discarded, and precipitates were washed with ethanol-DEPC (80% ethanol, DEPC 0.1% in water). After centrifugation (13 000 RPM, 5 min, 4 °C), supernatants were withdrawn, and total RNA was suspended in water-DEPC (0,1%) solution to determine the RNA concentration, and purity, was used a spectrophotometer for calculating the ratio of optical density at a wavelength ratio of 260/280 and 230/260 nm. After that, isopropanol (1 ml) was added and the total mRNA preparation was stored (at −20 °C) until complementary DNA synthesis procedure.

2.3.2. Complementary DNA synthesis. Complementary DNA (cDNA) synthesis was carried out using a two-steps cDNA synthesis kit (Promega, USA). One microgram of total RNA was reverse transcribed into cDNA using GoScipt reverse transcriptase according to the manufacturer's protocol using a total reaction of 20 μl.

2.3.3. Real-time polymerase chain reaction (RT-qPCR). The real-time quantitative polymerase chain reactions (RT-qPCR) were performed in Rotor-gene Q (Qiagen, Netherlands) using 2.5 μl of cDNA and 7.5 μl of mix containing free RNAse water (2.0 μl), primer of interest (0.5 μl) and sybr green (5.0 μl)

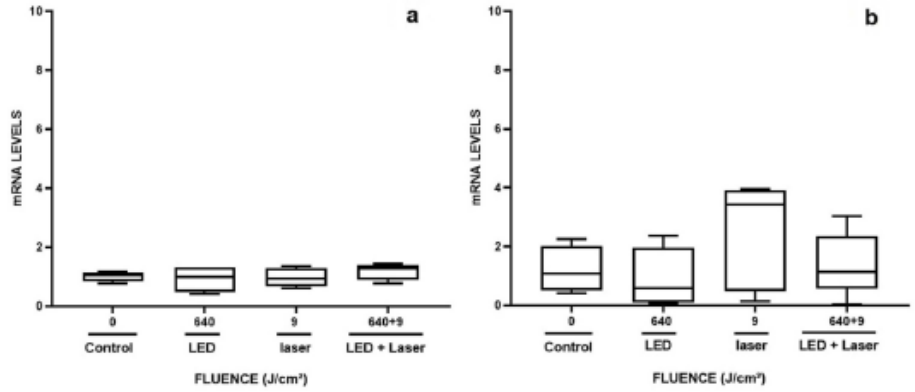

Figure 3. *PER2* relative mRNA levels in MCF-7 cells (a) and MDA-MB-231 (b) after exposure to low-power red laser and blue LED. Aliquots from MCF-7 and MDA-MB-231 cell cultures were exposed to low-power blue LED at 640 J cm^{-2}, low-power red laser 9 J cm^{-2}, and simultaneous low-power blue LED and red laser (640 and 9 J cm^{-2}, respectively). After that, *PER2* relative mRNA levels were evaluated by RT-qPCR.

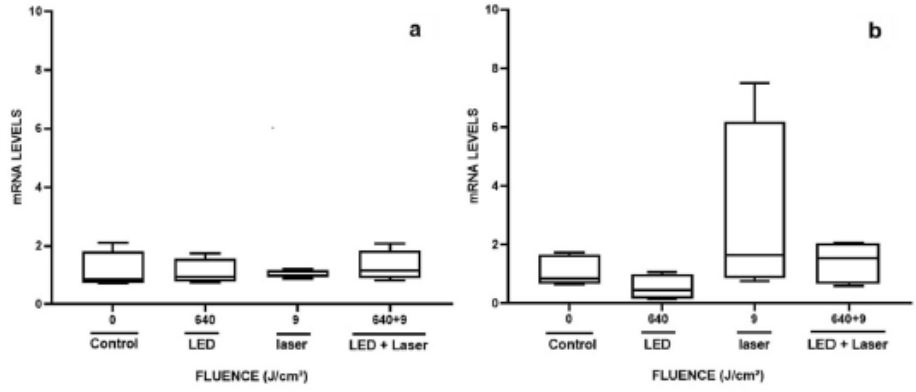

Figure 4. *BMAL1* relative mRNA levels in MCF-7 cells (a) and MDA-MB-231 (b) after exposure to low-power red laser and blue LED. Aliquots from MCF-7 and MDA-MB-231 cell cultures were exposed to low-power blue LED at 640 J cm^{-2}, low-power red laser 9 J cm^{-2}, and simultaneous low-power blue LED and red laser (640 and 9 J cm^{-2}, respectively). After that, *BMAL1* relative mRNA levels were evaluated by RT-qPCR.

LED (640 J cm^{-2}), red laser (9 J cm^{-2}) and simultaneously blue LED and red laser (640 + 9 J cm^{-2}). Similar to those *CRY1* and *CRY2* relative mRNA levels, data on this figure suggest that exposure to low-power red laser and blue LED, alone or simultaneously, did not significantly ($p > 0.05$) alter the *PER2* mRNA levels.

Figure 4 shows the *BMAL1* relative mRNA levels, in MCF-7 and MDA-MB-231 cells, after exposure to low-power blue LED (640 J cm^{-2}), red laser (9 J cm^{-2}) and simultaneously blue LED and red laser (640 + 9 J cm^{-2}). Similar to those *CRY1*, *CRY2* and *PER2* relative mRNA levels, data on this figure suggest that exposure to low-power red laser and blue LED, alone or simultaneously, did not significantly ($p > 0.05$) alter the *PER2* mRNA levels.

Figure 5 shows the *CLOCK* relative mRNA levels, in MCF-7 and MDA-MB-231 cells, after exposure to low-power blue LED (640 J cm^{-2}), red laser (9 J cm^{-2}) and simultaneously blue LED and red laser (640 + 9 J cm^{-2}). Similar to other genes, data on this figure suggest that exposure to low-power red laser and blue LED, alone or simultaneously, did not significantly ($p > 0.05$) alter the *CLOCK* mRNA levels.

4. Discussion

Studies on the PBM induced by exposure to low-power red laser and blue LED in MCF-7 and MDA-MB-231 cells have already been performed [21, 22]. However, there are no

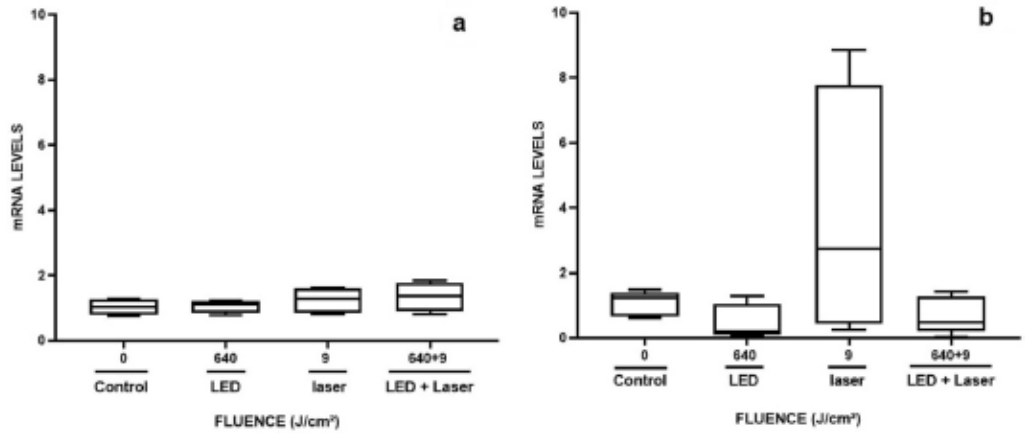

Figure 5. *CLOCK* relative mRNA levels in MCF-7 cells (a) and MDA-MB-231 (b) after exposure to low-power red laser and blue LED. Aliquots from MCF-7 and MDA-MB-231 cell cultures were exposed to low-power blue LED at 640 J cm^{-2}, low-power red laser 9 J cm^{-2}, and simultaneous low-power blue LED and red laser (640 and 9 J cm^{-2}, respectively). After that, *CLOCK* relative mRNA levels were evaluated by RT-qPCR.

experimental data of effects of radiations emitted from these low-power devices on circadian genes.

The RT-qPCR measurements are used to assess mRNA relative levels from genes in prokaryotic and eukaryotic cells [20, 23–27]. MCF-7 and MDA-MB-231 cells had their total mRNA extracted and their relative levels of circadian genes *CRY1, CRY2, PER2, BMAL1*, and *CLOCK* were evaluated after exposure to low-power red laser and blue LED, both alone and simultaneously. The results suggest that exposure to low-power blue LED and red laser does not alter the relative mRNA levels of these genes in both cell lines evaluated (figures 1–5).

The *CRY1* and *CRY2* genes also work on cell cycle regulation, such as deficient mice in these genes present deregulations in expression of WEE1 and cyclin D1 proteins, which lead disturbs in the cell cycle [28]. Studies demonstrated participation of CRY1 and CRY2 proteins in DNA repair in fibroblast knockout, which make such cells more sensitive to ionizing radiations [29, 30]. *CRY1* and *CRY2* mRNA relative levels were evaluated in MCF-7 and MDA-MB-231 cells. Exposure to low-power red laser and blue LED does not alter the *CRY1* and *CRY2* relative levels (figures 1 and 2), at least at radiation exposure evaluated.

PER genes have been reported in several types of cancer, where they are involved in tumorigenesis and tumor progression, due to such genes are related with cell cycle control, response to DNA damage, and apoptosis [31–33]. *PER2* gene has been reported as a gene involved in the cell cycle and apoptosis, through the regulation of c-MYC, cyclinD1, and GADD45 [14, 34, 35]. Expression of such proteins is associated with cell cycle arrest and proliferation control. Cultures of human breast cancer cells utilized in this study present expression of *PER2*, but the exposure to low-power red laser and blue LED did not alter the *PER2* mRNA levels in MCF-7 and MDA-MB-231 cells (figure 3). Deficient expression of *PER2* is related to higher incidence of tumors, due to a higher genomic stability and sensibility to radiation [14, 36]. Altered *PER3* gene expression is related to high risk of tumors, but the exact mechanism remains uncertain. Otherwise, studies have showed a relationship between mutations in *PER3* gene and recurrence of positive breast cancer to estrogen receptors [15, 31]. Exposure to low-power red laser and blue LED did not alter the expression profile of the *PER3* gene in MCF-7 and MDA-MB-231 cells.

The *BMAL1* and *CLOCK* genes are central regulators responsible to coordinate the expression of several genes, among them *PER1, PER2, PER3, CRY1*, and *CRY2*. Also, regulate the process of tumor suppression, such as cell cycle arrest by the expression of the *WEE1* gene and inhibition of CDK1 allowing G2/M transition and block of apoptosis by repression of DEC2 anti-apoptotic regulator [14, 37, 38]. The results suggest that do not have alterations in expression levels of *BMAL1* and *CLOCK* after exposure to low-power red laser and blue LED in both MCF-7 and MDA-MB-231 cells (figures 4 and 5).

5. Conclusion

Our research suggests the results suggested that exposure to low-power blue LED and red laser do not alter the mRNA levels from cryptochromes genes, and those involved in their regulation, in MCF-7 and MDA-MB-231 human breast cancer cells.

Acknowledgments

This research was supported by Fundação de Amparo à Pesquisa do Estado do Rio de Janeiro (FAPERJ), Conselho Nacional de Desenvolvimento Científico e Tecnológico

(CNPq), and Universidade do Estado do Rio de Janeiro (UERJ).

Compliance with ethical standards

Not applicable.

Conflict of interest

The authors declare that they have no conflict of interest

References

[1] Langella L G, Casalechi H L, Tomazoni S S, Johnson D S, Albertini R, Pallota R C, Marcos R L, Carvalho P T C and Leal-Junior E C P 2018 Photobiomodulation therapy (PBMT) on acute pain and inflammation in patients who underwent total hip arthroplasty—a randomized, triple-blind, placebo-controlled clinical trial *Lasers Med. Sci.* **33** 1933–40

[2] Petz F F C, Félix J V C, Roehrs H, Pott F S, Stocco J G D, Marcos R L and Meier M J 2020 Effect of photobiomodulation on repairing pressure ulcers in adult and elderly patients: a systematic review *Photochem. Photobiol.* **96** 191–9

[3] Diogo M L G *et al* 2021 Effect of blue light on acne vulgaris: a systematic review *Sensors* **21** 6943

[4] González-Muñoz A, Cuevas-Cervera M, Pérez-Montilla J J, Aguilar-Núñez D, Hamed-Hamed D, Aguilar-García M, Pruimboom L and Navarro-Ledesma S 2023 Efficacy of photobiomodulation therapy in the treatment of pain and inflammation: a literature review *Healthcare* **11** 938

[5] Smith K C 2005 Laser (and LED) therapy is phototherapy *Photomed. Laser Surg.* **23** 78–80

[6] Niemz M H 2007 *Laser-Tissue Interactions* (Springer)

[7] Silva T G, Ribeiro R S, Mencalha A L and Fonseca A S 2023 Photobiomodulation at molecular, cellular, and systemic levels *Lasers Med. Sci.* **38** 136

[8] Karu T I, Pyatibrat L V and Kalendo G S 2004 Photobiological modulation of cell attachment via cytochrome c oxidase *Photochem. Photobiol. Sci.* **3** 211–6

[9] Sancar A 2004 Regulation of the mammalian circadian clock by cryptochrome *J. Biol. Chem.* **279** 34079–82

[10] Sancar A, Lindsey-Boltz L A, Kang T-H, Reardon J T, Lee J H and Ozturk N 2010 Circadian clock control of the cellular response to DNA damage *FEBS Lett.* **584** 2618–25

[11] Masri S, Kinouchi K and Sassone-Corsi P 2015 Circadian clocks, epigenetics, and cancer *Curr. Opin. Oncol.* **27** 50–56

[12] Kavakli I H *et al* 2017 The photolyase/cryptochrome family of proteins as DNA repair enzymes and transcripional repressors *Photochem. Photobiol.* **93** 93–103

[13] Chan A B and Lamia K A 2020 Cancer, hear my battle CRY *J. Pineal Res.* **69** e12658

[14] Shafi A A and Knudsen K E 2019 Cancer and the circadian clock *Cancer Res.* **79** 3806–14

[15] Chen S-T, Choo K-B, Hou M-F, Yeh K-T, Kuo S-J and Chang J-G 2005 Deregulated expression of the PER1, PER2 and PER3 genes in breast cancers *Carcinogenesis* **26** 1241–6

[16] Oshima T *et al* 2011 Expression of circadian genes correlates with liver metastasis and outcomes in colorectal cancer *Oncol. Rep.* **25** 1439–46

[17] Rahman S, Pavelic S K and Markova-Car E 2019 Circadian (De)regulation in head and neck squamous cell carcinoma *Int. J. Mol. Sci.* **20** 2662

[18] Dong Z *et al* 2019 Targeting glioblastoma stem cells throught disruption of the circadian clock *Cancer Discovery* **9** 1556–73

[19] Koritala B S C *et al* 2021 Night shift schedule causes circadian dysregulation of DNA repair genes and elevated DNA damage in humans *J. Pineal Res.* **70** e12726

[20] Teixeira A F, Canuto K S, Rodrigues J A, Fonseca A S and Mencalha A L 2017 Low-level lasers alter mRNA levels from traditional reference genes used in breast cancer cells *Laser Phys.* **27** 075601

[21] Teixeira A F, Alves J R, Fonseca A S and Mencalha A L 2018 Low power blue LED exposure increases effects of doxorubicin on MDA-MB-231 breast cancer cells *Photodiagnosis Photodyn. Ther.* **24** 250–5

[22] Aniogo E C, George B P and Abrahamse H 2023 Photobiomodulation improves anti-tumor efficacy of photodynamic therapy against resistant MCF-7 cancer cells *Biomedicines* **11** 1547

[23] Teixeira A F, Machado Y L R C, Fonseca A S and Mencalha A L 2016 Low-level lasers and mRNA levels of reference genes used in *Escherichia coli Laser Phys. Lett.* **13** 115602

[24] Ribeiro R S, Rodrigues J A, Mencalha A L and Fonseca A S 2023 Low-power blue LED and red laser effects on plasmid DNA, survival, and photolyase mRNA levels in *Escherichia coli* cultures *Laser Phys. Lett.* **20** 085601

[25] Fonseca A S, Mencalha A L, Campos V M A, Machado S C F, Peregrino A A F, Geller M and Paoli F 2013 DNA repair gene expression. In biological tissues exposed to low-intensity infrared laser *Lasers Med. Sci.* **28** 1077–84

[26] Fonseca A S, Magalhães L A G, Mencalha A L, Geller M and Paoli F 2014 Low intensity infrared laser affects expression of oxidative DNA repair genes in mitochondria and nucleus *Laser Phys.* **24** 115605

[27] Trajano E T L, Mencalha A L, Costa A M-A, Pôrto L C and Fonseca A S 2014 Expression of DNA repair genes in burned skin exposed to low-level red laser *Lasers Med. Sci.* **29** 1953–7

[28] Matsuo T, Yamaguchi S, Mitsui S, Emi A, Shimoda F and Okamura H 2003 Control mechanism of the circadian clock for timing of cell division in vivo *Science* **302** 255–9

[29] Fu L, Pelicano H, Liu J, Huang P and Lee C 2002 The circadian gene Period2 plays an important role in tumor suppression and DNA damage response *in vivo Cell* **111** 41–50

[30] Gauger M A and Sancar A 2005 Cryptochrome, circadian cycle, cell cycle checkpoints, and cancer *Cancer Res.* **65** 6828–34

[31] Climent J, Perez-Losada J, Quigley D A, Kim I-J, Delrosario R, Jen K-Y, Bosch A, Lluch A, Mao J-H and Balmain A 2010 Deletion of the PER3 gene on chromosome 1p36 in recurrent ER-positive breast cancer *J. Clin. Oncol.* **28** 3770–8

[32] Wang Z, Wang H, Wang Z, He S, Jiang Z, Yan C, Zhang S and Wang T 2020 Associayed analysis of PER1/TUBB2B with endometrial cancer development caused by circadian rhythm disorders *Med. Oncol.* **37** 90

[33] Gong X, Tang H and Yang K 2021 PER1 suppresses glycolysis and cell proliferation in oral squamous cell carcinoma via the PER1/RACK1/PI3K signaling complex *Cell Death Dis.* **12** 276

[34] Blakeman V, Williams J L, Meng Q-J and Streuli C H 2016 Circadian clocks and breast cancer *Breast Cancer Res.* **18** 89

[35] Mitchell M I and Englebrecht A-M 2015 Circadian rhythms and breast cancer: the role of PE2 in doxorubicin-induced cell death *J. Toxicol.* **2015** 392360

[36] Wu Y, Sato F, Bhawal U K, Kawamoto T, Fujimoto K, Noshiro M, Morohashi S, Kato Y and Kijima H 2011 basic

helix-loop-helix transcription factors DEC1 and DEC2 regulate the paclitaxel-induced apoptotic pathway of MCF-7 human breast cancer cells *Int. J. Mol. Med.* **27** 491–5

[37] Bhattacharya A, Schmitz U, Wolkenhauer O, Schönherr M, Raatz Y and Kunz M 2013 Regulation of cell cycle checkpoint kinase WEE1 by miR-195 in malignant melanoma *Oncogene* **32** 3175–83

[38] Qu M *et al* 2023 Circadian regulator BMAL1::CLOCK promotes cell proliferation in hepatocellular carcinoma by controlling apoptosis and cell cycle *Proc. Natl Acad. Sci. USA* **120** e2214829120

APÊNDICE C – Photobiomodulation at molecular, cellular, and systemic levels (artigo publicado)

Lasers in Medical Science (2023) 38:136
https://doi.org/10.1007/s10103-023-03801-6

REVIEW ARTICLE

Photobiomodulation at molecular, cellular, and systemic levels

Thayssa Gomes da Silva[1] · Rickson Souza Ribeiro[1] · Andre Luiz Mencalha[1] · Adenilson de Souza Fonseca[1,2]

Received: 22 March 2023 / Accepted: 5 June 2023

Abstract
Since the reporting of Endre Mester's results, researchers have investigated the biological effects induced by non-ionizing radiation emitted from low-power lasers. Recently, owing to the use of light-emitting diodes (LEDs), the term photobiomodulation (PBM) has been used. However, the molecular, cellular, and systemic effects involved in PBM are still under investigation, and a better understanding of these effects could improve clinical safety and efficacy. Our aim was to review the molecular, cellular, and systemic effects involved in PBM to elucidate the levels of biological complexity. PBM occurs as a consequence of photon-photoacceptor interactions, which lead to the production of trigger molecules capable of inducing signaling, effector molecules, and transcription factors, which feature it at the molecular level. These molecules and factors are responsible for cellular effects, such as cell proliferation, migration, differentiation, and apoptosis, which feature PBM at the cellular level. Finally, molecular and cellular effects are responsible for systemic effects, such as modulation of the inflammatory process, promotion of tissue repair and wound healing, reduction of edema and pain, and improvement of muscle performance, which features PBM at the systemic level.

Keywords Laser · Light-emitting diodes · Photobiomodulation · Phototherapy

Introduction

Dr. Endre Mester, who can be considered the "father of photobiomodulation," was one of the pioneers in describing the photomodulatory effect. His research involved high-power lasers aimed at destroying malignant tumors implanted in the skin of rats. However, the ruby laser he customized did not have enough power to be considered a "high-power" laser according to the current parameters [1]. The results showed accelerated wound healing and hair growth stimulation in the skin of rats exposed to a laser. Although Mester described this effect in 1964 based on results observed in animal experiments, it was not conceptualized [2]. It was only in 1967 that these results were published and the observed effect was called "laser biostimulation" [1, 2].

Based on these results, other researchers began to study the biological effects of low-power lasers. In 1967, a group of researchers established the biostimulation effect of low-power laser irradiation, which stimulated metabolic reactions that potentiated cellular events related to hair growth in mice [3]. In 1974, biostimulation effect was first applied in clinical practice [4–7].

As the studies involving the light for therapeutic advanced, their terminology was changing. The effect reported by Mester has been described by different terms, such as "low-level laser therapy," "low-level laser irradiation," "non-thermal laser," "low-level laser," "cold laser," "soft laser," "low energy laser irradiation," "laser therapy," and more recently, "photobiomodulation" (PBM) [8].

Later, in 1990, light-emitting diodes (LEDs) were implemented. LEDs are radiation sources that emit almost monochromatic radiation, although they are not collimated or coherent. Similar to low-power lasers, LEDs can also induce biostimulation effects [6]. Thus, the term "laser" became inappropriate, as LEDs were also incorporated into basic research and clinical protocols based on effects induced by such lasers and LEDs. In addition, several

✉ Thayssa Gomes da Silva
thayssa.biomed@gmail.com

[1] Departamento de Biofísica e Biometria, Instituto de Biologia Roberto Alcantara Gomes, Universidade do Estado do Rio de Janeiro, Vila Isabel, Boulevard 28 de Setembro, 87, Rio de Janeiro 20551030, Brazil

[2] Departamento de Ciências Fisiológicas, Instituto Biomédico, Universidade Federal do Estado do Rio de Janeiro, Rua Frei Caneca, 94, Rio de Janeiro 20211040, Brazil

Published online: 13 June 2023

studies have reported not only a biostimulation effect but also the triggering of bioinhibition effects due to biphasic dose responses [9].

Therefore, a nomenclature consensus was reached in 2014 at a meeting where the American Association for Light Therapies and World Association of Laser Therapy members were brought together. At that meeting, appropriate scientific terminology was established to describe the effects induced by radiation emitted by low-power lasers and LEDs. PBM therapy was defined by Anders et al. (2015) as "a form of light therapy that utilizes non-ionizing light sources, including lasers, LEDs, and broadband light, in the visible and infrared spectrum" [10]. It is a non-thermal process involving endogenous chromophores that elicit photophysical (i.e., linear and nonlinear) and photochemical events at various biological scales. This process results in beneficial therapeutic outcomes including but not limited to the alleviation of pain or inflammation, immunomodulation, and promotion of wound healing and tissue regeneration.

Over the years, PBM has been reported in in vitro and in vivo studies, as well as in randomized clinical trials and case and series reports. However, what exactly is PBM? If we look for the etymology of the word: "photo" means "light," "bio" corresponds to "life." and "modulation" means "to modulate, to vary." Thus, PBM could be "roughly" understood as "modulation of life by light." Depending on the biological complexity of the study, PBM has been reported as a set of molecular, cellular, and tissue responses initiated by the absorption of energy from incident photons by endogenous chromophores (also called photoacceptors). Different irradiation parameters can vary the cellular response obtained.

PBM has acquired great attention in the field of regenerative medicine as the ability of radiation emitted from low-power lasers and LEDs to induce tissue repair has been reported. For example, exposure to radiation from such sources accelerates tissue repair, stimulates fibroblasts to produce more collagen fibers, and promotes extracellular matrix reorganization [11, 12]. In addition, radiation from low-power sources modulates cell proliferation and migration, as well as the secretion of inflammatory cytokines [13, 14]. Experimental and clinical data from studies on PBM have been used as a scientific basis for therapeutic protocols in different areas, such as medicine, dentistry, nursing, physiotherapy, and aesthetics [15]. However, the molecular, cellular, and systemic effects of PBM are still under investigation, and elucidating them could improve our understanding as well as their clinical safety and efficacy. Here, we aimed to review the molecular, cellular, and systemic effects of PBM at these levels of biological complexity.

PBM at different biological complexity levels

The therapeutic applications of PBM have advanced owing to a better understanding of its mechanisms of action at the molecular, cellular, and systemic levels. In fact, data from in vivo and in vitro studies as well as those from randomized clinical trials and case series on the effects of radiation emitted from low-power lasers and LEDs have allowed for a better understanding of the effects of PBM at different biological complexity levels.

The radiation-induced biological effects of PBM begin with the interaction of radiation photons with specific endogenous chromophores (or photoacceptors). Owing to photoreception, the photoacceptor molecule is excited, changing its energy state from a fundamental to an excited energy state. As the excited states are unstable, the excited photoacceptor molecule decays back to the fundamental energy state, transferring excess energy to other molecules, which leads to a set of biological processes, such as increasing electron transfer in the respiratory chain, NADH pool oxidation, free radical production, and alteration of proton motive force and mitochondrial membrane potential [16].

Cytochrome c oxidase (CCO), complex IV of the respiratory chain in mitochondria, is considered the main photoacceptor for visible light and infrared radiation (700–1100 nm) emitted from low-power light sources, such as low-power therapeutic lasers and LEDs [9, 16, 17]. Other photoacceptors have been suggested, such as flavins and flavoproteins that can absorb blue-green lights (400–550 nm), porphyrins that absorb yellow–red lights (560–700 nm), and opsins that absorb ultraviolet A-yellow lights (380–560 nm) [17–19]. Figure 1 shows the absorption of radiation by the photoacceptors.

CCO is the terminal enzyme of the electron transport chain and catalyzes the transfer of four electrons from cytochrome c to molecular oxygen, forming two water molecules. During this process, adenosine triphosphate (ATP) is produced by ATP synthases. Absorption of red-near infrared light at low-powers promotes the photodissociation of nitric oxide from CCO, which increases enzyme activity due to the non-covalent binding of nitric oxide between the heme centers a3 and CuB and inhibits CCO activity. This is considered the mechanism of increased ATP production involved in PBM induced by radiation emitted from low-power therapeutic lasers and LEDs.

Molecular level

Increased intracellular production of reactive oxygen species (ROS) has been associated with non-ionizing

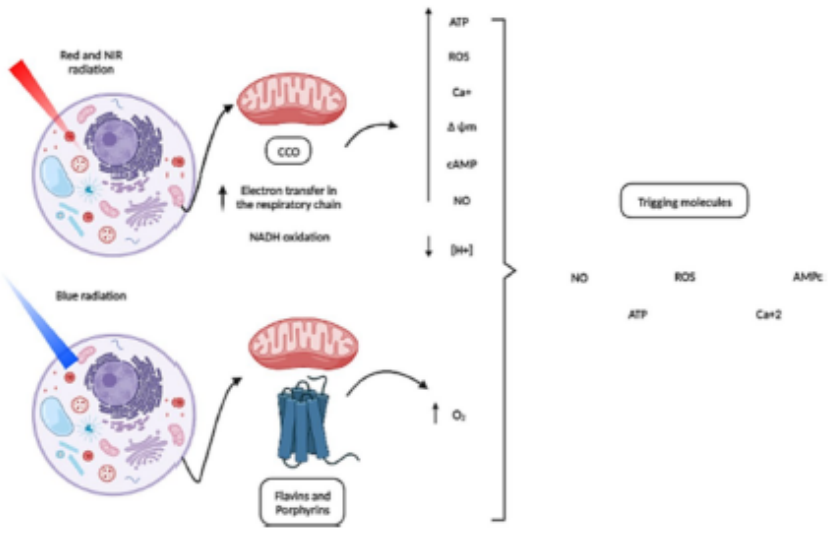

Fig. 1 Representation of the absorption of radiations by photoacceptors. Designed using BioRender. CCO, cytochrome c oxidase; ATP, adenosine triphosphate; ROS, reactive oxygen species; Ca^{2+}, calcium ions; $\Delta\psi m$, membrane potential; cAMP, cyclic adenosine monophosphate; NO, nitric oxide; [H +], hydrogen ions; O_2, oxygen

radiations at low-powers [20]. It has been suggested that CCO produces free radicals after absorption of red-near infrared light, and such chemical species are involved in the photosignal and transduction chains, which lead to PBM [16, 21]. On the other hand, photosensitization has been associated with the production of ROS by exposure of flavins to violet-blue lights [22] and porphyrins to yellow–red lights [23]. Free radicals have been suggested as second messengers participating in cell signaling cascades [24, 25] and can induce molecular events by stimulating signaling and effector molecules (second messengers) and activating transcription factors [26, 27]. Other chemical agents, such as nitric oxide (NO), ATP, cyclic AMP, and Ca^{2+} ions, have been related to radiation-induced effects involved in PBM [28–30].

ROS production has been associated with PBM; however, the role of these compounds remains controversial [31]. It was suggested that PBM reduces ROS levels in stressed cells [32]. On the other hand, Guo et al. (2021) indicated that low-level light absorbed by chromophores could lead to the production of NO and the modulation of ROS [33]. Other authors have suggested that the production of ROS after exposure to red-near infrared radiation could either be inhibited or, to some extent, increased depending on the irradiation conditions, such as radiation wavelength, irradiance, and exposure time [34]. Blue light–induced ROS production may be responsible for ocular phototoxicity [35].

These data suggest that exposure to red-near infrared light at low powers causes the displacement of NO from CCO, which is involved in PBM [36]. In addition, Chen et al. (2011) showed that exposure to red light at low-power could stimulate the nitrate reductase activity of CCO and induce NO release in the isolated mitochondria of yeast and mouse brain cells [37]. Moreover, an increase in NO levels in rat endothelial cells [38] and the restoring of NO levels in human-induced pluripotent stem cell-derived ventricular cardiomyocytes treated with doxorubicin [39] were detected after exposure to a low-power red laser.

In vitro and in vivo studies have demonstrated that intracellular ATP levels increase after irradiation with low-power therapeutic lasers and LEDs. Huang et al. (2014) reported increased ATP levels in primary cortical neurons exposed to low-level infrared laser therapy [40]. ATP synthesis increases in carcinoma cells and fibroblasts after exposure to infrared radiation from a LED array [41]. In addition, increased ATP synthesis in rat brains has been reported after exposure to red-near infrared radiation [42–44]. Furthermore, according to some experimental data, exposure to a low-power red laser accelerates ATP synthesis in rat skeletal muscle [45].

Taniguchi et al. (2009) suggested that cAMP is involved in PBM-induced synovial fibroblast proliferation following exposure to a low-power red laser [46]. Other authors have shown that a low-power red laser can increase cAMP levels in human skin fibroblasts subjected to hypoxia and acidosis [47].

PBM induced by violet-blue light increases Ca^{2+} ion levels in human adipose-derived stem cells [48], by low-power red laser increases intracellular Ca^{2+} content in rat liver cells [49], and low-power 980 nm, but not 810 nm, infrared laser increases cytosolic Ca^{2+}; otherwise, it decreases mitochondrial Ca^{2+} levels in adipose-derived stem cells [50]. In contrast, Amaroli et al. (2016) reported no alteration in the sequestered Ca^{2+} concentration after exposure to low-power infrared (808 and 908 nm) lasers [51], as well as

in dystrophic muscle cells after exposure to multiple LED wavelengths (420, 470, 660, and 850 nm) [52].

Some of such chemicals could act as trigger agents for the production and/or activation of signalizing molecules, transcription factors, and effector molecules in cells under PBM. Trigger agents could be able to start signaling pathways and activate transcription factors, explaining the long-lasting effects involved in PBM [53]. For example, ROS activates signaling pathways that are dependent on mitogen-activated protein kinase/extracellular signal-regulated protein kinase (MAPK/ERK) and protein kinase B (Akt), which are involved in activation of nuclear factor kappa-light-chain-enhancer of activated B cells (NF-κB) and vascular endothelial growth factor (VEGF) [54]. NO inhibits hypoxia-induced factor 1α (HIF-1α) expression and HIF-1 transcriptional activity [55]; however, but under non-hypoxic conditions, NO induces HIF-1α expression [56]. cAMP inhibits tumor necrosis factor-α (TNF-α) expression [57], induces NF-κB binding to the κ light chain enhancer and activates the κB reporter gene [58], stimulates late phase NF-κB activation, or inhibits early IL-1β-induced NF-κB [59]. In addition, intra-store Ca^{2+} mobilization mediates TNF-α- and IL-6-induced glial fibrillary acidic protein expression [60], and Ca^{2+}-dependent activation of Akt is inhibited by Ca^{2+}-chelating agents [61].

In fact, results have been reported on the relationship between such trigger agents and signaling molecules involved in PBM has been reported. For example, Agas et al. (2021) reported activation of the PI3K/Akt/Bcl-2 signaling pathway in pre-osteoblasts after exposure to a low-power infrared laser [62]. This signaling pathway is also activated in fibroblasts by a low-power red laser [63]. Using a low-power infrared laser, p38-MAPK mRNA expression was decreased in the dorsal root ganglion of diabetic neuropathic rats by a low-power infrared laser [64]. Also, it was demonstrated that the anti-inflammatory effects of the low-power red laser depend on the activation of ATP-dependent K + channels and the p38-MAPK signaling pathway [65]. Mohamed Abdelgawad et al. (2021) reported that exposure to a low-power infrared laser increases gene expression of Nrf2 in human periodontal ligament stem cells cultured in a high-glucose medium [66]. Curra et al. (2015) reported that preventive and/or therapeutic PBM using a low-power red laser reduces the severity of oral mucositis by activating the NF-kB pathway [67]. Other authors have shown that a low-power infrared laser reduces receptor activator of NF-κB ligand (RANKL) expression in an osteoblast/osteoclast co-culture system [68].

In addition, transcription factors could be related to trigger agents involved in PBM induced by non-ionizing radiations emitted from low-power lasers and LEDs. HIF-1α gene expression in human bone marrow mesenchymal stem cells was decreased by irradiation with a low-power infrared laser [69], and neurotoxic polarization of macrophages and secretion of inflammatory factors in mice with spinal cord injury was attenuated by inhibiting the Notch1-HIF-1α/NF-κB signaling pathway after exposure to low-power infrared laser [70]. However, a low-power infrared laser was not able to alter HIF-1α immunolabeling in rat pulp tissue after bleaching [71]. Tani et al. (2018) showed that exposure to low-power red and infrared laser, but not to blue LED, increases RUNX2 expression in osteoblast cultures [72]. In addition, de Lima and coworkers (2013) reported that exposure to low-power red laser increases PPARy expression in the lungs of rats affected by sepsis [73], and Mohamed and coworkers (2022) showed an increase in PPARy gene and protein expression in rat liver fibrosis by exposure to low-power red-near infrared lasers [74].

Moreover, PBM has been proposed to act on effector molecules in certain signaling pathways. For example, a low-power infrared, but not red, laser was able to increase TGF-β mRNA expression in rat macrophages [75], but there was no significant change in TGF-β1, and pTGF-β1R1 was verified in fibroblasts in normal, normally wounded, diabetic, and diabetic wound models exposed to a low-power red laser [76]. Ruh et al. (2018) reported an increase in VEGF gene expression in pressure ulcers of human diabetic patients after exposure to a low-power red laser [77], and the low-power red laser was also able to decrease VEGF in gingival crevicular fluid [78]. A low-power infrared laser reduced TNF-α secretion from neurons under oxidative stress simulated in vitro [79], and TNF-α expression in rat skin flaps was reduced by irradiation with a low-power red laser [80]. Yin et al. (2017) reported the upregulation of hepatocyte growth factor (HGF) in mesenchymal stem cell cultures upon exposure to a low-power laser [81], and other authors have demonstrated that red LED is able to increase the expression of HGF in tonsil-derived mesenchymal stem cells [82]. Red LED was also able to increase BDNF expression in mouse hippocampal organotypic slices [83], and low-power red laser increased BNDF expression in cultures of neural stem cells from the mouse hippocampus [84]. It was reported that low-power laser and LED decreased pro-inflammatory interleukin (IL) levels, such as IL-6 levels, in diabetic fibroblast cell models after red laser exposure [85], and low-power infrared laser decreased the immunoexpression of IL-1β in an experimental model of COVID-19 infection [86]. In addition, radiation from such light sources was able to increase anti-inflammatory interleukin levels, as IL-10 levels were increased in individuals with relapsing–remitting multiple sclerosis after sublingual exposure to a low-power infrared (808 nm) laser [87], and low-power red (635 nm) increased IL-10

expression in the mouse hippocampus of Alzheimer's disease models [84]. However, red (630 nm) and infrared (850 nm) LEDs decreased IL-10 gene expression in an acute radiodermatitis animal model [88]. In addition, heat shock proteins (HSP-90 and HSP-60) were upregulated in rat burn wounds exposed to a low-power infrared (904 nm) laser [89], and HSP-90 expression is upregulated in rat skin wound tissues after exposure to another low-power infrared (830 nm) laser [90].

Thus, the data obtained from available studies suggest that PBM at the molecular level can be understood as the ability of non-ionizing radiation emitted from low-power sources, such as low-power therapeutic lasers and LEDs, to modulate the levels of signaling, effector molecules, and transcription factors. Figure 2 shows the radiation-induced signaling, effector molecules, and transcription factors involved in PBM at the molecular level.

Cellular level

The cellular effects involved in PBM occur as a consequence of those molecular effects, caused by the actions of signaling and effector molecules, as well as transcription factors, which in turn are induced by trigger agents. Cellular effects induced by exposure to radiation emitted from low-power lasers and LEDs have been reported, including cell proliferation, viability, differentiation, apoptosis, and migration [91, 92]. In fact, it was demonstrated that exposure to a low-power green laser increases dental pulp stem cell proliferation [93], and a low-power infrared laser increases the viability and proliferation of normal unstressed, normal wounded, diabetic, diabetic wounded, and hypoxic diabetic wounded fibroblasts [94]. However, other studies have shown that the viability of oral squamous carcinoma cells decreased after repetitive exposure to low-power infrared [95] and red lasers [96], and a low-power blue laser decreased cell viability in bladder cancer cell cultures [97]. Chaweewannakorn et al. (2021) showed that red (630 and 608 nm) LEDs were more efficient than infrared (830 nm) LED in inducing osteoblastic differentiation of periodontal ligament stem cells in vitro [98]. George et al. (2022) suggested that exposure to a low-power infrared laser can promote the neuronal differentiation potential of primary adipose stem cells [99], and other authors have shown that a low-power red laser induces the osteogenic and chondrogenic differentiation of dental pulp stem cells [100]. A low-power infrared laser increased the apoptosis of polymorphonuclear cells in the talocrural and subtalar joints of mice affected by arthritis [101] and the mRNA levels of pro-apoptotic genes in tissues from the talocrural joint of mice [102]. However, a low-power infrared laser decreased apoptosis markers in the prefrontal cortex and hippocampus of mice subjected to subchronic restraint stress [103], and exposure to red LED reduced apoptosis in organotypic slice-cultured hippocampal tissue of rats [104]. Zaccara et al. (2020) demonstrated that exposure to a low-power red laser increases cell migration in human dental pulp stem cell cultures [105], and Oyebode et al. (2022) reported increased cell migration in diabetic wounds in vitro after exposure to another

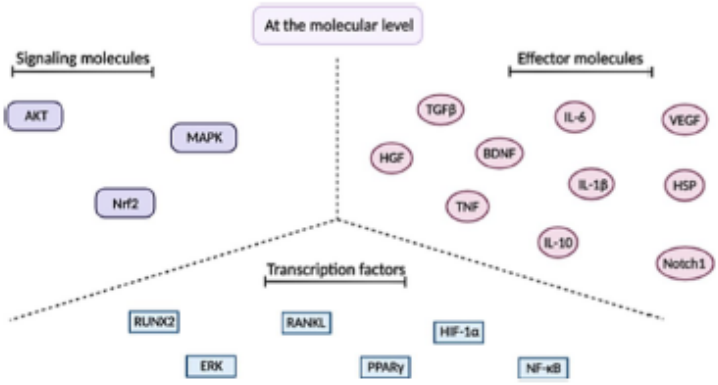

Fig. 2 Schematic representation for radiation-induced signaling and effector molecules, and transcription factors involved in PBM at the molecular level. Designed using BioRender. MAPK, mitogen-activated protein kinases; Akt, protein kinase B; Nrf2, nuclear factor erythroid 2-related factor 2; HGF, hepatocyte growth factor; TGF-β, transforming growth factor beta; VEGF, vascular endothelial growth factor; BDNF, brain-derived neurotrophic factor; HSP, heat shock proteins; TNF, tumor necrosis factor; RUNX2, Runt-related transcription factor 2; ERK, extracellular signal-regulated kinases; RANKL, receptor activator of nuclear factor kappa-B ligand; PPARγ, peroxisome proliferator-activated receptor gamma; HIF-1α, hypoxia-inducible factor; NF-κB, nuclear factor-κB; Notch1, neurogenic locus notch homolog protein 1; IL-1β, interleukin-1 beta; IL-6, interleukin 6; IL-10, interleukin 10

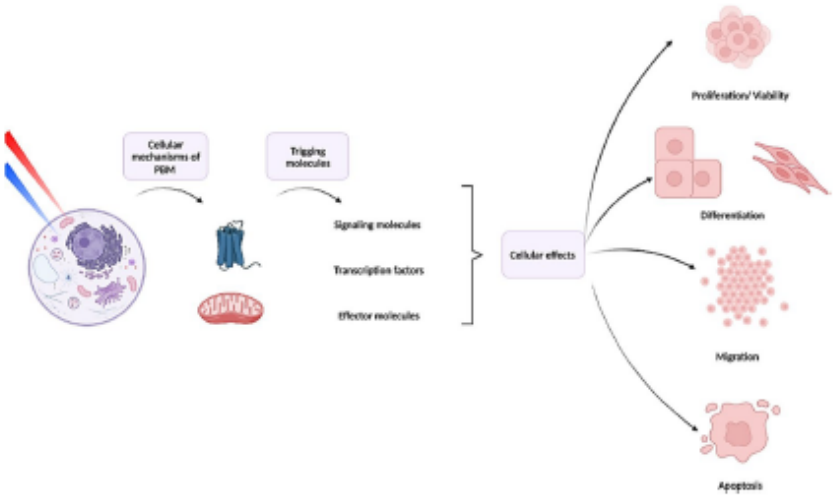

Fig. 3 Representation of radiation-induced cellular effects involved in PBM at the cellular level. Designed using BioRender

low-power infrared (830 nm) laser [94]. However, Schalch et al. (2019) reported decreased cell migration of carcinoma cells after exposure to low-power infrared radiation (780 nm) [95].

Thus, the data obtained from the studies suggest that PBM at the cellular level could be understood as the ability of non-ionizing radiation emitted from low-power sources, such as low-power therapeutic lasers and LEDs, to modulate cellular responses such as cell proliferation, viability, differentiation, apoptosis, and migration, which are consequences of those radiation-induced molecular effects. Figure 3 shows the radiation-induced effects involved in PBM at the cellular level.

Systemic level

The systemic effects involved in PBM occur as a consequence of radiation-induced molecular (signaling and effector molecules, and transcription factors) and cellular effects (cell proliferation, viability, differentiation, apoptosis, and migration). In fact, radiations emitted from these devices induce the systemic effects involved in PBM, such as modulation of the inflammatory process, promotion of tissue repair and wound healing, reduction of edema and pain, and improvement in muscle performance. Although the mechanisms related to some systemic effects involved in PBM are still not understood, these effects have been demonstrated in experimental models and clinical studies, and are being considered in therapeutic protocols based on radiation emitted from low-power lasers and LEDs for the treatment of diseases and clinical conditions. For example, Pigatto et al. (2019) reported that a red LED reduced the migration of inflammatory cells induced by a single application of croton oil in rat ears [106], and Wang et al. (2021) reported the alleviation of neuroinflammation in an experimental model of spinal cord injury after exposure to a low-power infrared laser [107]. In addition, Le et al. (2022) demonstrated the anti-inflammatory effect of a low-power infrared laser after the surgical removal of mandibular third molars in a clinical model [108], and Alonso et al. (2022) reported that transcutaneous systemic irradiation with a red LED reduced lung inflammation in rats [109]. Exposure to both low-power red and infrared lasers enhances the repair of acute muscle injury in rats by modulating the inflammation phase, optimizing the transition from the inflammatory to the regeneration phase, and improving the final step of tissue regeneration [75]. Red (630 nm) light from a low-power LED improved the dermo-epidermal junction and modulated the expression of proteins related to tissue repair in rat full-thickness skin grafts [110], and red light at the same wavelength from a low-power LED also enhanced the number of fibroblasts and amount of collagen in acute Achilles tendinitis in rats [111]. Based on histopathological and immunohistochemical analyses, Astuti et al. (2022) showed that a low-power red laser accelerated the process of proliferation in wound healing after molar extraction [112]. Other authors have demonstrated that exposure to a low-power red laser is effective in decreasing the rate of scar formation and hypertrophic scar formation in children with deep burn ulcers [113]. Cai et al. (2022) reported that a combination of red and blue light accelerated the healing process by increasing angiogenesis density and collagen deposition and alleviating inflammation in diabetic rat wounds [114]. Red LED showed an anti-edematogenic effect on rat ear edema [105], a low-power red laser reduced edema formation in

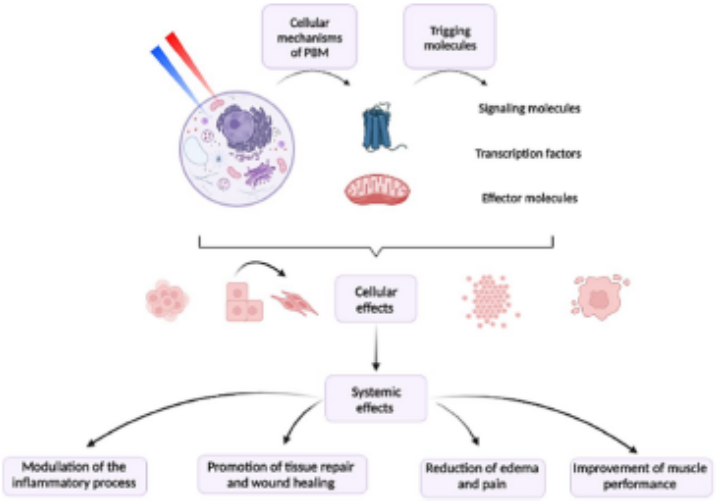

Fig. 4 Representation of radiation-induced effects involved in PBM at the systemic level. Designed using BioRender

a myositis model in rats [115], and a low-power infrared laser promoted edema reduction after third molar surgery in a clinical trial [116]. In acute nociception models, pre-exposure to red LED reduced nociceptive neurogenic and inflammatory pain [105], and a low-power infrared (810 nm) laser was able to promote pain relief after the surgical removal of mandibular third molars in a clinical trial [107]. Another low-power infrared (850 nm) laser reduced pain levels in the short and medium term in patients with symptomatic knee osteoarthritis [117]. In one clinical trial, exposure to an infrared (810 nm) LED cluster before exercise enhanced muscular performance and post-exercise recovery [114], and in another clinical trial, exposure to a low-power infrared laser before physical exercise enhanced athletic performance and improved post-exercise recovery [118]. Moreover, treatment with red (630 nm) and infrared (940 nm) LED before eccentric exercise attenuated exercise-induced muscle damage without impairing repeated bouts of exercise in healthy men [119]. However, data from another study suggested that infrared radiation from a multidiode array did not have a beneficial effect on muscle fatigue, cycling performance, metabolic parameters, or muscle activity in male recreational cyclists [120], and exposure to a low-power infrared laser did not improve biceps brachii performance to exhaustion, rating of perceived exertion, or delayed onset muscle soreness in untrained women [121].

Thus, the data obtained from these studies suggest that the effect of PBM at the systemic level can be understood as the ability of non-ionizing radiation emitted by low-power sources, such as low-power lasers and LEDs, to modulate systemic responses, including the modulation of inflammatory processes, promotion of tissue repair and wound healing, reduction of edema and pain, and improvement of muscle performance, which are consequences of those radiation-induced molecular and cellular effects. Figure 4 shows the radiation-induced effects involved in PBM at the systemic level.

Conclusion

Radiation emitted by low-power lasers and LEDs has been increasingly used for the treatment of diseases and clinical conditions through therapeutic protocols based on PBM. Experimental and clinical studies have advanced our understanding the effects involved in PBM. For PBM-based therapeutic protocols to become safer and more effective, it is essential to understand the PBM at molecular, cellular, and systemic levels. PBM can occur because of photon-photoacceptor interactions, which lead to the production of trigger molecules. These molecules induce a cascade of events that lead to the molecular, cellular, and systemic effects involved in PBM. Non-ionizing radiation emitted by low-power sources induces signaling, effector molecules, and transcription factors that feature PBM at the molecular level. In turn, these molecules are responsible for cellular effects such as cell proliferation, migration, differentiation, and apoptosis, which feature PBM at the cellular level. Finally, molecular and cellular effects are responsible for systemic effects, such as modulation of the inflammatory process, promotion of tissue repair and wound healing, reduction of edema and pain, and improvement of muscle performance, which are features of PBM at the systemic level.

Author contribution Thayssa G. da Silva and Rickson Souza Ribeiro prepared the manuscript. Adenilson de Souza Fonseca conceived the original idea of the article, as well as helped in the elaboration and correction. Andre Luiz Mencalha contributed to the writing and correction. All authors contributed to the manuscript.

Funding This study was supported by the Coordenação de Aperfeiçoamento de Pessoal de Nível Superior (CAPES) (88887.636295/2021–00).

Declarations

Conflict of interest The authors declare no competing interests.

References

1. Gáspar L (2009) Endre Mester, the father of photobiomodulation. J Laser Dentist 17(3):146–148
2. Mester A, Mester A (2017) The history of photobiomodulation: Endre Mester (1903–1984). Photomed Laser Surg 35:393–394
3. Mester E, Szende B, Gärtner P (1968) Die Wirkung der Lasstrahlen auf den Haarwuchs der Maus [The effect of laser beams on the growth of hair in mice]. Radiobiol Radiother 9(5):621–626
4. Abergel RP, Lyon RF, Castel JC, Dwyer RM, Uitto LL (1987) Biostimulation of wound healing by lasers: experimental approaches in animal models and in fibroblast cultures. J Dermato Surg Oncol 13:127–133
5. Karu T (1990) Effects of visible radiation on cultured cells. Photoschem Photobiol 52:1089–1098
6. Emelyanov AN, Kiryanova VV (2015) Photomodulation of proliferation and differentiation of stem cells by the visible and infrared light. Photomed Laser Surg 33:164–174
7. Lins RD, Dantas EM, Lucena KC, Catão MH, Granville-Garcia AF, Carvalho Neto LG (2010) Biostimulation effects of low-power laser in the repair process. An Bras Dermatol 85:849–855
8. Mester A (2013) Laser Biostimulation. Photomed Laser Surg 31:237–239
9. Hamblin MR (2018) Mechanisms and mitochondrial redox signaling in photobiomodulation. Photochem Photobiol 94:199–212
10. Anders JJ, Lanzafame RJ, Arany PR (2015) Low-level light/laser therapy versus photobiomodulation therapy. Photomed Laser Surg 33:183–184
11. Deana NF, Alves N, Zaror C, Del Sol M, Bagnato VS (2021) Photobiomodulation therapy in burn wound healing: systematic review and meta-analysis of preclinical studies. Photobiomodul Photomed Laser Surg 39:439–452
12. Rahmannia M, Amini A, Chien S, Bayat M (2022) Impact of photobiomodulation on macrophages and their polarization during diabetic wound healing: a systematic review. Lasers Med Sci 37:2805–2815
13. Ahrabi B, Rezaei Tavirani M, Khoramgah MS, Noroozian M, Darabi S, Khoshsirat S, Abbaszadeh HA (2019) The effect of photobiomodulation therapy on the differentiation, proliferation, and migration of the mesenchymal stem cell: a review. J Lasers Med Sci 10(Suppl 1):S96–S103
14. da Cruz TD, Silva T, Araujo T, Andreo L, Malavazzi TCDS, Horliana ACRT, Fernandes KPS, Bussadori SK, Mesquita-Ferrari RA (2022) Effects of photobiomodulation in experimental spinal cord injury models: a systematic review. J Biophotonics 15:e202200059
15. Hamblin MR (2016) Photobiomodulation or low-level laser therapy. J Biophotonics 9:1122–1124
16. Karu T (1999) Primary and secondary mechanism of action of visible to near-IR radiation on cell. J Photochem Photobiol B Biol 49:1–17
17. Chen Z, Huang S, Liu M (2022) The review of the light parameters and mechanisms of photobiomodulation on melanoma cells. Photodermatol Photoimmunol Photomed 38:3–11
18. Yamashita T, Ono K, Ohuchi H, Yumoto A, Gotoh H, Tomonari S et al (2014) Evolution of mammalian Opn5 as a specialized UV-absorbing pigment by a single amino acid mutation. J Biol Chem 289:3991–4000
19. Buhr ED, Vemaraju S, Diaz N, Lang RA, Van Gelder RN (2019) Neuropsin (OPN5) mediates local light-dependent induction of circadian clock genes and circadian photoentrainment in exposed murine skin. Curr Biol 29:3478–3487
20. Rai V (2017) Role of reactive oxygen species in low-level laser therapy. Handbook of Low-Level Laser Therapy. Pan Stanford Publishing Pte Ltd
21. Karu T (1989) Laser biostimulation: a photobiological phenomenon. J Photochem Photobiol B 3:638–640
22. Eichler M et al (2005) Flavins are source of visible-light-induced free radical formation in cells. Lasers Surg Med 37:314–319
23. Kolarova H, Nevrelova P, Tomankova K, Kolar P, Bajgar R, Mosinger J (2008) Production of reactive oxygen species after photodynamic therapy by porphyrin sensitizers. Gen Physiol Biophys 27:101–105
24. Valko M, Leibfritz D, Moncol J, Cronin MT, Mazur M, Telser J (2007) Free radicals and antioxidants in normal physiological functions and human disease. Int J Biochem Cell Biol 39:44–84
25. Migliario M, Pittarella P, Fanuli M, Rizzi M, Renò F (2014) Laser-induced osteoblast proliferation is mediated by ROS production. Lasers Med Sci 29:1463–1467
26. de Freitas LF, Hamblin MR (2016) Proposed mechanisms of photobiomodulation or low-level light therapy. IEEE J Sel Top Quantum Electron 22:7000417
27. Schröder K (2019) Redox control of angiogenesis. Antioxid Redox Signal 30(7):960–971
28. Hashmi JT, Huang YY, Osmani BZ, Sharma SK, Naeser MA (2010) Hamblin MR (2010) Role of low-level laser therapy in neurorehabilitation. PM R 2(12 Suppl 2):S292–S305
29. Serrage H, Heiskanen V, Palin WM, Cooper PR, Milward MR, Hadis M, Hamblin MR (2019) Under the spotlight: mechanisms of photobiomodulation concentrating on blue and green light. Photochem Photobiol Sci 18:1877–1909
30. Khorsandi K, Hosseinzadeh R, Abrahamse H, Fekrazad R (2020) Biological responses of stem cells to photobiomodulation therapy. Curr Stem Cell Res Ther 15:400–413
31. Garzón J, Baldion PA, Grajales M, Escobar LM (2022) Response of osteoblastic cells to low-level laser treatment: a systematic review. Lasers Med Sci 37:3031–3049
32. Huang YY, Nagata K, Tedford CE, McCarthy T, Hamblin MR (2013) Low-level laser therapy (LLLT) reduces oxidative stress in primary cortical neurons in vitro. J Biophotonics 6:829–838
33. Guo Y, Qu Q, Chen J, Miao Y, Hu Z (2021) Proposed mechanisms of low-level light therapy in the treatment of androgenetic alopecia. Lasers Med Sci 36:703–713
34. Walski T, Dąbrowska K, Drohomirecka A, Jędruchniewicz N, Trochanowska-Pauk N, Witkiewicz W, Komorowska M (2019) The effect of red-to-near-infrared (R/NIR) irradiation on inflammatory processes. Int J Radiat Biol 95:1326–1336
35. Shang YM, Wang GS, Sliney DH, Yang CH, Lee LL (2017) Light-emitting-diode induced retinal damage and its wavelength dependency in vivo. Int J Ophthalmol 10(2):191–202

36. Sarti P, Giuffre A, Forte E, Mastronicola D, Barone MC, Brunori M (2000) Nitric oxide and cytochrome c oxidase: mechanisms of inhibition and NO degradation. Biochem Biophys Res Commun 274:183–187
37. Chen ACH, Arany PR, Huang YY et al (2011) Low-level laser therapy activates NF-kB via generation of reactive oxygen species in mouse embryonic fibroblasts. PLoS ONE 6(7):e22453
38. Buzinari TC, de Moraes TF, Conceição-Filho JC, Cárnio EC, Almeida-Lopes L, Salgado HC, Rodrigues GJ (2022) Nitric oxide storage levels modulate vasodilation and the hypotensive effect induced by photobiomodulation using an aluminum gallium arsenide (AlGaAs) diode laser (660 nm). Lasers Med Sci 37:2753–2762
39. Atum ALB, da Silva JAA, Marques D, Prates RA, Consolim-Colombo FM, Irigoyen MCC, Dalboni MA, Chavantes MC, Silva JA Jr (2022) Photobiomodulation therapy preconditioning modifies nitric oxide pathway and oxidative stress in human-induced pluripotent stem cell-derived ventricular cardiomyocytes treated with doxorubicin. Lasers Med Sci 37:1667–1675
40. Huang YY, Nagata K, Tedford CE, Hamblin MR (2014) Low-level laser therapy (810-nm) protects primary cortical neurons against excitotoxicity in vitro. J Biophotonics 7:656–664
41. Gonçalves de Faria CM, Ciol H, Salvador Bagnato V, Pratavieira S (2021) Effects of photobiomodulation on the redox state of healthy and cancer cells. Biomed Opt Express 12:3902–3916
42. Uozumi Y et al (2010) Targeted increase in cerebral blood flow by transcranial near-infrared laser irradiation. Lasers Surg Med 42:566–576
43. Rojas JC, Bruchey AK, Gonzalez-Lima F (2012) Low-level light therapy improves cortical metabolic capacity and memory retention. J Alzheimers Dis 32:741–752
44. Radziuk JM (2013) The suprachiasmatic nucleus, circadian clocks, and the liver. Diabetes 62:1017–1019
45. Gong L, Zou Z, Liu L, Guo S, Xing D (2021) Photobiomodulation therapy ameliorates hyperglycemia and insulin resistance by activating cytochrome c oxidase-mediated protein kinase B in muscle. Aging (Albany NY) 13:10015–10033
46. Taniguchi D, Dai P, Hojo T, Yamaoka Y, Kubo T, Takamatsu T (2009) Low-energy laser irradiation promotes synovial fibroblast proliferation by modulating p15 subcellular localization. Lasers Surg Med 41:232–239
47. Zungu IL, Hawkins Evans D, Abrahamse H (2009) Mitochondrial responses of normal and injured human skin fibroblasts following low level laser irradiation—an in vitro study. Photochem Photobiol 85:987–996
48. Wang Y, Huang YY, Wang Y, Lyu P, Hamblin MR (2016) Photobiomodulation (blue and green light) encourages osteoblastic-differentiation of human adipose-derived stem cells: role of intracellular calcium and light-gated ion channels. Sci Rep 6:33719
49. Guo S, Gong L, Shen Q, Xing D (2022) Photobiomodulation reduces hepatic lipogenesis and enhances insulin sensitivity through activation of CaMKKβ/AMPK signaling pathway. Photochem Photobiol Sci 21:1257–1272
50. Wang Y, Huang YY, Wang Y, Lyu P, Hamblin MR (2017) Photobiomodulation of human adipose-derived stem cells using 810 nm and 980 nm lasers operates via different mechanisms of action. Biochim Biophys Acta Gen Subj 1861:441–449
51. Amaroli A, Benedicenti A, Ferrando S, Parker S, Selting W, Gallus L, Benedicenti S (2016) Photobiomodulation by infrared diode laser: effects on intracellular calcium concentration and nitric oxide production of paramecium. Photochem Photobiol 92:854–862
52. da Rocha GL, Mizobuti DS, da Silva HNM, Covatti C, de Lourenço CC, Salvador MJ, Pereira ECL, Minatel E (2022) Multiple LEDT wavelengths modulate the Akt signaling pathways and attenuate pathological events in mdx dystrophic muscle cells. Photochem Photobio Sci 21(7):1257–1272
53. Kohlgrüber S, Upadhye A, Dyballa-Rukes N, McNamara CA, Altschmied J (2017) Regulation of transcription factors by reactive oxygen species and nitric oxide in vascular physiology and pathology. Antioxid Redox Signal 26(13):679–699
54. Aggarwal V, Tuli HS, Varol A, Thakral F, Yerer MB, Sak K, Varol M, Jain A, Khan MA, Sethi G (2019) Role of reactive oxygen species in cancer progression: molecular mechanisms and recent advancements. Biomolec 9:735
55 Huang LE, Willmore WG, Gu J, Goldberg MA, Bunn HF (1999) Inhibition of hypoxia-inducible factor 1 activation by carbon monoxide and nitric oxide. Implications for oxygen sensing and signaling. J Biol Chem 274(13):9038–44
56 Palmer LA, Gaston B, Johns RA (2000) Normoxic stabilization of hypoxia inducible factor 1 expression and activity: redox-dependent effect of nitrogen oxides. Mol Pharmacol 58:1197–1203
57. Medzhitov R, Horng T (2009) Transcriptional control of the inflammatory response. Nat Rev Immunol 9:692–703
58. Shirakawa F, Chedid M, Suttles J, Pollok BA, Mizel SB (1989) Interleukin 1 and cyclic AMP induce kappa immunoglobulin light-chain expression via activation of an NF-kappa B-like DNA-binding protein. Mol Cell Biol 9(3):959–964
59. Bomsztyk K, Toivola B, Emery DW, Rooney JW, Dower SK, Rachie NA, Sibley CH (1990) Role of cAMP in interleukin-1-induced kappa light chain gene expression in murine B cell line. J Biol Chem 265(16):9413–9417
60. Sticozzi C, Belmonte G, Frosini M, Pessina F (2021) Nitric oxide/cyclic GMP-dependent calcium signalling mediates IL-6- and TNF-α-induced expression of glial fibrillary acid protein. J Mol Neurosci 71:854–866
61. Divolis G, Mavroeidi P, Mavrofrydi O, Papazafiri P (2016) Differential effects of calcium on PI3K-Akt and HIF-1α survival pathways. Cell Biol Toxicol 32:437–449
62. Agas D, Hanna R, Benedicenti S, De Angelis N, Sabbieti MG, Amaroli A (2021) Photobiomodulation by near-infrared 980-nm wavelengths regulates pre-osteoblast proliferation and viability through the PI3K/Akt/Bcl-2 pathway. Int J Mol Sci 22:7586
63. Jere SW, Houreld NN, Abrahamse H (2022) Photobiomodulation activates the PI3K/AKT pathway in diabetic fibroblast cells in vitro. J Photochem Photobiol B 237:112590
64. Vieira WF, Malange KF, de Magalhães SF, Lemes JBP, Dos Santos GG, Nishijima CM, de Oliveira ALR, da Cruz-Höfling MA, Tambeli CH, Parada CA (2022) Anti-hyperalgesic effects of photobiomodulation therapy (904 nm) on streptozotocin-induced diabetic neuropathy imply MAPK pathway and calcium dynamics modulation. Sci Rep 12:16730
65. Neves LMS, Gonçalves ECD, Cavalli J, Vieira G, Laurindo LR, Simões RR, Coelho IS, Santos ARS, Marcolino AM, Cola M, Dutra RC (2018) Photobiomodulation therapy improves acute inflammatory response in mice: the role of cannabinoid receptors/ATP-sensitive K^+ channel/p38-MAPK signalling pathway. Mol Neurobiol 55(7):5580–5593
66. Mohamed Abdelgawad L, Abd El-Hamed MM, Sabry D, Abdelgwad M (2021) Efficacy of photobiomodulation and metformin on diabetic cell line of human periodontal ligament stem cells through Keap1/Nrf2/Ho-1 pathway. Rep Biochem Mol Biol 10:30–40
67. Curra M, Pellicioli AC, Filho NA, Ochs G, Matte Ú, Filho MS, Martins MA, Martins MD (2015) Photobiomodulation reduces oral mucositis by modulating NF-kB. J Biomed Opt 20:125008
68. Hong JU, Kwon JJ, Heo SC, Shin SH, Kim HJ, Lee JY (2022) Effects of photobiomodulation on bone remodeling in an osteoblast-osteoclast co-culture system. Lasers Med Sci 37:1049–1059

69. Fridoni M, Kouhkheil R, Abdollhifar MA, Amini A, Ghatr-ehsamani M, Ghoreishi SK, Chien S, Bayat S, Bayat M (2019) Improvement in infected wound healing in type 1 diabetic rat by the synergistic effect of photobiomodulation therapy and conditioned medium. J Cell Biochem 120:9906–9916
70. Ma Y, Li P, Ju C, Zuo X, Li X, Ding T, Liang Z, Zhang J, Li K, Wang X, Zhu Z, Zhang Z, Song Z, Quan H, Hu X, Wang Z (2022) Photobiomodulation attenuates neurotoxic polarization of macrophages by inhibiting the Notch1-HIF-1α/NF-κB signalling pathway in mice with spinal cord injury. Front Immunol 13:816952
71. Silva IJP, Cintra LTA, Ervolino E, Chaves HGDS, Sivieri-AraúJo G, Briso ALF, Cosme-Silva L, Benetti F (2022) Photobiomodulation reduces inflammation but does not influence the hypoxia-inducible factor-1α in pulp tissue of rats after bleaching. J Appl Oral Sci 30:e20210559
72. Tani A, Chellini F, Giannelli M, Nosi D, Zecchi-Orlandini S, Sassoli C (2018) Red (635 nm), Near-infrared (808 nm) and violet-blue (405 nm) photobiomodulation potentiality on human osteoblasts and mesenchymal stromal cells: a morphological and molecular in vitro study. Int J Mol Sci 19:1946
73. de Lima FM, Albertini R, Dantas Y, Maia-Filho AL, Santana Cde L, Castro-Faria-Neto HC, França C, Villaverde AB, Aimbire F (2013) Low-level laser therapy restores the oxidative stress balance in acute lung injury induced by gut ischemia and reperfusion. Photochem Photobiol 89:179–188
74. Mohamed AE, Mahmoud AM, Mohamed WR, Mohamed T (2022) Femtosecond laser attenuates oxidative stress, inflammation, and liver fibrosis in rats: Possible role of PPARγ and Nrf2/HO-1 signaling. Life Sci 307:120877
75. Souza NHC, Mesquita-Ferrari RA, Rodrigues MFSD, da Silva DFT, Ribeiro BG, Alves AN, Garcia MP, Nunes FD, da Silva Junior EM, França CM, Bussadori SK, Fernandes KPS (2018) Photobiomodulation and different macrophages phenotypes during muscle tissue repair. J Cell Mol Med 22:4922–4934
76. Mokoena DR, Houreld NN, Dhilip Kumar SS, Abrahamse H (2020) Photobiomodulation at 660 nm stimulates fibroblast differentiation. Lasers Surg Med 52:671–681
77. Ruh AC, Frigo L, Cavalcanti MFXB, Svidnicki P, Vicari VN, Lopes-Martins RAB, Leal Junior ECP, De Isla N, Diomede F, Trubiani O, Favero GM (2018) Laser photobiomodulation in pressure ulcer healing of human diabetic patients: gene expression analysis of inflammatory biochemical markers. Lasers Med Sci 33:165–171
78. Angiero F, Ugolini A, Cattoni F, Bova F, Blasi S, Gallo F, Cossellu G, Gherlone E (2020) Evaluation of bradykinin, VEGF, and EGF biomarkers in gingival crevicular fluid and comparison of PhotoBioModulation with conventional techniques in periodontitis: a split-mouth randomized clinical trial. Lasers Med Sci 35:965–970
79. Zheng Q, Zhang J, Zuo X, Sun J, Liang Z, Hu X, Wang Z, Li K, Song J, Ding T, Shen X, Ma Y, Li P (2021) Photobiomodulation promotes neuronal axon regeneration after oxidative stress and induces a change in polarization from M1 to M2 in macrophages via stimulation of CCL2 in neurons: relevance to spinal cord injury. J Mol Neurosci 71:1290–1300
80. Esteves GR, Junior IE, Masson IFB, Machado AFP, Oliveira MCD, Baldan CS, Farcic TS, Liebano RE, Plapler H (2022) Photobiomodulation effect in tumoral necrosis factor-alpha(TNF-α) on the viability of random skin flap in rats. Lasers Med Sci 37:1495–1501
81. Yin K, Zhu R, Wang S, Zhao RC (2017) Low-level laser effect on proliferation, migration, and antiapoptosis of mesenchymal stem cells. Stem Cells Dev 26:762–775
82. Park IS, Kim DK, Kim JH, Bae JS, Kim EH, Yoo SH, Chung YJ, Lyu L, Mo JH (2022) Increased anti-allergic effects of secretome of low-level light treated tonsil-derived mesenchymal stem cells in allergic rhinitis mouse model. Am J Rhinol Allergy 36:261–268
83. Heo JC, Park JA, Kim DK, Lee JH (2019) Photobiomodulation (660 nm) therapy reduces oxidative stress and induces BDNF expression in the hippocampus. Sci Rep 9:10114
84. Wu X, Shen Q, Chang H, Li J, Xing D (2022) Promoted CD4+ T cell-derived IFN-γ/IL-10 by photobiomodulation therapy modulates neurogenesis to ameliorate cognitive deficits in APP/PS1 and 3xTg-AD mice. J Neuroinflammation 19:253
85. Shaikh-Kader A, Houreld NN, Rajendran NK, Abrahamse H (2021) Levels of cyclooxygenase 2, interleukin-6, and tumour necrosis factor-α in fibroblast cell culture models after photobiomodulation at 660 nm. Oxid Med Cell Longev 2021:6667812
86. Macedo DB, Tim CR, Kido HW, Macedo JB, Martignago CCS, Renno ACM, Macedo GB, Assis L (2022) Influence of photobiomodulation therapy on the treatment of pulmonary inflammatory conditions and its impact on COVID-19. Lasers Med Sci 37:1921–1929
87. Silva T, Fragoso YD, Destro Rodrigues MFS, Gomes AO, da Silva FC, Andreo L, Viana A, Teixeira da Silva DF, Chavantes MC, Tempestini Horliana ACR, De Angelis K, Deana AM, Branco LP, Santos Fernandes KP, Motta LJ, Mesquita-Ferrari RA, Bussadori SK (2020) Effects of photobiomodulation on interleukin-10 and nitrites in individuals with relapsing-remitting multiple sclerosis - Randomized clinical trial. PLoS ONE 15:e0230551
88. Camargo CP, Forner-Cordero A, Silva BM, de Souza VM, Cunha HS, de Oliveira FY, Campello GA, Dos Santos PHG, Rego CL, Carvalho H, Gemperli R (2023) Effect of photobiomodulation with different wavelengths on radiodermatitis treatment. Plast Reconstr Surg Glob Open 11:e4809
89. Gupta A, Keshri GK, Yadav A, Gola S, Chauhan S, Salhan AK, Bala Singh S (2015) Superpulsed (Ga-As, 904 nm) low-level laser therapy (LLLT) attenuates inflammatory response and enhances healing of burn wounds. J Biophotonics 8:489–501
90. Keshri GK, Gupta A, Yadav A, Sharma SK, Singh SB (2016) Photobiomodulation with pulsed and continuous wave near-infrared laser (810 nm, Al-Ga-As) augments dermal wound healing in immunosuppressed rats. PLoS ONE 11:e0166705
91. Tam SY, Tam VCW, Ramkumar S, Khaw ML, Law HKW, Lee SWY (2020) Review on the cellular mechanisms of low-level laser therapy use in oncology. Front Oncol 10:1255
92. Zhu Q, Xiao S, Hua Z, Yang D, Hu M, Zhu YT, Zhong H (2021) Near infrared (NIR) light therapy of eye diseases: a review. Int J Med Sci 18:109–119
93. Malthiery E, Chouaib B, Hernandez-Lopez AM, Martin M, Gergely C, Torres JH, Cuisinier FJ, Collart-Dutilleul PY (2021) Effects of green light photobiomodulation on dental pulp stem cells: enhanced proliferation and improved wound healing by cytoskeleton reorganization and cell softening. Lasers Med Sci 36:437–445
94. Oyebode OA, Houreld NN (2022) Photobiomodulation at 830 nm stimulates migration, survival and proliferation of fibroblast cells. Diabetes Metab Syndr Obes 15:2885–2900
95. Schalch TD, Fernandes MH, Destro Rodrigues MFS, Guimarães DM, Nunes FD, Rodrigues JC, Garcia MP, Mesquita Ferrari RA, Bussadori SK, Fernandes KPS (2019) Photobiomodulation is associated with a decrease in cell viability and migration in oral squamous cell carcinoma. Lasers Med Sci 34:629–636
96. Ibarra AMC, Garcia MP, Ferreira M, de Fátima Teixeira da Silva D, Pavani C, Mesquita-Ferrari RA, Fernandes KPS, Nunes FD, Rodrigues MFSD, (2021) Effects of photobiomodulation on cellular viability and cancer stem cell phenotype in oral squamous cell carcinoma. Lasers Med Sci 36:681–690

97. Xia Y, Yu W, Cheng F, Rao T, Ruan Y, Yuan R, Ning J, Zhou X, Lin F, Zheng D (2021) Photobiomodulation with blue laser inhibits bladder cancer progression. Front Oncol 11:701122
98. Chaweewannakorn C, Santiwong P, Surarit R, Sritanaudomchai H, Chintavalakorn R (2021) The effect of LED photobiomodulation on the proliferation and osteoblastic differentiation of periodontal ligament stem cells: in vitro. J World Fed Orthod 10:79–85
99. George S, Hamblin MR, Abrahamse H (2022) Neuronal differentiation potential of primary and immortalized adipose stem cells by photobiomodulation. J Photochem Photobiol B 230:112445
100. Dawoud LE, Hegazy EM, Galhom RA, Youssef MM (2022) Photobiomodulation therapy upregulates the growth kinetics and multilineage differentiation potential of human dental pulp stem cells-an in vitro Study. Lasers Med Sci 37:1993–2003
101. Dos Anjos LMJ, da Fonseca AS, Gameiro J, de Paoli F (2017) Apoptosis induced by low-level laser in polymorphonuclear cells of acute joint inflammation: comparative analysis of two energy densities. Lasers Med Sci 32:975–983
102. da Silva PAV, Dos Anjos LMJ, Abduch TF, Pereira R, da Fonseca AS, de Paoli F (2019) Photobiomodulation can alter mRNA levels cell death-related. Lasers Med Sci 34(7):1373–1380
103. Salehpour F, Farajdokht F, Cassano P, Sadigh-Eteghad S, Erfani M, Hamblin MR, Salimi MM, Karimi P, Rasta SH, Mahmoudi J (2019) Near-infrared photobiomodulation combined with coenzyme Q10 for depression in a mouse model of restraint stress: reduction in oxidative stress, neuroinflammation, and apoptosis. Brain Res Bull 144:213–222
104. Davies DJ, Hadis M, Di Pietro V, Lazzarino G, Forcione M, Harris G, Stevens AR, Soon WC, Goldberg Oppenheimer P, Milward M, Belli A, Palin WM (2022) Photobiomodulation reduces hippocampal apoptotic cell death and produces a Raman spectroscopic "signature." PLoS ONE 17:e0264533
105. Zaccara IM, Mestieri LB, Pilar EFS, Moreira MS, Grecca FS, Martins MD, Kopper PMP (2020) Photobiomodulation therapy improves human dental pulp stem cell viability and migration in vitro associated to upregulation of histone acetylation. Lasers Med Sci 35:741–749
106. Pigatto GR, Silva CS, Parizotto NA (2019) Photobiomodulation therapy reduces acute pain and inflammation in mice. J Photochem Photobiol B 196:111513
107. Wang X, Li X, Zuo X, Liang Z, Ding T, Li K, Ma Y, Li P, Zhu Z, Ju C, Zhang Z, Song Z, Quan H, Zhang J, Hu X, Wang Z (2021) Photobiomodulation inhibits the activation of neurotoxic microglia and astrocytes by inhibiting Lcn2/JAK2-STAT3 crosstalk after spinal cord injury in male rats. J Neuroinflammation 18:256
108. Le HT, Huynh NC, Nguyen-Ho QA, Nguyen TT, Le SH, Nguyen LT (2022) Effect of photobiomodulation therapy on reducing acute pain and inflammation following surgical removal of impacted mandibular third molars: a randomized, split-mouth clinical trial. Photobiomodul Photomed Laser Surg 40:245–251
109. Alonso PT, Schapochnik A, Klein S, Brochetti R, Damazo AS, de Souza Setubal Destro MF, Lino-Dos-Santos-Franco A, (2022) Transcutaneous systemic photobiomodulation reduced lung inflammation in experimental model of asthma by altering the mast cell degranulation and interleukin 10 level. Lasers Med Sci 37:1101–1109
110. Martignago CCS, Tim CR, Assis L, Da Silva VR, Santos ECBD, Vieira FN, Parizotto NA, Liebano RE (2020) Effects of red and near-infrared LED light therapy on full-thickness skin graft in rats. Lasers Med Sci 35:157–164
111. Evangelista AN, Dos Santos FF, de Oliveira Martins LP, Gaiad TP, Machado ASD, Rocha-Vieira E, Costa KB, Santos AP, Oliveira MX (2021) Photobiomodulation therapy on expression of HSP70 protein and tissue repair in experimental acute Achilles tendinitis. Lasers Med Sci 36:1201–1208
112. Astuti SD, Sulistyo A, Setiawatie EM, Khasanah M, Purnobasuki H, Arifianto D, Susilo Y, Alamsyah KA, Suhariningsih SA (2022) An in-vivo study of photobiomodulation using 403 nm and 649 nm diode lasers for molar tooth extraction wound healing in wistar rats. Odontology 110:240–253
113. Kazemikhoo N, Ghadimi T, Vaghardoost R, Momeni M, Nilforoushzadeh MA, Ansari F, Dahmardehei M (2022) Effects of photobiomodulation and split-thickness skin grafting in the prognosis of wound healing in children with deep burn ulcers. Photobiomodul Photomed Laser Surg 40:148–154
114. Cai W, Hamushan M, Zhang Y, Xu Z, Ren Z, Du J, Ju J, Cheng P, Tan M, Han P (2022) Synergistic effects of photobiomodulation therapy with combined wavelength on diabetic wound healing in vitro and in vivo. Photobiomodul Photomed Laser Surg 40:13–24
115. Oliveira CG, Freitas MF, de Sousa MVP, Giorgi R, Chacur M (2020) Photobiomodulation reduces nociception and edema in a CFA-induced muscle pain model: effects of LLLT and LEDT. Photochem Photobiol Sci 19:1392–1401
116. Hadad H, Santos AFP, de Jesus LK, Poli PP, Mariano RC, Theodoro LH, Maiorana C, Souza FÁ (2022) Photobiomodulation therapy improves postoperative pain and edema in third molar surgeries: a randomized, comparative, double-blind, and prospective clinical trial. J Oral Maxillofac Surg 80:37.e1-37.e12
117. Pinto NC, de MVP, Ferreira NL, Braga NA, Aldred A, Gomes G, Freire GMG, Ashmawi HA, Chacur M (2022) Customized photobiomodulation modulates pain and alters thermography pattern in patients with knee osteoarthritis: a randomized double-blind pilot study. Photobiomodul Photomed Laser Surg 40:698-707
118. Tomazoni SS, Machado CDSM, De Marchi T, Casalechi HL, Bjordal JM, de Carvalho PTC, Leal-Junior ECP (2019) Infrared low-level laser therapy (photobiomodulation therapy) before intense progressive running test of high-level soccer players: effects on functional, muscle damage, inflammatory, and oxidative stress markers—a randomized controlled trial. Oxid Med Cell Longev 2019:6239058
119. Padoin S, Zeffa AC, Molina Corrêa JC, de Angelis TR, Moreira TB, Barazetti LK, de Paula RS (2022) Phototherapy improves muscle recovery and does not impair repeated bout effect in plyometric exercise. J Strength Cond Res 36:3301–3310
120. Dutra YM, Claus GM, Malta ES, Brisola GMP, Esco MR, Ferraresi C, Zagatto AM (2020) Acute photobiomodulation by LED does not alter muscle fatigue and cycling performance. Med Sci Sports Exerc 52:2448–2458
121. Azuma RHE, Merlo JK, Jacinto JL, Borim JM, da Silva RA, Pacagnelli FL, Nunes JP, Ribeiro AS, Aguiar AF (2021) Photobiomodulation therapy at 808 nm does not improve biceps brachii performance to exhaustion and delayed-onset muscle soreness in young adult women: a randomized, controlled, crossover trial. Front Physiol 12:664582

APÊNDICE D – Could violet-blue lights increase the bacteria resistance against ultraviolet radiation mediated by photolyases? (artigo publicado)

Lasers in Medical Science (2023) 38:253
https://doi.org/10.1007/s10103-023-03924-w

REVIEW ARTICLE

Could violet-blue lights increase the bacteria resistance against ultraviolet radiation mediated by photolyases?

Rickson Souza Ribeiro[1] · Andre Luiz Mencalha[1] · Adenilson de Souza da Fonseca[1,2,3]

Received: 16 August 2023 / Accepted: 26 October 2023

Abstract
Studies have demonstrated bacterial inactivation by radiations at wavelengths between 400 and 500 nm emitted by low-power light sources. The phototoxic activity of these radiations could occur by oxidative damage in DNA and membrane proteins/lipids. However, some cellular mechanisms can reverse these damages in DNA, allowing the maintenance of genetic stability. Photoreactivation is among such mechanisms able to repair DNA damages induced by ultraviolet radiation, ranging from ultraviolet A to blue radiations. In this review, studies on the effects of violet and blue lights emitted by low-power LEDs on bacteria were accessed by PubMed, and discussed the repair of ultraviolet-induced DNA damage by photoreactivation mechanisms. Data from such studies suggested bacterial inactivation after exposure to violet (405 nm) and blue (425–460 nm) radiations emitted from LEDs. However, other studies showed bacterial photoreactivation induced by radiations at 348–440 nm. This process occurs by photolyase enzymes, which absorb photons at wavelengths and repair DNA damage. Although authors have reported bacterial inactivation after exposure to violet and blue radiations emitted from LEDs, pre-exposure to such radiations at low fluences could activate the photolyases, increasing resistance to DNA damage induced by ultraviolet radiation.

Keywords Bacteria · DNA repair · LED · Photobiomodulation · Photoreactivation · Ultraviolet radiation

Introduction

Non-ionizing radiations emitted from low-power light sources into the violet-near to infrared range (400–1100 nm, approximately) can induce effects on bacteria [1–4]. These effects can be characterized as stimulation effects, such as cell proliferation and DNA and RNA synthesis, or inhibition effects, such as cell inactivation by generating reactive oxygen species and DNA damage [1, 2, 5, 6]. It seems that lights from low-power lasers (light amplification by stimulation of emitted radiation) and LED (light-emitting diode) can induce stimulation or inhibition effects on bacteria depending on endogenous chromophores, which could act as photosensitizers or as photoacceptors [7].

Endogenous photoacceptors absorb radiation at the highest wavelengths (600–1100 nm) and lead to the production of free radicals at low levels, which in turn could cause bacterial proliferation, characterizing a photostimulation effect [7–9]. On the other hand, endogenous photosensitizers absorb radiations at the lowest wavelengths (400–500 nm) and produce free radicals at high levels, which in turn could cause bacterial inactivation, characterizing a photoinactivation effect [1, 10, 11].

Radiations belonging to the ultraviolet spectrum can cause bacterial inactivation, but this effect could not depend on those endogenous chromophores that behave as photosensitizers because proteins and nucleic acids are chromophores for ultraviolet radiation, mainly at 260–280 nm [12].

Interestingly, radiations at wavelengths ranging from 300 up to 500 nm (ultraviolet A radiation up to blue light) can activate enzymes (photolyases) involved in the repair

✉ Adenilson de Souza da Fonseca
adnfonseca@yahoo.com.br

[1] Departamento de Biofísica e Biometria, Instituto de Biologia Roberto Alcantara Gomes, Universidade do Estado do Rio de Janeiro, Boulevard Vinte e Oito de Setembro, 87, Fundos, Vila Isabel, Rio de Janeiro 20551030, Brazil

[2] Departamento de Ciências Fisiológicas, Instituto Biomédico, Universidade Federal do Estado do Rio de Janeiro, Rua Frei Caneca, 94, Rio de Janeiro 20211040, Brazil

[3] Centro de Ciências da Saúde, Centro Universitário Serra dos Órgãos, Avenida Alberto Torres, Teresópolis, Rio de Janeiro 11125964004, Brazil

Published online: 06 November 2023

of DNA damages induced by ultraviolet radiation, the so-called photorepair or photoreactivation mechanism [13, 14]. Figure 1 is a schematic representation of radiation-induced photoinactivation and photostimulation mediated by photosensitizers and photoacceptors.

Ultraviolet radiation causes DNA damage through two pathways: direct and indirect. In the direct pathway, the DNA absorbs the ultraviolet photon energy in DNA sequences containing adjacent pyrimidine bases [12, 15]. By absorbing ultraviolet energy, these bases form covalent bonds with each other, generating deformation in DNA strands, which prevents DNA transcription and replication [16, 17]. These damages are so-called pyrimidine dimers and can be of two types: (i) cyclobutane pyrimidine (CPD) and (ii) 6–4 photoproducts (6–4 PP) and the difference between such DNA damages is the covalent bound between the carbons of the adjacent pyrimidine bases [18]. In bacteria, ultraviolet-induced pyrimidine dimers are reversed by photolyases. Figure 2 is a schematic representation of ultraviolet-induced pyrimidine dimer production and the action of photolyases.

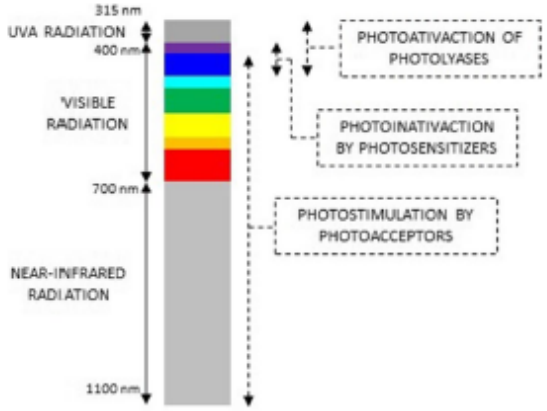

Fig. 1 Schematic representation for radiation-induced photoinactivation and photostimulation mediated by photosensitizers and photoacceptors as well as photoactivation of photolyases in bacteria. UVA, ultraviolet A

Photolyases have two cofactors: (i) a flavin adenine dinucleotide (FAD) responsible for the catalytic repair of UV-induced pyrimidine dimers [19] and (ii) secondary chromophores or antenna chromophores. Such secondary chromophores are methyltetrahydrofolate (MTHF), flavin mononucleotide (FMN), 8-hydroxy-7,8 dimethyl-5 deazariboflavin (8-HDF), and 6,7-dimethyl-8-ribityllumazine (DMRL), the type of secondary chromophore of photolyases, which depends on the organism [20–22].

The photolyase enzyme recognizes pyrimidine dimers in DNA strands and binds in these locations. The DNA repair process initializes through direct absorption of photon energy from incident radiation by a reduced form of FAD, which raises it to excited form ($FADH^{-*}$) or through energy transfer from the excited secondary chromophores [16, 17, 19]. Radiations absorbed by photolyases are those in the wavelength range between 315 and 500 nm (ultraviolet A up to violet/blue lights) [16, 21]. After energy absorption, electron excitation occurs in the catalytic cofactor FAD, which results in a reduced instability form ($FADH^{-*}$), and electrons are transferred to covalent bonds that form apyrimidine dimers in the DNA strand. Due to electron transfer, covalent bonds in the pyrimidine dimer are broken, restructuring the adjacent pyrimidine bases and the hydrogen bonds between nitrogenous bases, resulting in the integrity of genetic material [19–21].

Also, exposure to ultraviolet radiations and violet-blue lights could increase reactive oxygen species. Such chemical compounds are produced in the skin following

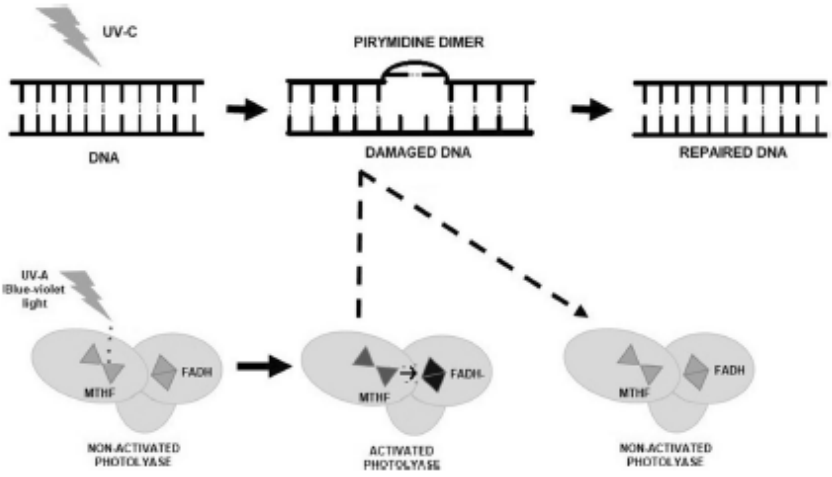

Fig. 2 Schematic representation for ultraviolet-induced pyrimidine dimer production and ultraviolet-induced photolyases, and for mechanism that would lead to an increase in bacterial resistance to ultraviolet radiation due to the activation of photolyase by pre-exposure to violet-blue lights. T, thymine; DR, deoxyribose; P, phosphorous; T^T, thymine dimers; triangles, secondary chromophores and FAD

exposure to ultraviolet radiation and are key mediators of oxidative damage to the skin [23]. Nakashima and coworkers [24] suggested that blue light causes oxidative stress in keratinocyte mitochondria. Transient formation of superoxide anion and accumulation of hydrogen peroxide in the nucleus of insect cell cultures were increased after exposure to blue light [25]. In addition, exposure to blue light increased reactive oxygen species in normal human epidermal keratinocytes and oral squamous cell carcinoma [26].

On the other hand, there have been suggested bactericidal effects of blue-violet radiation [27]. Blue light inactivates Gram-positive and Gram-negative bacteria at high radiation fluences [28–30]. However, despite the blue-violet radiations being proposed as bactericidal agents, using these radiations emitted by low-power sources at low fluences could increase the bacterial resistance to ultraviolet radiation due to the increased action of the photoreactivation mechanism through photolyases. Also, pre-exposure to radiations at other wavelengths, such as white light (from illumination in intensive care units, burn units of hospitals, corridors of hospitals, and medical applications), might affect overall ultraviolet C sterilization. Such an effect could decrease the effectiveness of ultraviolet disinfection and infection control in controlled environments [31]. Also, the increased action of photolyases could alter the bacteria load in foods sterilized by ultraviolet radiation. Blue-violet radiation can acquire such resistance through the activation of photolyase enzymes. Activated photolyase can repair damages caused by ultraviolet in DNA, which could increase bacteria survival in harmful environments.

In this review, studies on the effects of violet and blue lights emitted by low-power LEDs on bacteria were accessed by PubMed and discussed the repair of ultraviolet-induced DNA damages by a photoreactivation mechanism.

Material and methods

Studies performed using blue-violet radiations and bacteria were those written in English and assessed by MEDLINE/PubMed. No limit of time was specified for searches by PubMed, and headings and keywords used were "Blue LED and bacteria inactivation," "violet LED and bacteria inactivation," "Blue light and bacteria inactivation," and "violet light and bacteria inactivation." A total of 538 articles were retrieved from PubMed, with only abstracts, and full texts in English considered. Articles in repetitions/duplicates were 74. Articles on bacterial inactivation induced by exogenous photosensitizers in photodynamic therapy were not considered.

Results

The data obtained from a search performed by PubMed about the inactivation effect of violet-blue lights emitted from LEDs on Gram-positive and Gram-negative bacterial cultures are listed in Tables 1 and 2, respectively. The studies show that the radiation emitted by low-power violet-blue LEDs and lasers ranged from 405 to 470 nm of wavelengths. The fluence was from 0 up to 3060 J/cm^2, but most studies used the fluence between 0 up to 300 J/cm^2. The irradiance was from 0.17 up to 1260 mW/cm^2 (most commonly irradiance between 2.2 up to 400 mW/cm^2), and the exposure time was 38 s up to 24 h (most commonly exposure time between 4.3 up to 240 min). Several Gram-positive bacteria have been used, such as *Bacillus cereus*, *Listeria monocytogenes*, *Staphylococcus aureus* (and MRSA), *Staphylococcus epidermalis*, *Streptococcus pyogenes*, *Streptococcus mutans*, *Enterococcus faecalis*, *Clostridium perfringens*, *Leuconostoc mesenteroides*, and *Bacillus atrophaeus*. Several Gram-negative bacteria have also been used, such as the following: *Pseudomonas aeruginosa*, *Pseudomonas flurescens*, *Salmonella typhimurium*, *Salmonella enteritidis*, *Escherichia coli*, *Porphyromonas gengivalis*, *Klebsiella pnumoniae*, *Acinetobacter baumannii*, *Neisseria gonorrhoeae*, *Proteus mirabilis*, *Proteus vulgaris*, and *Aggregatibacter actinomycetemcomitans*.

The bactericidal effect of violet light emitted from a low-power violet (405 nm) laser on in vitro and in vivo *H. pylori* was reported by Ganz and coworkers [46]. Such light from a low-power LED was also effective on other Gram-negative and Gram-positive bacteria, as reported by Maclean and coworkers [32]. Also, violet light (405 nm) from a single-emitter diode lamp was able to inactivate and reduce the virulence factor of *P. aeruginosa* [33]. Exposure to blue light (470 nm) from low-power LED was able to inactivate *Leuconostoc mesenteroides* and *P. aeruginosa* cells, but *P. aeruginosa* cells were more sensitive to blue light than *L. mesenteroides* cells [34]. Also, blue light (470 nm) was able to inactivate *L. monocytogenes* cells in stationary and exponential growth phases [35]. The exposure to blue light (425 nm) emitted from low-power LEDs reduced survival in *Porphyromonas gengivalis*, *S. aureus*, and *Escherichia coli* cultures, whereas exposure to red light (625 nm) emitted from another low-power LED increases bacterial proliferation in cultures of these bacteria at similar irradiation conditions used for blue and violet irradiation. A multidrug-resistant *A. baumannii* also showed sensibility to violet light (415 nm) emitted by a low-power LED [9, 36]. Blue light (460 nm) emitted by a LED proved effective against *Aggregatibacter actinomycetemcomitans*, but no bactericidal activity was found

Table 1 Inactivation effects induced by exposure to blue-violet radiations emitted by low-power light sources on gram-positive bacteria

Title	Light parameters	Bacteria	Main biological end point	Method used	Exposure time	Reference
Kinetics of bacterial inactivation by 405-nm and 520-nm light emitting diodes and the role of endogenous coproporphyrin on bacterial susceptibility	405 and 520 nm; 306 and 3060 J/cm2; 21 and 210 mW/cm2	*Bacillus cereus* *Listeria monocytogenes* *Staphylococcus aureus*	Cell death	Counting of colony-forming units	Not clear	[8]
In vitro bacterial effects of 625-, 525-, and 425-nm wavelength (red, green, and blue) light-emitting diode irradiation	425, 525, and 625 nm; 21.6–172.8 J/cm2; 6 mW/cm2/h	*Staphylococcus aureus*	Cell death	Counting of colony-forming units	1–8 h	[9]
Antimicrobial blue light inactivation of microbial isolates in biofilms	405 nm; 108 and 216 J/cm2; 60 mW/cm2	*Enterococcus faecalis*	Cell death	Counting of colony-forming units	30 and 60 min	[30]
Inactivation of bacterial pathogens following exposure to light from a 405-nm light-emitting diode array	405 nm; 36–216 J/cm2; 10 mW/cm2	*Staphylococcus aureus* *Staphylococcus epidermalis* *Streptococcus pyogenes* *Enterococcus faecalis* *Clostridium perfringens*	Survival loss	Counting of colony-forming units	360 min	[32]
Blue light (470 nm) effectively inhibits bacterial and fungal growth	470 nm; 2–300 J/cm2; 2.2 and 80 mW/cm2	*Leuconostoc mesenteroides* *Bacillus atrophaeus*	Survival loss	Counting of colony-forming units	4.3–21.5 min	[34]
Blue light sensing in *Listeria monocytogenes* is temperature-dependent and the transcriptional response to it is predominantly sigb-dependent	470 nm; 35 mW/cm^2	*Listeria monocytogenes*	Global transcriptional response	RNAseq-based approach	8 h	[35]
A new proof of concept in bacterial reduction: antimicrobial action of violet-blue light (405 nm) in ex vivo stored plasma	405 nm; 0–250, 0–1200 J/cm2; 5 and 100 mW/cm2	*Staphylococcus aureus* *Staphylococcus epidermalis*	Cell death	Counting of colony-forming units	Not clear	[38]
Blue/violet laser inactivates methicillin-resistant *Staphylococcus aureus* by altering its transmembrane potential	405 ±1 nm; 500 mW; 121 J/cm^2; 135 mW/cm^2	*Staphylococcus aureus*	Membrane potential	Laser-scanning microscopy	15 min	[39]
Porphyrins and flavins as endogenous acceptors of optical radiation of blue spectral region determining photoinactivation of microbial cells	405, 445 nm; 50–500 mW; 50 ±3 mW/cm^2	*Staphylococcus aureus*	Survival loss	Counting of colony-forming units	0–180 min	[40]
Photo inactivation of *Streptococcus mutans* biofilm by violet-blue light	405 nm; 3 W; 0–9.26 J/cm2; 13 mW/cm2	*Streptococcus mutans*	Biofilm formation	Absorbance	5 min	[41]

Table 1 (continued)

Title	Light parameters	Bacteria	Main biological end point	Method used	Exposure time	Reference
Visible light as an antimicrobial strategy for inactivation of *Pseudomonas fluorescens* and *Staphylococcus epidermidis* biofilms	410 ± 10, 440 ± 20 nm; 10.1–420.5, 2.5–6.9 J/cm2; 0.7–29.2, 0.17–0.49 mW/cm2	*Pseudomonas fluorescens* *Staphylococcus epidermidis*	Survival loss	Counting of colony-forming units	30–240 min	[43]

against *E. coli* [37]. Also, violet light (405 nm) was able to inactivate *S. aureaus*, *S. epidermidis*, and *E. coli* cells in plasma bags [38]. Similarly, violet light (405 nm) from a low-power laser was able to alter membrane integrity and inactivate *S. aureus* [39]. A more significant bactericidal effect was induced by exposure to violet light (405 nm) emitted from low-power LED than that induced by green light (520 nm) in *S. aureus*, *Listeria monocytogenes*, *Bacillus cereus*, *P. aeruginosa*, *Salmonella typhimurium*, and *E. coli* cells, even at low fluence [8]. Violet light at 405 nm from a low-power laser was more effective in inactivating *E. coli* and *S. aureus* than violet light at 445 nm from another low-power laser [40]. The inactivation of *Streptococcus mutans* and the reduction of biofilms were found after exposure to violet light (405 nm) [41]. Exposure of *P. gengivalis* cells to blue light (460 nm) emitted from a low-power LED decreased cell viability and increased reactive oxygen species production [11]. Inhibition of growth in *P. gengivalis* cultures was obtained after exposure to violet light (405 nm) [28]. Survival of *E. coli* multidrug-resistant strains was decreased after exposure to violet light (410 nm) emitted from low-power LED [42]. Cultures of a *K. pneumonie* β-lactamase-resistant strain showed were more tolerant to the antimicrobial effect of blue light (410 nm) when compared to other clinically important bacteria, such as *S. aureus*, *E. coli*, and *P. aeruginosa* [29].

Discussion

Bactericidal effects of violet and blue lights on Gram-positive bacteria

Maclean and coworkers [32] demonstrated that Gram-positive bacteria of medical interest (*S. aureus*, *S. epidermidis*, *S. pyogenes*, *E. faecalis*, *C. perfringens*) were in vitro susceptible to exposure to violet light (405 nm) emitted from LEDs. The authors did not use photosensitizing agents and proposed that the photoinactivation was due to high levels of coproporphyrin, a natural endogenous photosensitizer that absorbs violet light and generates reactive oxygen species. These results were reinforced by Kumar and coworkers [8], who demonstrated that three Gram-positive bacteria of medical interest (*B. cereus*, *L. monocytogenes*, and *S. aureus*) had high inactivation rates after in vitro exposure to violet light at 405 nm from LEDs. Also, the authors carried out porphyrin quantification in such Gram-positive bacteria and reported high levels of endogenous coproporphyrin. However, in addition to the concentration of endogenous porphyrins, the authors proposed that other factors should be considered, such as metabolic burden and bacterial response to free radicals. Biener and coworkers [39] reported that a

Table 2 Inactivation effects induced by exposure to blue-violet radiations emitted by low-power light sources on gram-negative bacteria

Title	LED parameters	Bacteria	Main biological end point	Method used	Exposure time	Reference
Kinetics of bacterial inactivation by 405-nm and 520-nm light emitting diodes and the role of endogenous coproporphyrin on bacterial susceptibility	405 and 520 nm; 306 and 3060 J/cm2; 21 and 210 mW/cm2	*Pseudomonas aeruginosa* *Salmonella typhimurium* *Escherichia coli*	Cell death	Counting of colony-forming units	Not clear	[8]
In vitro bacterial effects of 625-, 525-, and 425-nm wavelength (red, green, and blue) light-emitting diode irradiation	425, 525, and 625 nm; 21.6–172.8 J/cm2; 6 mW/cm2/h	*Porphyromonas gengivalis* *Escherichia coli*	Cell death	Counting of colony-forming units	1–8 h	[9]
Antimicrobial effects of blue light using *Porphyromonas gengivalis* pigment	460 nm; 1–100 J/cm2; 400 mW/cm2	*Porphyromonas gengivalis*	Survival loss	Counting of colony-forming units	Not clear	[11]
Specific-wavelength visible light irradiation inhibits bacterial growth of *Porphyromonas gingivalis*	405 nm; 15 J/cm2; 50, 200, 400 mW/cm2	*Porphiromonas gengivalis*	Cell death	Counting of colony-forming units	38–300 s	[28]
Antimicrobial blue light and photodynamic therapy inhibit clinically relevant β-lactamases with extended-spectrum (ESBL) and carbapenemase activity	410 nm; 0–126 J/cm2; 38.2 mW/cm2	*Klebsiella pneumoniae*	Inhibition of hydrolytic activity of β-lactamase enzymes	Measurement of chromogenic β-lactam substrate nitrocefin	Not clear	[29]
Antimicrobial blue light inactivation of microbial isolates in biofilms	405 nm; 108, 216 J/cm2; 60 mW/cm2	*Acinetobacter baumannii* *Escherichia coli* *Neisseria gonorrhoeae* *Pseudomonas aeruginosa* *Proteus mirabilis*	Cell death	Counting of colony-forming units	30 and 60 min	[30]
Inactivation of bacterial pathogens following exposure to light from a 405-nm light-emitting diode array	405 nm; 36–216 J/cm2; 10 mW/cm2	*Acinetobacter baumannii* *Pseudomonas aeruginosa* *Escherichia coli* *Proteus vulgaris* *Klebsiella pneumoniae*	Survival loss	Counting of colony-forming units	360 min	[32]
Blue light treatment of *Pseudomonas aeruginosa*: Strong bactericidal activity, synergism with antibiotics, and inactivation of virulence factors	405 nm; 120 W; 0–50 J/cm^2; 15.7 mW/cm^2	*Pseudomonas aeruginosa*	Survival loss	Counting of colony-forming units	0–3184 s	[33]
Blue light (470 nm) effectively inhibits bacterial and fungal growth	470 nm; 2–300 J/cm2; 2.2, 80 mW/cm2	*Pseudomonas aeruginosa*	Survival loss	Counting of colony-forming units	4.3–21.5 min	[34]

Table 2 (continued)

Title	LED parameters	Bacteria	Main biological end point	Method used	Exposure time	Reference
Antimicrobial blue light therapy for multidrug-resistant *Acinetobacter baumannii* infection in a mouse burn model: implications for prophylaxis and treatment of combat-related wound infections	415 nm; 0–70.2 J/cm2; 19.5 mW/cm2	*Acinetobacter baumannii*	Survival loss	Counting of colony-forming units	0–60 min	[36]
Blue light kills *Aggregatibacter actinomycetemcomitans* due to its endogenous photosensitizers	460 nm; 0–150 J/cm2; 1260 mW/cm2	*Aggregatibacter actinomycetemcomitans*	Survival loss	Counting of colony-forming units		[37]
A new proof of concept in bacterial reduction: antimicrobial action of violet-blue light (405 nm) in ex vivo stored plasma	405 nm; 250–1200 J/cm2; 5 and 100 mW/cm2	*Escherichia coli*	Cell death	Counting of colony-forming units	Not clear	[38]
Porphyrins and flavins as endogenous acceptors of optical radiation of blue spectral region determining photoinactivation of microbial cells	405, 445 nm; 50–500 mW; 50 ± 3 mW/cm^2	*Escherichia coli*	Survival loss	Counting of colony-forming units	0–180 min	[40]
Antimicrobial blue light inactivation of international clones of multidrug-resistant *Escherichia coli* ST10, ST131, and ST648	410 nm; 0–412.5 J/cm2; 38.2 mW/cm2	*Escherichia coli*	Survival loss	Counting of colony-forming units	30–180 min	[42]
Visible light as an antimicrobial strategy for inactivation of *pseudomonas fluorescens* and *Staphylococcus epidermidis* biofilms	410 ± 10 and 440 ± 20 nm; 10.1–420.5, 2.5–6.9 J/cm2; 0.7–29.2, 0.17–0.49 mW/cm2	*Pseudomonas fluorescens*	Survival loss	Counting of colony-forming units	30–240 min	[43]
Inactivation efficacy of 405 nm light emitting diodes (LEDs) on *Salmonella enteritidis* at different illumination temperatures	405 nm; 10 W; 0–2332,8 J/cm2; 27.7 mW/cm2	*Salmonella enteritidis*	Survival loss	Counting of colony-forming units	7.5 h 24 h	[45]
Helicobacter pylori in patients can be killed by visible light	405 ± 2 nm; 4–32 J/cm^2, 100 mW/cm^2	*Helicobacter pylori*	Cell death	Counting of colony-forming units	40–320 s	[46]

multi-resistant *S. aureus* is also susceptible to exposure to violet at 405 nm from a low-power diode laser. The authors suggested that the antimicrobial activity of blue light was due to the alteration of membrane integrity, which caused a decrease in membrane polarization and rapid alteration of vital cellular functions. In addition, Plavskii and coworkers [40] compared bacterial inactivation by violet light at two wavelengths from low-power lasers. Data from such study showed that violet light at 405 nm is more effective than 445 nm in inactivating *S. aureus* and that the contribution of porphyrin photosensitizers is most pronounced for violet light at 405 nm, and flavins for violet-blue light at 445 nm.

In the food industry, violet light at 405 nm was reported to inactivate bacteria, such as *S. aureus*, *B. cereus*, *L. monocytogenes*, and *P. aeruginosa* in food packaging, work surfaces, liquid foods, horticultural, meat, and seafood products [44]. Dorey and coworkers [35] also reported that blue light at 470 nm inactivates *L. monocytogenes* but that light-induced bacterial inactivation was more effective in exponential bacterial cultures than in stationary bacterial cultures as well as in bacterial cultures at 37°C than in bacterial cultures at 30°C.

The contamination of injectable stored biological fluids, such as blood plasma and platelet concentrates preserved in plasma, is also a major health risk. Maclean and coworkers [38] evaluated the effect of violet light at 405 nm on *S. aureus* and *S. epidermidis* seeded in stored plasma ex vivo in different volumes and found significant inactivation of those bacteria. However, the light fluence should be increased according to plasma volumes to achieve similar bacterial inactivation to small volumes due to the optical transmission proprieties.

In addition to bacterial inactivation, biofilm formation could be reduced by exposure to violet light at 405 nm. Gomez and coworkers [41] reported a decrease in biofilm formation and reduced viability in planktonic cells of *S. mutans*. The mechanism involved in the photoinactivation of *S. mutans* is unknown, but it is attributed to endogenous photosensitizers, such as porphyrins, which are excited by this radiation and cause cytotoxic effects. However, Angarano and coworkers [43] demonstrated that blue light at 420 nm cannot inhibit biofilms from *S. epidermidis*, while violet light at 400 nm can cause such an effect.

Bactericidal effects of violet and blue lights on Gram-negative bacteria

Similar to the studies based on Gram-positive bacterial, photoinactivation by violet-blue lights has potential against Gram-negative bacteria, including multidrug-resistant [36], periodontal [9, 11, 28, 37], and foodborne [44, 45] bacteria, enterobacteria [8, 9, 30, 32, 38, 42], as well as biofilm formation [30, 43].

Regarding multidrug-resistant bacteria, *A. baumannii* is considered one of the most dangerous pathogens due to its capability to develop resistance to antibiotics and adaptation to adverse environmental conditions [32], which increases interest in alternative bactericidal agents. Zhang and coworkers [36] demonstrated that violet light at 415 nm is efficient against *A. baumannii* at a single exposure. The authors showed higher susceptibility to blue light than human keratinocytes and did not develop resistance after 10 cycles of sublethal bacterial inactivation. The photoinactivation was related to the presence of porphyrins (coproporphyrin III), as shown by the fluorescence spectrum.

P. gengivalis is an infectious agent associated with the initiation and progression of periodontitis [9, 11, 28]. Fukui and coworkers [28] demonstrated that exposure to violet light at 405 nm emitted from a LED device could significantly inhibit *P. gengivalis*. This effect was attributed to protoporphyrins at high levels, which act as natural photosensitizers and alter the proteolytic activity of this bacterium, reducing its growth and viability. Kim and coworkers [9] reported similar effects on *P. gengivalis* after exposure to the blue range at 425 nm emitted from a LED device. However, photoinactivation was related to the production of reactive oxygen species. Also, Yoshida and coworkers [11] demonstrated bacterial inactivation in *P. gengivalis* cultures after exposure to blue light at 460 nm, and the authors quantified the concentration of endogenous porphyrins from lysed bacterial cells, in particular protoporphyrin IX, which is an intracellular pigment able to generate reactive oxygen species after exposure to blue light.

A. actinomycetemcomitans is another periodontal pathogen in which Cieplik and coworkers [37] demonstrated the bactericidal effects of blue light at 460 nm emitted from a LED device. The authors also examined the production of reactive oxygen species from lysed bacterial cells and detected oxygen singlet production, suggesting the presence of endogenous photosensitizers, such as porphyrins and flavins, which are chemical compounds involved in phototoxicity.

A non-pathogenic *E. coli* strain was more susceptible to violet light at 425 nm than green light at 525 nm and not susceptible to red light at 625 nm from LEDs [9]. Kumar and coworkers [8] also reported bacterial inactivation in *E. coli* cultures exposed to violet light at 405 nm from a LED and that such an effect could be related to endogenous coproporphyrin. In another study, the antibacterial effect of violet light at 405 nm from a LED array on *E. coli* in biological fluids was reported, which suggests that such light permits bacterial reduction in biological fluids, especially those injectable fluids relevant to transfusion medicine [38]. Plavskii and coworkers [40] showed that violet lights (405 and 445 nm) from low-power lasers were able to inactivate *E. coli*, but the contribution of porphyrin photosensitizers is

most pronounced for violet light at 405 nm, and flavins for violet-blue light at 445 nm. A multidrug-resistant *E. coli* was also inactivated by violet light at 410 nm from a LED, which supports using of blue light as an antimicrobial against such pathogens [42]. In addition, Ferrer-Espada and coworkers [30] reported that *E. coli* and *E. faecali* were inactivated by violet light at 405 nm from a LED, reinforcing that violet-blue lights can inactivate pathogenic microorganisms.

P. aeruginosa thrives in most natural and man-made environments, including soil, water, plants, and animals, and infects multiple hosts [33]. Violet light at 405 nm from a single-emitter diode lamp was able to inactivate and reduce the virulence of this bacterium [33]. Moreover, violet light at 405 nm from LEDs could inactivate in vivo and in vitro *H. pylori*, particularly in those patients who have failed standard antibiotic treatment [46].

Some studies have demonstrated that bacteria develop resistance to violet-blue lights. Development of tolerance to blue light (415 nm) was reported in subsequently irradiated *E. coli*, *K. pneumoniae*, and *P. aeruginosa* cultures, which could result in genetic alterations driven by SOS mutagenesis [47]. Metzger and coworkers [48] reported that the recA gene increases survival in *E. coli* and *S. carnosus* cultures exposed to blue light (475 nm), indicating a protective mechanism conveyed by the bacterial SOS response.

However, Amin and coworkers [49] reported no tolerance development to blue light (415 nm) in *P. aeruginosa* cultures after 10 cycles of sub-lethal inactivation. Also, repeated sub-lethal exposure of non-proliferating *S. aureus* populations did not affect the susceptibility to violet-blue light (405 nm) [50]. Leanse and coworkers [51] reported the absence of resistance in *P. aeruginosa*, *A. baumannii*, and *E. coli* cultures after sequential exposure to blue light (405 nm).

The irradiation parameters such as fluence, irradiance, and exposure time demonstrated in Tables 1 and 2 did not vary much due to these studies which used different bacteria, Gram-positive and Gram-negative, as a comparison to evaluate the effects of violet-blue lights from low-power light sources in these organisms and verify the cytotoxic effects generated by exposure to these radiations at different fluences.

Violet-blue lights on photolyase action

The bactericidal effect of violet-blue lights, at wavelengths ranging between 405 and 470 nm, has been reported to *P. gengivalis*, *E. coli*, *S. aureus*, *B. cereus*, *L. monocytogenes*, and *S. typhimurium* [8, 9, 11]. The photoinactivation effect of these lights is related to the stimulation of endogenous photosensitizers, such as porphyrins, which can absorb the energy of radiation at specific wavelengths. Consequently, free radicals are produced, such as singlet oxygen, which react with endogenous molecules, including the DNA, generating oxidative damage [1, 10, 11]. Free radicals at low concentrations could cause sub-lethal DNA damage and active DNA repair, and pre-exposure to red light and infrared radiation from low-power lasers seems to increase free radical levels and induce DNA repair [6]. Such an effect could explain protection against DNA damage by red light (632.8 nm) from low-power lasers in *E. coli* [52]. On the other hand, other studies have suggested that such violet-blue lights are used in therapeutic protocols for the treatment of several conditions, such as reduction of ulcers in diabetic patients, recovery of injured tissues, and treatment of acne [3, 53].

However, violet-blue lights can also activate photolyases, which are enzymes involved in repairing of damages induced in DNA by direct absorption of ultraviolet radiation, mainly the pyrimidine dimers, reverting such DNA damages [16, 17, 19, 21]. The activation of these enzymes in *E. coli* cells occurs at maximum level by exposure to ultraviolet radiation at 384 nm, despite such radiation at wavelengths higher than 450 nm being less absorbed by photolyases; they can significantly activate photolyases [20]. Violet-blue lights are absorbed by the chromophore antennas (MTHF and 8-HDF) in photolyases, as well as by secondary chromophores, such as flavin mononucleotide (FMN), flavin adenine dinucleotide (FAD), and 6,7-dimethyl-8-ribityllumazine (DMRL), depending on the cell type [20–22]. As a consequence of such absorption, the redox state of FAD changes to $FADH^-$, activating the photolyase to reverse lesions caused by ultraviolet radiations as the pyrimidine dimers. Therefore, the photolyase could be activated by exposition to violet-blue lights emitted from low-power LEDs. Then, the catalytic cofactor, FADH, is reduced, which enables the photolyase to repair direct damages caused by ultraviolet radiation in DNA (Fig. 2).

Sancar (1994) [21] explained the structure and function of photolyase on DNA damages, summarizing the process in four steps: (i) the second chromophore or antenna chromophore (MTHF or 8-HDF) absorbs a photon of incident radiation; (ii) transfers the energy to FADH by dipole–dipole interaction; (iii) the excited singlet state $FADH^-$ transfers an electron to pyrimidine dimer, resulting in a pyrimidine anion; and (iv) which is later oxidized by the FADH to restore the pyrimidine and the functional form of flavin ($FADH^-$), which is ready for a new cycle of catalysis.

The mechanism involved in this process consists in the activation of photolyase by lights into the violet-blue spectrum; this phenomenon generates the reduction of catalytic cofactor $FADH^-$, which could remain in this state until the formation of pyrimidine dimers. When DNA damages occur, the photolyases recognize them and bind at the pyrimidine dimer, carry out transfer electrons, and undo the covalent bound, leading to the repair of the DNA. Thus, the repair capacity of the pyrimidine dimers in DNA could be increased without the necessity of a posterior exposition to radiation if the photolyases are in reduced form before exposure to ultraviolet radiation and induction of pyrimidine dimers in DNA.

Conclusion

Although several studies have reported the application of radiations in the violet and blue range (400 nm up to 500 nm) to inactivate bacteria, the previous exposure of such radiations at low fluences could generate the reduction of cofactors FADH of photolyases. This effect could increase the bacteria's resistance to ultraviolet radiation and reduce its effectivity on decontamination and sterilization procedures of environments and foods depending on the bacteria type.

Author contribution Rickson Souza Ribeiro: conceptualization, methodology, resources, and writing of the original draft. Andre Luiz Mencalha: data curation, visualization, review, and editing. Adenilson de Souza da Fonseca: conceptualization, methodology, review, editing, and supervision.

Funding This research was supported by Fundação de Amparo à Pesquisa do Estado do Rio de Janeiro (FAPERJ), Conselho Nacional de Desenvolvimento Científico e Tecnológico (CNPq), and Universidade do Estado do Rio de Janeiro (UERJ).

Declarations

Ethics approval Not applicable.

Conflict of interest The authors declare no competing interests.

References

1. Lubart R, Lipovsky A, Nitzan Y, Friedmann H (2011) A possible mechanism for the bactericidal effect of visible light. Laser Ther 20(1):17–22. https://doi.org/10.5978/islsm.20.17
2. Fonseca AS, Teixeira AF, Presta GA, Geller M, Valença SS, Paoli F (2012) Low intensity infrared laser effects on escherichia coli cultures and plasmid DNA. Laser Phys 22:1635–164. https://doi.org/10.1134/S1054660X12100076
3. Diogo MLG, Campos TM, Fonseca ESR, Pavini C, Horliana ACRT, Fernandes KPS, Bussadori SK, Fantin FGMM, Leite DPV, Yamamoto ATA, Navarro RS, Motta LJ (2021) Effect of blue light on acne vulgaris: a systematic review. Sensors 21(20):6943. https://doi.org/10.3390/s21206943
4. Ribeiro RS, Rodrigues JA, Mencalha AL, Fonseca AS (2023) Low-power blue LED and red laser effects on plasmid DNA, survival and photolyase mRNA levels in Escherichia coli cultures. Laser Phys Lett 20(8):085601. https://doi.org/10.1088/1612-202X/ace0b1
5. Karu T, Tiphlova O, Esenaliev R, Letokhov V (1994) Two different mechanisms of low-intensity laser photobiological effects on Escherichia coli. J Photochem Photobiol B 24(3):155–161. https://doi.org/10.1016/1011-1344(94)07016-4
6. Fonseca AS, Moreira TO, Paixão DL, Farias FM, Guimarães OR, Paoli S, Geller M, Paoli F (2010) Effect of laser therapy on DNA damage. Laser Surg Med 42:481–488. https://doi.org/10.1002/lsm.20921
7. Lima AMCT, Sergio LPD, Fonseca AS (2020) Photobiomodulation via multilple-wavelenght radiations. Lasers Med Sci 35:307–316. https://doi.org/10.1007/s10103-019-02879-1
8. Kumar A, Ghate V, Kim M-J, Zhou W, Khoo GH, Yuk H-G (2015) Kinetics of bacterial inactivation by 405 nm and 520 nm light emitting diodes and the role of endogenous coproporphyrin on bacterial susceptibility. J Photochem Photobiol B 149:37–44. https://doi.org/10.1016/j.jphotobiol.2015.05.005
9. Kim S, Kim J, Lim WB, Jeon S, Kim O, Koh JT, Kim C-S, Choi H, Kim, (2013) In vitro bactericidal effects of 625, 525, and 425nm wavelength (red, green, and blue) light-emitting diode irradiation. Photomed Laser Surg 31(11):554–562. https://doi.org/10.1089/pho.2012.3343
10. Wang Y, Wang Y, Wang Y, Murray CK, Hamblin MR, Hooper DC, Dai T (2017) Antimicrobial blue light inactivation of pathogenic microbes: state of art. Drug Resis Updat 33–35:1–22. https://doi.org/10.1016/j.drup.2017.10.002
11. Yoshida A, Sasaki H, Toyama T, Araki M, Fujioka J, Tsukiyama K, Hamada N, Yoshino F (2017) Antimicrobial effect of blue light using Porphyromonas gengivalis pigment. Sci Rep 7(1):5225. https://doi.org/10.1038/s41598-017-05706-1
12. Sinha RP, Häder DP (2002) UV-induced DNA damage and repair: a review. Photochem Photobiol Sci 1(4):225–236. https://doi.org/10.1039/b201230h
13. Schleicher E, Hessling B, Illarionova V, Bacher A, Weber S, Richter G, Gerwert K (2005) Light-induced reactions of Escherichia coli DNA photolyase monitored by Fourier transform-infrared spectroscopy. FEBS J 272(8):1855–1866. https://doi.org/10.1111/j.1742-4658.2005.04617.x
14. Harper JW, Elledge SJ (2007) The DNA damage response: ten years after. Mol Cell 28(5):739–745. https://doi.org/10.1016/j.molcel.2007.11.015
15. Jiang Y, Rabbi M, Kim M, Ke C, Lee W, Clark RL, Mieczkowski PA, Marszalek PE (2009) UVA generates pyrimidine dimers in DNA directly. Biophys J 96(3):1151–1158. https://doi.org/10.1016/j.bpj.2008.10.030
16. Zhang M, Wang L, Zhong D (2017) Photolyase: dynamics and mechanisms of repair of sun-induced DNA damage. Photochem Photobiol 93(1):78–92. https://doi.org/10.1111/php.12695
17. Zhang M, Wang L, Zhong D (2017) Photolyase: dynamics and electron-transfer Mechanisms of DNA repair. Arch Biochem Biophys 632:158–174. https://doi.org/10.1016/j.abb.2017.08.007
18. Chatterjee N, Walker GC (2017) Mechanisms of DNA damage, repair and mutagenesis. Environ Mol Mutagen 58(5):235–263. https://doi.org/10.1002/em.22087
19. Liu Z, Wang L, Zhong D (2015) Dynamics and mechanisms of DNA repair by photolyase. Phys Chem Chem Phys 17(18):11933–11949. https://doi.org/10.1039/C4CP05286B
20. Sancar GB, Smith FW, Reid R, Payne G, Levy M, Sancar A (1987) Action mechanism of Escherichia coli DNA photolyase I Formation of the enzyme-substrate complex. J Biol Chem 262(1):478–485
21. Sancar A (2008) Structure and function of photolyase and in vivo Enzymology: 50th Anniversary. J Biol Chem 283(47):32153–32157. https://doi.org/10.1074/jbc.R800052200
22. Terai Y, Sato R, Matsumura R, Iwai S, Yamamoto J (2020) Enhanced DNA repair by DNA photolyase bearing an artificial light-harvesting chromophore. Nucleic Acids Res 48(18):10076–10086. https://doi.org/10.1093/nar/gkaa719
23. Liebel F, Kaur S, Ruvolo E, Kollias N, Southall MD (2012) Irradiation of skin with visible light induces reactive oxygen species and matrix-degrading enzymes. J Invest Dermatol 132(7):1901–1907. https://doi.org/10.1038/jid.2011.476
24. Nakashima Y, Ohta S, Wolf AM (2017) Blue light-induced oxidative stress in live skin. Free Radic Biol Med 108:300–310. https://doi.org/10.1016/j.freeradbiomed.2017.03.010
25. Arthaut LD, Jourdan N, Mteyrek A, Procopio M, El-Esawi M, d'Harlingue A, Bouchet PE, Witczak J, Ritz T, Klarsfeld A, Birman S, Usselman RJ, Hoecker U, Martino CF, Ahmad M (2017) Blue-light induced accumulation of reactive oxygen species is a consequence of the Drosophila cryptochrome photocycle. PLoS ONE 12(3):e0171836. https://doi.org/10.1371/journal.pone.0171836

26. Omata Y, Lewis JB, Rotenberg S, Lockwood PE, Messer RL, Noda M, Hsu SD, Sano H, Wataha JC (2006) Intra- and extracellular reactive oxygen species generated by blue light. J Biomed Mater Res A 77(3):470–477. https://doi.org/10.1002/jbm.a.30663
27. Bae S, Oh T (2018) In vitro bactericidal activity of 465–470 nm blue light phototherapy and aminolevulinic acid on Staphylococcus pseudintermedius. Vet Dermatol. https://doi.org/10.1111/vde.12651
28. Fukui M, Yoshioka M, Satomura K, Nakanishi H, Nagayama M (2008) Specific-wavelength visible light irradiation inhibits bacterial growth of Porphyromonas gingivalis. J Periodont Res 43(2):174–178. https://doi.org/10.1111/j.1600-0765.2007.01009.x
29. Dos Anjos C, Sellera FP, Ribeiro MS, Baptista MS, Pogliani FC, Lincopan N, Sabino CP (2020) Antimicrobial blue light and photodynamic therapy inhibit clinically relevant β-lactamases with extended-spectrum (ESBL) and carbapenemase activity. Photodiagnosis Photodyn Ther 32:102086. https://doi.org/10.1016/j.pdpdt.2020.102086
30. Ferrer-Espada R, Wang Y, Goh XS, Dai T (2020) Antimicrobial blue light inactivation of microbial isolates in biofilms. Lasers Surg Med 52(5):472–478. https://doi.org/10.1002/lsm.23159
31. Beck SE, Ryu H, Boczek LA, Cashdollar JL, Jeanis KM, Rosenblum JS, Lawal OR, Linden KG (2017) Evaluating UV-C LED disinfection performance and investigating potencial dual-wavelenght synergy. Water Res 109:207–216. https://doi.org/10.1016/j.watres.2016.11.024
32. Maclean M, MacGregor SJ, Anderson JG, Woolsey G (2009) Inactivation of bacterial pathogens following exposure to light from a 405-nanometer light-emitting diode array. Appl Environ Microbiol 75(7):1932–1937. https://doi.org/10.1128/AEM.01892-08
33. Fila G, Kawiak A, Grinholc MS (2017) Blue light treatment of Pseudomonas aeruginosa: strong bactericidal activity, synergism with antibiotics and inactivation of virulence factors. Virulence 8(6):938–958. https://doi.org/10.1080/21505594.2016.1250995
34. De Lucca AJ, Carter-Wientjes C, Williams KA, Bhatnagar D (2012) Blue light (470 nm) effectively inhibits bacterial and fungal growth. Lett Appl Microbiol 55(6):460–466. https://doi.org/10.1111/lam.12002
35. Dorey AL, Lee B-H, Rotter B, O'Byrne CP (2019) Front microbiol blue light sensing in listeria monocytogenes is temperature-dependent and the transcriptional response to it is predominantly SigB-dependent. Front Microbiol 10:2497. https://doi.org/10.3389/fmicb.2019.02497
36. Zhang Y, Zhu Y, Gupta A, Huang Y, Murray CK, Vrahas MS, Sherwood ME, Baer DG, Hamblin MR, Dai T (2014) Antimicrobial blue light therapy for multidrug-resistant Acinetobacter baumannii Infection in a mouse burn model: implications for prophylaxisand treatment of combat-related wound infections. J Infect Dis 209(12):1963–1971. https://doi.org/10.1093/infdis/jit842
37. Cieplik F, Späth A, Leibl C, Gollmer A, Regensburger J, Tabenski L, Hiller K-A, Maisch T, Schmalz G (2014) Blue light kills Aggregatibacter actinomycetemcomitans due to its endogenous photosensitizers. Clin Oral Invest 18(7):1763–1769. https://doi.org/10.1007/s00784-013-1151-8
38. Maclean M, Anderson JG, MacGregor SJ, White T, Atreya CD (2016) A new proof of concept in bacterial reduction: antimicrobial action of violet-blue light (405 nm) in *ex vivo* stored plasma. J Blood Trans 2016:2920514. https://doi.org/10.1155/2016/2920514
39. Biener G, Masson-Meyers DS, Bumah VV, Hussey G, Stoneman MR, Enwemeka CS, Raicu V (2017) Blue/violet laser inactivates methicillin-resistant Staphylococcus aureus by altering its transmembrane potential. J Photochem Photobiol B 170:118–124. https://doi.org/10.1016/j.jphotobiol.2017.04.002
40. Plavskii VY, Mikulich AV, Tretyakova AI, Leusenka IA, Plavskaya LG, Kazyuchits OA, Dobysh II, Krasnenkova TP (2018) Porphyrins and flavins as endogenous acceptors of optical radiation of blue spectral region determining photoinactivation of microbial cells. J Photochem Photobiol B 183:172–183. https://doi.org/10.1016/j.jphotobiol.2018.04.021
41. Gomez GF, Huang R, MacPherson M, Zandona AGF, Gregory RL (2016) Photo inactivation of Streprococcus mutans biofilm by violet-blue light. Curr Microbiol 73(3):426–433. https://doi.org/10.1007/s00284-016-1075-z
42. Dos Anjos C, Sabino CP, Bueris V, Fernandes MR, Pogliani FC, Lincopan N, Sellera FP (2019) Antimicrobial blue light inactivation of international clones of multidrug-resistant Escherichia coli ST10, ST131 and ST648. Photodiagnosis Photodyn Ther 27:51–53. https://doi.org/10.1016/j.pdpdt.2019.05.014
43. Angarano V, Smet C, Akkermans S, Watt C, Chieffi A, Impe JFMV (2020) Visible light as an antimicrobial strategy for inactivation of Pseudomonas fluorescens and Staphylococcus epidermidis Biofilms. Antibiotics (Basel) 9(4):171. https://doi.org/10.3390/antibiotics9040171
44. Hadi J, Wu S, Brightwell G (2020) Antimicrobial blue light versus pathogenic bacteria: mechanism, application in the food industry, hurdle technologies and potential resistance. Foods 9(12):1895. https://doi.org/10.3390/foods9121895
45. Keyvan E, Kahraman HA, Tutun H, Donmez S, Sen E, Demirtas A, Akyuz AO (2021) Inactivation efficacy of 405 nm light emitting diodes (LEDs) on Salmonella Enteritidis at different illumination temperatures. Food Sci Technol 42:e08721. https://doi.org/10.1590/fst.08721
46. Ganz RA, Viveiros J, Ahmad A, Ahmadi A, Khalil A, Tolkoff MJ, Nishioka NS, Hamblin MR (2005) Helicobacter pylori in patients can be killed by visible light. Lasers Surg Med 36(4):260–265. https://doi.org/10.1002/lsm.20161
47. Rapacka-Zdonczyk A, Wozniak A, Kruszewska B, Waleron K, Grinholc M (2021) Can Gram-negative bacteria develop resistance to antimicrobial blue light treatment? Int J Mol Sci 22(21):11579. https://doi.org/10.3390/ijms222111579
48. Metzger M, Hacobian A, Karner L, Krausgruber L, Grillari J, Dungel P (2022) Resistance of bacteria toward 475 nm blue light exposure and the possible role of the SOS response. Life 12(10):1499. https://doi.org/10.3390/life12101499
49. Amin RM, Bhayana B, Hamblin MR, Dai T (2016) Antimicrobial blue light inactivation of Pseudomonas aeruginosa by photo-excitation of endogenous porphyrins: in vitro and in vivo studies. Lasers Surg Med 48(5):562–568. https://doi.org/10.1002/lsm.22474
50. Tomb RM, Maclean M, Coia JE, MacGregor SJ, Anderson JG (2017) Assessment of the potential for resistance to antimicrobial violet-blue light in Staphylococcus aureus. Antimicrob Resist Infect Control 29(6):100. https://doi.org/10.1186/s13756-017-0261-5
51 Leanse LG, Harrington OD, Fang Y, Ahmed I, Goh XS, Dai T (2018) Evaluating the potential for resistance development to antimicrobial blue light (at 405 nm) in Gram-negative bacteria: In vitro and in vivo Studies. Front Microbiol 16(9):2403. https://doi.org/10.3389/fmicb.2018.02403
52. Kohli R, Gupta PK, Dube A (2000) Helium-neon laser preirradiation induces protection against UVC radiation in wild-type E. colistrain K12AB1157. Radiat Res 153:181–185. https://doi.org/10.1667/0033-7587(2000)153[0181:HNLPIP]2.0.CO;2
53. Purbhoo-Makan M, Houreld NN, Enwemeka CS (2022) The effects of blue light on human fibroblasts and diabetic wound healing. Life (Basel) 12(9):1431. https://doi.org/10.3390/life12091431